

SYNCHRONOUS GENERATOR FAULT DIAGNOSIS USING SHAFT SIGNAL MEASUREMENTS

Simon John Hoffe

A dissertation submitted to the Faculty of Engineering and the Built Environment,
University of the Witwatersrand, Johannesburg, in fulfilment of the requirements
for the degree of Master of Science in Engineering.

Johannesburg, 2006

Declaration

I declare that this dissertation is my own, unaided work, except where otherwise acknowledged. It is being submitted for the degree of Master of Science in Engineering in the University of the Witwatersrand, Johannesburg. It has not been submitted before for any degree or examination in any other university.

Signed this ____ day of _____ 20__

Simon John Hoffe

Abstract

Shaft voltages and currents are an unavoidable characteristic of rotating machines, though they are typically a nuisance this work shows that shaft signals can be used for fault diagnosis. This work focussed on shaft voltages present on synchronous generators. Measurements on a 4-pole generator found that the angular position of the shaft could be determined from the shaft voltage. An experimental 20 kVA 2-pole synchronous generator was designed and built which resembled a full-size 600 MVA turbo-generator. The effects of a static eccentricity on the shaft voltage were successfully determined firstly through FEM simulation and then verified with physical measurements. Shaft voltages can be used to diagnose static eccentricity, future work should investigate other faults. In addition, computer simulation was found to be effective and simulation and measurements of operating machines (such as turbo-generators) should be considered.

*Dedicated to the friendly and hardworking staff of the School of Electrical and
Information Engineering. God bless you all.*

Acknowledgements

Thanks to my supervisor past, Mr Andre ‘Fuzzy’ Van Zyl who got me started and to my supervisor present Prof Willie Cronje for patience and support. Thanks also to Mr Alan Meyer of Wits and to Mr Verdun Pardini of Trans Vaal Electric who together have played a crucial role in the design and construction of the experimental mini-gen which will hopefully fuel many more research projects. Finally, this whole avenue of research is indebted to Dr Simon Higgins and Eskom (through TESP) for their motivation and financial support respectively.

Contents

Declaration	i
Abstract	ii
Acknowledgements	iv
Contents	v
List of Figures	xii
List of Tables	xvi
1 Introduction	2
1.1 In general	2
1.2 Thesis plan	3
1.2.1 Chapter 2 – Background	3
1.2.2 Chapter 3 – Measurement system	3
1.2.3 Chapter 4 – Shaft position determination	4
1.2.4 Chapter 5 – Mini-gen design	4
1.2.5 Chapter 6 – Mini-gen simulation	4
1.2.6 Chapter 7 – Mini-gen measurements	5

2	Background	6
2.1	Introduction	6
2.2	Typical machine failures	7
2.2.1	Stator core defects	8
2.2.2	Winding insulation defects	8
2.2.3	Winding subconductor faults	9
2.2.4	Stator end winding faults	10
2.2.5	Water coolant faults	10
2.2.6	Rotor winding faults	11
2.2.7	Rotor body defects	11
2.2.8	Bearing failure	12
2.3	Condition monitoring	13
2.4	Established techniques	14
2.4.1	Electrical techniques	15
2.4.2	Chemical techniques	16
2.4.3	Vibrational techniques	17
2.4.4	Temperature techniques	17
2.5	Proposed technique – shaft signals	19
2.5.1	History – Cause, effect and minimisation	19
2.5.2	Application to condition monitoring	20
2.6	Testing platform	23
2.6.1	Introduction and goals	23

2.6.2	Simulation	24
2.6.3	Physical measurements	25
2.6.4	Signal processing	25
2.7	Conclusion	26
3	Measurement system	27
3.1	Introduction	27
3.2	Power supply	27
3.2.1	Requirements	27
3.2.2	Design	28
3.3	Angular position measurement	28
3.3.1	Requirements	28
3.3.2	Encoder interface and isolation design	29
3.4	Shaft voltage measurement	30
3.4.1	Requirements	30
3.4.2	Design	31
3.4.3	Characterisation	31
3.5	Additional line current and voltage measurements	33
3.6	Conclusion	33
4	Shaft position determination	35
4.1	Introduction	35
4.2	Experimental setup	36
4.3	Measurement system	36

4.4	Algorithm	37
4.5	Discussion	38
4.6	Conclusion	40
5	Mini-gen design	41
5.1	Introduction	41
5.2	Generator requirements	41
5.2.1	Experimental capability	42
5.2.2	Similarity to full-sized machine	43
5.2.3	Economic decisions	43
5.3	Generator design	43
5.3.1	General	43
5.3.2	Constructional features	44
5.3.3	Design	45
5.4	Final specification	45
5.4.1	Stator	45
5.4.2	Rotor	46
5.5	Operating characteristics	47
5.5.1	Measured winding resistances	47
5.5.2	Open and short-circuit tests	48
5.5.3	Rotor temperature rise	48
5.6	Conclusion	50
6	Mini-gen simulation	51

6.1	Introduction	51
6.2	Modelling	52
6.2.1	Simulation types	52
6.2.2	Drawing the model	53
6.2.3	Choosing materials	54
6.2.4	Setting up boundaries and sources	56
6.2.5	Setting up executive parameters	58
6.2.6	Setting up the solution	58
6.3	Areas to investigate	61
6.4	Data analysis technique	62
6.5	Results	62
6.5.1	Usefulness of transient simulations	62
6.5.2	Influence of steps per revolution	64
6.5.3	Feasibility of using linear approximations of materials	66
6.5.4	Affect of static eccentricity on shaft voltage	66
6.5.5	Affect of machine output loading on shaft voltage	68
6.5.6	Affect of reduced excitation current on shaft voltage	68
6.5.7	Affect of reduced angular velocity on shaft voltage	70
6.5.8	Affect of damper bars on shaft voltage	73
6.5.9	Affect of stator slot count on shaft voltage	75
6.6	Computing observations and recommendations	80
6.7	Conclusion	81

7	Mini-gen measurements	83
7.1	Introduction	83
7.2	Experimental set up	83
7.3	Eccentricity adjustment	86
7.4	Experiments	87
7.5	Measured results	88
7.5.1	No Eccentricity	88
7.5.2	+0,65 mm eccentricity	91
7.5.3	+1,9 mm eccentricity	91
7.5.4	-3,1 mm eccentricity	91
7.5.5	Waveform comparison	94
7.6	Conclusion	96
8	Conclusion	97
8.1	Outcomes	97
8.2	Recommendations for future research	98
	References	100
A	Minigen drawings	102
B	Matlab source code	108
B.1	Introduction	108
B.2	sjh_process_sims.m	109
B.3	sjh_process_measured.m	112

B.4	sjhspec.m	114
B.5	loaddat.m	116
B.6	loadmeas.m	118
B.7	loadsig.m	119
B.8	ave_data.m	121
B.9	rmssim.m	122
C	Datasheets	123

List of Figures

3.1	Power supply schematic	28
3.2	Encoder interface schematic	30
3.3	Shaft voltage interface schematic	32
3.4	Measured interface gain	32
3.5	Photograph of signal interface box (with cover removed)	33
4.1	Diagram of experimental setup	36
4.2	Time domain plot of the recorded shaft signal and the shaft absolute position	39
4.3	Super-imposed plot of shaft signal cycles, referenced against the shaft position	39
4.4	Averaged plot of shaft signal cycles over 20 s, referenced using shaft position recording	39
4.5	Averaged plot of shaft signal cycles over 1 s, referenced using an estimated fundamental frequency	39
4.6	Time domain plot of a signal recorded at 90% excitation	39
4.7	Averaged plot of 90% excitation shaft signal. Averaged over 1 s, referenced using an estimated fundamental frequency	39
4.8	The reference plot and the 90% excitation plot after correlation with each other	39
4.9	Estimated shaft position versus actual shaft position	39

5.1	Assembly diagram of mini-gen	44
5.2	Photograph of the stator before winding	46
5.3	Photograph of the rotor in the process of winding	47
5.4	Open circuit characteristic of the mini-gen	48
5.5	Short circuit characteristic of the mini-gen	49
6.1	Possible drawing geometries for MAXWELL 2D TM models [1]	52
6.2	MAXWELL 2D TM model of the mini-generator	55
6.3	MAXWELL 2D TM model external circuit for stator and shaft	55
6.4	B-H curve for laminated steel M400	56
6.5	Mini-generator model mesh	59
6.6	Output node voltages relative to ground	63
6.7	Shaft voltage relative to ground	63
6.8	Shaft voltage frequency spectrum	63
6.9	Comparison of shaft voltage frequency power spectrums	65
6.10	Comparison of shaft voltage frequency power spectrums for linear vs non-linear materials	65
6.11	Model of the generator with no eccentricity	67
6.12	Model of the generator with 5 mm of eccentricity	67
6.13	Time domain plot of shaft-voltage at full load for different simulated eccentricities	67
6.14	Relative frequency spectrum of shaft-voltage at full load for different simulated eccentricities	67
6.15	Comparison plot of shaft voltage power frequency spectrum for dif- ferent load conditions with no eccentricity	69

6.16	Comparison plot of shaft voltage power frequency spectrum for different load conditions with 2,5 mm eccentricity	71
6.17	Comparison plot of shaft voltage power frequency spectrum for different excitation currents with no eccentricity	72
6.18	Comparison plot of shaft voltage power frequency spectrum for different excitation currents with 2,5 mm eccentricity	72
6.19	Comparison plot of shaft voltage power frequency spectrum for different rotational speeds with no eccentricity	74
6.20	Comparison plot of shaft voltage power frequency spectrum for different rotational speeds with 2,5 mm eccentricity	76
6.21	Time domain plot of the bar currents for the full load model with no eccentricity	76
6.22	Flux density normal to the air-gap for the full load model with no eccentricity	77
6.23	Time domain plot of the rotor torque with a 5 mm eccentricity	77
6.24	Comparison plot of shaft voltage power frequency spectrum for simulations with and without damper bars (no eccentricity)	78
6.25	Comparison plot of shaft voltage power frequency spectrum for simulations with and without damper bars (5 mm eccentricity)	78
6.26	Model of the 48 slot generator with 5 mm of eccentricity	79
6.27	Model of the 42 slot generator with 4 mm of eccentricity	79
6.28	Comparison plot of shaft voltage power frequency spectrum for no eccentricity and 4mm eccentricity of a machine with a 42 slot stator	79
7.1	Experimental setup	84
7.2	Photograph of the coupled miniature turbo-generator and 2-pole induction motor	85
7.3	Closeup of the NDE shaft brush, slip rings and incremental encoder	86

7.4	Closeup of a stator mounting bracket, showing the oblong locating holes and removable shim	87
7.5	Position referenced average shaft voltage for no eccentricity and full load	89
7.6	Normalised power spectrum of the shaft voltage for no eccentricity and full load	89
7.7	Position referenced average shaft voltage for +0,65 mm eccentricity and full load	90
7.8	Normalised power spectrum of the shaft voltage for +0,65 mm eccentricity and full load	90
7.9	Position referenced average shaft voltage for +1,9 mm eccentricity and full load	92
7.10	Normalised power spectrum of the shaft voltage for +1,9 mm eccentricity and full load	92
7.11	Position referenced average shaft voltage for -3,1 mm eccentricity and full load	93
7.12	Normalised power spectrum of the shaft voltage for -3,1 mm eccentricity and full load	93
7.13	Position referenced average shaft voltage for +0,65 mm and +1,9 mm eccentricity at full load	95
7.14	Position referenced average shaft voltage for +1,9 mm and -3,1 mm eccentricity at full load	95

List of Tables

2.1	Pros and cons of condition monitoring techniques	14
5.1	Mini-gen winding resistances	47
5.2	Temperature rise of the rotor during no-load operation	49
6.1	Phase output voltage (RMS) with different loads and no eccentricity	69
6.2	Shaft voltage (RMS) with different loads and no eccentricity	69
6.3	Shaft voltage (RMS) with different loads and 2,5 mm eccentricity . .	69
6.4	Phase output voltage (RMS) with different excitation currents and no eccentricity	71
6.5	Shaft voltage (RMS) with different excitation currents and no eccen- tricity	71
6.6	Shaft voltage (RMS) with different excitation currents and 2,5 mm eccentricity	71
6.7	Phase output voltage (RMS) with different rotational speeds and no eccentricity	74
6.8	Shaft voltage (RMS) with different rotational speeds and no eccentricity	74
6.9	Shaft voltage (RMS) with different rotational speeds and 2,5 mm eccentricity	74
6.10	Phase output voltage (RMS) with and without damper bars (no ec- centricity)	76
6.11	Shaft voltage (RMS) with and without damper bars (no eccentricity)	77

6.12	Shaft voltage (RMS) with and without damper bars (5 mm eccentricity)	77
7.1	dSPACE TM channel connections	86
7.2	Measured rms voltages for no eccentricity	89
7.3	Measured rms voltages for +0,65 mm eccentricity	90
7.4	Measured rms voltages for +1,9 mm eccentricity	92
7.5	Measured rms voltages for -3,1 mm eccentricity	93

Chapter 1

Introduction

1.1 In general

Constantly increasing demands for electrical energy is, in the short-term, resulting in a decrease in spare generating capacity. Accurate condition monitoring of electrical generators is becoming of greater importance, as the consequences of unforeseen or emergency generator shutdown is becoming more and more difficult to mitigate as spare capacity is simply not available. While the problem of managing South Africa's generating capacity and the development of new capacity is far beyond the scope of this dissertation, this work is concerned with shedding light on, and developing expertise in a relatively unexplored area of condition monitoring known as shaft signal analysis.

A synchronous generator is typically designed to produce a voltage and a current at the stator terminals through the rotation of a d.c. magnetic field within the stator windings. A voltage at the terminals of the stator windings is, however, not the only e.m.f. generated by the changing flux. A voltage also develops between either end of the rotating shaft. This e.m.f. is not a design trait and is as a result of unavoidable dissymmetries in the physical construction of the machine. Due to imperfect manufacturing shaft voltages will be developed even in healthy machines; a fault generally introduces some kind of disturbance into the magnetic fields within the machine, and this is manifested as a change in the shaft voltage waveform. This research concerns itself with the simulation and measurement of shaft voltages under normal and fault conditions.

Extensive use was made of multi-step finite element simulations in order to predict

anticipated changes in the shaft signal when a fault was introduced. For the purposes of this work, the fault in question is a static eccentricity of the rotor. This fault has the benefit of being simple to simulate with a 2-D model and, using the custom built miniature turbo-generator, easy to physically demonstrate.

This report documents the various stages of the project, starting with a background on available condition monitoring techniques and moving through the development of a measurement system, preliminary experiments carried out with a standard 4-pole generator, the design of the miniature turbo-generator, the simulation of the mini-gen and finally the physical measurements and conclusion.

1.2 Thesis plan

1.2.1 Chapter 2 – Background

Starts by presenting a general overview of rotating machine components and the types of failures which can affect them. The subject of condition monitoring and its importance is introduced, followed by an overview of the established monitoring techniques. The different monitoring techniques are listed under the categories of electrical, chemical, vibrational and temperature. A background is then given of the proposed technique of shaft signal analysis, which is the principal topic of this study. Both the history and anticipated application to condition monitoring are given. In particular, the work of Nippes and Torlay is presented and discussed. Finally the testing platform which is used to investigate shaft voltages is introduced and the goals of the testing and of this research are given. Three aspects of the testing platform, namely simulation, physical measurements and signal processing are elucidated.

1.2.2 Chapter 3 – Measurement system

This chapter presents a detailed design of the necessary signal interface and power supply circuits. There are three circuits which were designed and constructed. The first is a general purpose regulated dual-rail supply, the second is an incremental encoder interface and isolation circuit needed to obtain angular position information, and the third is an anti-alias, gain and protection circuit used for measuring the shaft voltage.

1.2.3 Chapter 4 – Shaft position determination

While the 2-pole miniature generator was being manufactured experiments were conducted on a 4-pole Siemens generator. The 4-pole generator was retro-fitted with an insulated bearing on the driven-end. The result of those experiments was the identification of a technique which could locate the angular position of the shaft. This technique makes use of an extended capture time to average out the shaft-voltage, producing a clear waveform which is periodic about a mechanical revolution. These results were presented at the IEEE International Symposium on Diagnostics for Electric Machines, Power Electronics and Drives (SDEMPED) in September 2005 [2].

1.2.4 Chapter 5 – Mini-gen design

This chapter details the design objectives for the experimental miniature generator (or mini-gen). In summary, the mini-gen must be suited to experimentation in the University's machines laboratory, it must closely resemble the key characteristics of a full size turbo-generator and cost of materials and manufacture must be minimised. The design, final specification and operating characteristics are presented.

1.2.5 Chapter 6 – Mini-gen simulation

This chapter and the next present the focus of this research project. This chapter details the methodology used and the results obtained from transient finite element method (FEM) simulations. MAXWELL 2DTM from Ansoft was used to perform these simulations and MATLAB from The Mathworks was used to plot and analyse the results. One of the objectives of this research project is to build expertise in transient simulations using MAXWELL 2DTM and this is reflected in the detailed product-specific content of this chapter. Background on the model setup, meshing and related activities is given. Once a consistent approach to the simulations is established, various questions are posed concerning the suitability of FEM simulation to shaft voltage prediction and then further, the effect of various machine parameters on the shaft voltage. These can be looked up using the section titles in the chapter. The use of the MAXWELL 2DTM package to simulate shaft voltage was highly successful, and the simulation results strongly support the use of shaft voltage measurement as a condition monitoring tool.

1.2.6 Chapter 7 – Mini-gen measurements

This chapter follows on from the last by showing how the FEM simulation results were verified against physical measurements. It begins by detailing the experimental setup and means by which a static eccentricity can be introduced into the machine. The primary goal of the experiments was to verify whether or not the shaft voltage frequency spectrum would behave in a similar manner to the simulations. Experiments were conducted with no eccentricity and at three different levels of eccentricity. The results obtained in these four cases are presented and discussed. It is concluded that the FEM simulations were accurate in their prediction of an increased fifth harmonic in the shaft voltage when the machine was run with a misaligned shaft.

Chapter 2

Background

2.1 Introduction

This research is concerned with synchronous machines in general, and synchronous generators in particular. Failures prevalent in other machines (such as squirrel-cage faults) will not be presented here.

Rotating machines are made up of two key components: a stator and a rotor. Both are made up of different materials with substantially different properties. The three basic materials are steel, which gives structural strength and forms the magnetic circuit in the machine, copper which forms the electrical circuit and carries power into and out of the machine and finally, various types of insulation which keep the current flowing where it should. Additional mechanical components such as fans, bearings, slip-rings, brushes, ducting and casings are also present. In very large machines (upwards of about 20 MVA) it becomes necessary to include more sophisticated cooling systems. A common cooling strategy on large turbo-generators is forced water circulation in the stator and hydrogen circulation in the rotor.

The purpose of any generator or motor is to convert mechanical energy to electrical energy, or visa-versa. On a large machine, large forces will be present. These forces act on all parts of the machine to greater and lesser extents. As such, all parts of the machine are subject to some degree of aging and deterioration. It is the job of the designer and manufacturer to minimise these effects for specified operating conditions.

To this end, machine design and manufacturing techniques are very mature and the risk of sudden failure on most machines is low. Failure becomes a risk where

machines are operated outside of their design specification or in extremely harsh environments. Design specifications will include (but are not limited to) the necessary voltage, current and power ratings, intended operating environment (ambient temperature, humidity, vibration, etc.) and intended machine lifespan. The issue of design life-span is now highly topical as machines installed many years ago may now be technically running outside of their design specification, and hence are at a higher risk of failure.

Risk of failure must also be balanced with the consequences of failure. Unfortunately, the machines most depended upon often have the greatest complexity and operate under high levels of mechanical and/or electrical stress. Thus the machines with the highest risk of failure are also those with the most severe consequences! This is especially true for the large synchronous turbo-generators employed by power utilities. However, an important digression needs to be made. Very often, a large mission-critical machine such as a turbo-generator will be last in a line consisting of a complex process of pumps, burners, conveyers and the like. A simple conveyer driver can be overlooked because of its simplicity, low-cost and high reliability – but should it fail, it could cause a plant shut-down of the same extent as a turbo-generator failure!

As will be discussed in *Section 2.3*, any plant monitoring system does need to take a holistic approach and incorporate the monitoring of supporting as well as primary plant components. Digression aside, this research is concerned with the condition monitoring of synchronous generators. A brief overview of machine failures will be given in *Section 2.2* and various established monitoring techniques will be presented in *Section 2.4*. A background and motivation of the relatively new technique, and the focus of this dissertation, of shaft signal monitoring will be presented in *Section 2.5*. Finally the proposed testing platform will be discussed in *Section 2.6*.

2.2 Typical machine failures

Before looking at techniques of condition monitoring, it is wise to consider what faults are most likely to occur. Eskom does not publicly release its synchronous machine failure statistics, but the following common faults are documented in the literature. Tavner and Penman [3] gives a dated but relevant overview of condition monitoring and typical faults on a wide range of machine types, and is the primary

source for the material presented below¹. Vas [4] presents a more technical approach to machine diagnostics incorporating parameter estimation. Alger and Samson [5], Ammann et al. [6], Costello [7] and Verma et al. [8] discuss failures relating to shaft currents and/or voltages.

2.2.1 Stator core defects

Core faults are rare and usually only occur in very large turbo-generators where the laminated steel cores are sufficiently massive, and carry a sufficiently high magnetic flux density, that when shorting occurs between laminations potentially damaging currents can flow. Laminations can be shorted together during manufacture or as a result of poor rotor insertion. The circulating currents can cause heating which can be severe enough to melt the core steel, the molten steel then runs into the slots and burns through the winding insulation. This would trip the earth-fault protection relay, at this stage the damage to the stator core and windings would result in them being written off.

Early indications of this type of fault are the flowing of large circulating currents, high temperatures and the pyrolysing of the insulation material. On smaller machines similar damage can occur. In this case, damage can be caused by manufacturing defects. However, the stator is often damaged in service through excessive vibration or as a result of an earlier bearing failure resulting in the rotor rubbing the stator.

Lee et al. [9] presented a paper on inter-laminar stator core insulation failure detection techniques for generators based on low flux core excitation.

2.2.2 Winding insulation defects

One of the intrinsically weakest components of an electrical machine, both mechanically and electrically, is the insulation system. This was especially true of earlier machines, however, modern materials and techniques have greatly improved the mechanical and electrical strength of the insulation system. Failure due to simple ageing is now very rare. Most failures are as a result of either manufacturing defects or mechanical damage caused by foreign materials while the machine is in operation.

¹The material presented here is largely a summary of Tavner and Penman [3] Chap. 2, please refer to it if you require greater background or depth.

With the exception of a sudden massive physical trauma, insulation failure will be preceded by an increase in partial discharge activity. The increase can be gradual, and depending on the location of the defect, symptoms of failure can be observed days or weeks in advance. Partial discharge detection is a very active area of research, though it does not fall in the immediate scope of this study.

Winding insulation, in this context, refers to the primary insulation between intended current paths (the copper windings) and surrounding components (such as the stator and rotor). A failure of this insulation will typically cause a ground fault which will result in the immediate shut-down of the machine. However, depending on the electrical connection of the machine with respect to ground it is possible that a single failure will not result in a fault, but a second failure will complete the circuit and cause a very serious fault condition.

2.2.3 Winding subconductor faults

These faults are generally confined to large generators where the electrical loadings are such that the stator winding is very highly stressed, electrically, thermally and mechanically. It is normal to subdivide the conductor into a large number of subconductors and to insulate and transpose them to minimise winding losses. In modern machines the transposition is distributed throughout the conductor length by the use of the Roebel technique. This gives a uniform current distribution and minimises the voltages between subconductors. Older machines, however, have the transpositions made in the end winding at the knuckle joint and quite large voltages, up to 50 V rms, can exist between subconductors. If severe mechanical movement of the winding occurs during operation and the subconductor insulation fails then subconductors can short together causing arcing.

The early indicators of such faults are arcing activity within the winding and the pyrolysing of insulation. Although the fact that burning is taking place deep within a conductor bar usually means that, initially at least, only small quantities of particulate and gaseous matter produced by the burning are released into the cooling gas circuit. Where water-cooled subconductors are present, the fault causes a leakage of gas into the winding cooling system.

2.2.4 Stator end winding faults

A lot of effort has gone into the design of end winding structures. The end winding must be restrained against the large forces on the winding during transient loading, it also needs to cushion the conductor bars against the smaller forces during steady, continuous running. End winding movements in normal operation are quite significant and can be as much as a few millimetres on a large turbogenerator. Faults occur in the end winding when the bracing structure slackens, either as a result of a succession of unusual overloads or because of an extended period of continuous running. In some cases the end winding insulation becomes cracked, fretted or worn away.

Foreign bodies inside a machine, such as steel washers, nuts or small portions of insulation, get thrown around by the rotor. Damage is caused by these objects, usually in the stator end winding region, where the insulation is damaged by the impact or eroded by debris worming into it under the action of electromagnetic forces (such a piece of debris is colloquially known as a “magnetic termite”).

The early indications of problems are an increase in end winding vibration and the possibility of electrical discharge activity to nearby earth planes.

2.2.5 Water coolant faults

In water-cooled machines it is possible for a coolant blockage to occur, either in the pipework leading to or from the conductor bars or in a subconductor itself. This can be caused by either debris (though filters should protect against this) or by gas entrainment resulting in gas-locking. Coolant blockage will eventually lead to machine overheating and ultimately the burning of insulation. It is possible, however, to operate a machine with some blocked pathways if restrictions on load are acceptable. The normal vibration of a machine in service can excite resonances in an improperly designed cooling pipework system and this can cause fatigue failure of a pipe and loss of coolant.

The early indications of these kinds of fault are high indicated conductor or cooling water temperatures, possible gas release from the water system and pyrolysing insulation leading eventually to damaging discharge activity which will be electrically detectable at the machine terminals.

2.2.6 Rotor winding faults

In turbine-type generators the rotor winding insulation and bracing system must be designed to withstand exceptionally high centrifugal forces imposed upon them, and the faults are usually associated with these forces. A short can occur between rotor turns, due to cracking of the winding insulation. The shorting current which then flows creates a local hot-spot leading to further insulation degradation and the possibility of further shorted turns. Once a short has occurred there is an asymmetry in the flux in the machine and an unbalanced force on the rotor which causes rotor vibrations. This is usually the first evidence that a shorted turn is present. Shorts are also sometimes promoted by copper dust produced by fretting action in the rotor winding. This occurs because of the cyclic movement which a large winding experiences relative to the rotor, partly due to the self-weight bending of the long thin rotor and partly due to thermal cycling. If an insulation fault occurs between the winding and rotor body then an earth fault current flows which can be detected by an earth leakage relay. If only a single earth fault occurs then the fault current is limited, but if a second earth fault occurs then very large circulating currents can flow.

The early indications of these faults are a distortion of the air gap flux and associated stray leakage flux around the machine and an increase in bearing vibration. Further, it is a proposal of this research that rotor faults can be detected through the measurement and trending of shaft voltages and currents.

2.2.7 Rotor body defects

The high centrifugal stresses in machine rotors can also lead to problems in the rotor body as well as in the windings. The propagation of cracks from surface defects in the rotor material, or its associated components, due to high-cycle fatigue under the action of the self-weight forces during rotation, can lead to catastrophic rotor failures. This situation is exacerbated if the cooling gas contains moisture or other impurities which encourage corrosion and can lower the resistance of the rotor material to fatigue failure. Excessive heating of the rotor can also weaken the rotor material. This can be caused by eddy current losses due to negative sequence in the supply. But it is not only high-cycle fatigue which can cause a rotor to fail. Large transients on the electrical system to which a machine is connected can also impose sudden strains on its rotor. If a resonant condition exists between the machine and the system the sudden transients can excite torsional oscillations which can lead to

rotor or coupling failure.

Eccentricity of the rotor can lead to vibration due to unbalanced magnetic pull and this can be compounded when the asymmetric heating leads to thermal bending of the rotor. Two and four pole totally enclosed machines are particularly prone to these problems especially if they have a small air-gap.

The early indications of these types of faults are usually excessive transverse bearing vibrations, attention has also been given to measuring the torsional oscillations of the shaft itself. The influence that static eccentricity has on shaft currents and voltages will be investigated in this study using both transient simulations and physical measurements.

2.2.8 Bearing failure

Bearings are a critical component of all rotating machines and their design and specification is a mature science. The rate of wear with correct installation and consistent running conditions is reasonably predictable; in addition, bearings are usually renewed when the machine is serviced. Premature breakdown of bearings can still occur and can result in excessive vibration and even rotor eccentricity to the point of contact between the stator and the rotor on small air-gap machines.

Bearing failure can be caused by a number of factors [10]. Poor lubrication will shorten the life of a bearing, with both under and over lubrication being a problem. Faulty mounting which can result from poor alignment or other pre-loading conditions, is evidenced by an unusual running band pattern or local injury to the races such as nicks, score marks or dents. Design faults are less common but can arise where a bearing is improperly modified after manufacture. Corrosion of bearings can result from poor sealing, acid fumes, lubricants containing acids, condensation or unsuitable storage. Dirt and/or other foreign particles in the lubricant can cause damage. Chatter marks can be caused by static overload, vibrations and knocks when the bearing was stationary and also by current passing through the bearing.

Shaft currents and voltages are generally regarded as a nuisance feature of rotating machines because of the damage they can cause to the bearings. This was documented by Alger and Samson [5] in 1924 along with machine design techniques which will minimise shaft currents. None-the-less, the damage done to bearings by shaft currents and voltages has continued to be an operating concern on rotating machines in general and large generators in particular [6–8, 11].

2.3 Condition monitoring

The goal of condition monitoring is to save money and/or safeguard reliability and safety. In most circumstances, up-time and financial cost are directly linked. In extreme cases (such as nuclear power), reliability and safety must be guaranteed at (almost) any cost.

With this in mind, it is easy to see why industry should react to recent advances in the digital arena which have brought down the capital cost of condition monitoring systems. But what is condition monitoring?

Condition monitoring is the name given to the discipline of monitoring machine related variables, and inferring the condition of the machine from those variables. It is desirable to know far more than whether or not a machine is simply working or broken. A failure on a machine which results in it requiring immediate shut down is usually preceded by one or more much smaller, less severe, and less expensive to repair failures. Such as in the example of insulation failure where the failure is preceded by an increase in partial discharge.

Condition monitoring greatly aids forward planning in production environments. If it is known that a machine needs to be taken down in the next 6 weeks, then a time can be chosen which will minimise disruption and production losses. If it is expected that spares will be needed, these can also be ordered ahead of time.

Because of the varied types, designs and ages of machine as well as the many different applications, it is very difficult to prescribe and quantify a single measurable characteristic which will give a yes or no answer in terms of machine condition. As already mentioned, one usually wants far more than a “yes” or “no” anyway. Effective condition monitoring depends on the trending of measured variables.

The cost of measuring equipment for some variables of interest has, in the past, resulted in a single instrument being purchased which is then used on each machine in rotation, and samples are separated by days or weeks. The steadily decreasing cost of online measurement instruments and the associated network connectivity is now making full-time online measurements of machines feasible. See *Table 2.1* for the tradeoffs between discrete monitoring where a single instrument is used discretely on several machines, and continuous monitoring where instrumentation is installed on each machine.

When deciding what to, and what not to monitor, it is important to take into

Table 2.1: Pros and cons of condition monitoring techniques

	Discrete monitoring	Continuous monitoring
Capital investment	Low	High
Sampling interval	Long	Short
Repeatability	Fair (risk of instrument damage between measurements as well as inconsistent probe placement)	Good (probes and instrument are fixed)
Freedom of probe placement	Poor (probe placement must be accessible while the machine is running)	Good (probes can be placed during maintenance)
Ease of trending	Fair (samples have to be captured manually)	Good (samples are captured automatically and can be graphed in real time)
Application of online technologies	Limited	Unlimited
Application of expert knowledge	Naturally facilitated (expert consultants can meet with machine operators when measurements are made)	Restricted (in-house expertise may be insufficient to diagnose some problems)

account not just the repair or replacement cost of the individual machine, but also the predicted loss of earnings due to production stoppage. It can be worthwhile to monitor a relatively inexpensive machine because of the impact that that machine's failure will have on the plant as a whole.

There is plethora of machine parameters which can be recorded, and while they are generally all useful for some purpose, some may offer more insight into the machine's condition and possible failure than others. An overview of established monitoring techniques is given in *Section 2.4*. This research is concerned with the monitoring of shaft currents and voltages, the merits of which are discussed in *Section 2.5*.

2.4 Established techniques

There are numerous machine characteristics which can be monitored. They can be roughly divided into the four categories given below [3]². Each of these characteristics can be translated into a technique by which the condition of a machine is monitored.

- Electrical

²This material is largely a summary of Tavner and Penman [3] Chapters 4, 5, 6 and 7, please refer to it if you require greater background or depth.

- Chemical
- Vibrational
- Temperature

2.4.1 Electrical techniques

Protection relays which monitor for overload, phase faults, ground faults and the like have been around for some time. Unfortunately they generally only react when a fault has already occurred and therefore do not serve to identify incipient faults. They should therefore be regarded as a last line of defence and as a backup to other more advanced techniques.

Within the machine there is a magnetic flux and electric field which varies, circumferentially in the airgap, periodically in space and, for an a.c. machine, periodically with time. Under ideal conditions these magnetic flux and electric field waveforms will be symmetrical but electrical defects in the machine will distort them. Rotor defects could be detected by electrical sensors fixed to the rotor. Defects on either rotor or stator disrupt the radial and circumferential patterns of flux in the machine causing changes which can be detected outside the machine [12]. These internal magnetic and electric field distortions will also alter the machine terminal quantities, the voltage and current, which can be measured to give an indication of machine condition.

Partial discharge is an early indicator of many electrical faults in machine stators. A number of techniques have been, and continue to be developed to measure this phenomenon. These techniques generally operate in the HF realm and involve measurements and connections to just about all aspects of the machine, including stator windings, rotor windings and external broadband antennas.

Brushgear faults can be picked up by recording a temperature rise of the brushes, or increased RF emissions from the brushes as a consequence of sparking.

Rotor mounted search coils may be useful, but problems with access and the reliability of instrument slip rings has resulted in limited to no application in industry.

Techniques for generator rotor fault detection are well documented [3]. Earth faults can be detected using earth leakage protection relays, potential difference measurements or winding resistance to earth measurements. Turn-to-turn faults can be

detected online with an air-gap search coil and by circulating current measurement. An off-line quality control technique utilising rapid rise-time surges injected into the winding between the slip-ring and the earthed body of the rotor has also been developed.

The principal shortcoming of an air-gap search coil is that it needs to be incorporated into the machine at manufacture. Online monitoring of shaft voltage may prove to be an effective alternative, as this research will investigate.

2.4.2 Chemical techniques

Both insulating materials and lubricating oils are complex organic materials which, when they are degraded by heat or electrical action, produce a very large number of chemical products in the gas, liquid and solid states. Lubrication oils also carry, not only the products of their own degradation, but also those from the wear of the bearings and seals they cool and lubricate. Any technique to detect degradation needs to measure the concentration of one or more of these complex products in the most appropriate state, at the most convenient location in the machine.

Heat will break down insulation in a process which usually starts with the volatile solvents used in manufacture and continues by breaking down the resin. If temperatures continue to rise the binder material (e.g. wood, paper, mica or glass fibre) will also break down until the insulation is charred and no longer has significant mechanical strength.

Pyrolysing activity gives rise to a wide range of gases, liquid droplets and even some solid particulates which together make up the smoke being driven off the insulation.

Electrical discharge activity, within or adjacent to the insulation system, also releases chemical degradation products as a result of the very high temperatures associated with sparking.

Various methods exist for detecting the byproducts of insulation break down, be they particulate or molecular in nature. Some methods, such as coolant/lubricant flow or purity monitors operate full-time. Other methods, such as dissolved gas analysis usually require a sample of coolant/lubricant to be drawn and analysed off-line. Newer methods of continuous online monitoring of dissolved gas have also been developed.

In addition to monitoring the various lubricants and coolants for insulation breakdown byproducts, they can also be monitored for debris from wear and tear. Such methods usually exploit the ferromagnetic and/or electrical properties of metallic debris.

2.4.3 Vibrational techniques

Vibration is a long known, and much studied feature of electrical machines. An electrical machine is a complex mechanical system, made up of internal components (such as bearings), its associated support structure and the load to which it is coupled. It is free to vibrate at its own natural frequency, or can be forced to vibrate at many different frequencies.

The principal causes of vibration in electrical machines are [3]:

1. The stator core response to the attractive force developed between rotor and stator.
2. The response of the stator end windings to the electromagnetic forces on the conductors.
3. The dynamic behaviour of the rotor.
4. The response of the shaft bearings to vibration transmitted from the rotor.

These four areas are inter-related. For example, bearing misalignment or wear can quite easily result in eccentric running which will in turn stimulate the vibrational modes of the stator.

Each of these four areas exert their own influence on the total machine vibration, and characterising each area is a work in itself. That said, vibration monitoring is technically straight-forward to implement and can give a good indication of the overall health of the machine. However, expert analysis is usually required to diagnose specific faults from machine vibration.

2.4.4 Temperature techniques

The temperatures within a machine are perhaps the best indicators of impending failure, but obtaining high spacial resolution is difficult and/or expensive.

There are three basic approaches to temperature monitoring [3]:

1. Measurement of local temperatures at points in the machine using embedded temperature detectors.
2. Obtaining a thermal image, fed with suitable variables, to monitor the temperature of what is perceived to be the hottest spot in the machine.
3. Measurement of the distributed temperatures in the machine, or the bulk temperatures of coolant fluids.

These approaches demonstrate the fundamental difficulty of thermal monitoring, which is resolving the conflict between the fact that point temperature measurements are easy to make, but give only local information, whereas bulk temperature measurements are more difficult and run the risk that local hot-spots can be overlooked.

Local temperature measurement is usually accomplished with thermocouples or resistance temperature detectors (RTD). They are usually embedded at manufacture in areas of interest, such as in the stator windings, stator core or even the bearings. Measurement of local rotor temperatures is more difficult, but can be done using a self-contained circuit which is powered by the changing flux in the machine and transmits data via a contact-less infrared link or similar.

Hot-spot measurement and thermal images are concerned with knowing the temperature at the hottest point. Unfortunately this point may not be conveniently located at a local thermocouple or RTD. Performing this type of measurement is technically difficult, but it can be done. One solution for a rotating machine involves programming a microprocessor with a thermal model of that machine and then feeding it information from key points in the machine.

Bulk measurement of coolant temperatures is simple and is frequently implemented. A sudden rise can give an indication of the machine being overloaded or of a coolant system failure, though obtaining information about localised hot-spots is near to impossible.

2.5 Proposed technique – shaft signals

“Shaft signals” is used to refer to both shaft voltages and shaft currents. Though the two are inextricably linked by Ohm’s Law, it is useful to treat them separately. Where the shaft is correctly insulated, shaft currents are kept to a minimum and shaft voltages can be measured. It is also possible to monitor the shaft current itself using Rogowski coils [13].

2.5.1 History – Cause, effect and minimisation

An alternating flux which encircles the shaft can occur if there is a magnetic imbalance in the machine. Two common causes are stator segmentation and residual magnetism [5]. This flux will produce a potential difference across the shaft. When spinning, the shaft is typically insulated at both ends by a thin film of oil in the bearings, thus there are two oil-films in series in the circuit. If the potential difference (shaft voltage) exceeds twice the breakdown voltage of the oil-film [6] (because of the two films), breakdown occurs and a shaft current flows. In the case where a grounding brush is used at one end of the shaft, the potential difference only needs to exceed the break-down voltage of a single oil-film in order for a current to flow to ground. Repeated breakdown usually results in damage to the bearings which can eventually lead to the failure of the machine [7] (as discussed in *Section 2.2.8*).

Due to the destructive nature of shaft-currents, much work has gone into construction and/or grounding methodologies which will limit or manage the shaft currents [3-8].

The causes of shaft voltages and currents can be summarised as follows:

1. Magnetic Asymmetries, e.g. due to
 - joints in the stator laminations
 - rotor eccentricity
 - rotor or stator sagging producing variable magnetic flux
2. Axial Shaft Flux, e.g. due to
 - residual magnetisation
 - rotor eccentricity
 - saturation

- asymmetrical rotor winding
3. Electrostatic charge, e.g. due to
 - steam brushing turbine blade
 4. External voltages on rotor windings, e.g. due to
 - static excitation equipment
 - voltage source and/or rotor winding insulation asymmetries
 - active rotor winding protection

On large machines it is common for one end of the shaft to be grounded and the other to be insulated. Nippes [14] stated that shaft grounding current peaks range from 10 mA to 20 A on healthy rotating machines rated above 75 kW up to the largest, 1200 MW. Voltage on the electrical machine shaft end opposite from the grounding brush location (the insulated end) can be very high, reaching hundreds of volts.

2.5.2 Application to condition monitoring

While shaft currents are a known characteristic of machines, and effort is made to minimise them, shaft voltage analysis and consequent fault diagnosis has received little in-depth attention. This is owed to the difficulties encountered in obtaining accurate measurements and due to the difficulty in generalising results from one machine to another. The other possibility is that the research has been found to be extremely useful by the utility companies and any further research was kept out of the public domain by commercial interest.

There is some work which has focused on the diagnostic aspects of shaft voltage measurement and how different fault conditions might influence those measurements. Ong et al. [13] looked at different techniques for the measurement of shaft currents. Their research utilised one or more Rogowski coils to perform the measurement on motors. Hsu and Stein [15, 16] looked firstly at the effect of eccentricities on shaft signals and then on the use of shaft signals for eccentricity and/or shorted field coil detection. Their work does not directly relate to this research as they focused on motors rather than on generators. Their results are promising none-the-less, though evidence of further work could not be found.

Torlay et al. [17, 18] presented papers on the analysis of shaft voltages in large synchronous generators. They started with a small 30 kVA synchronous machine and concerned themselves with both the measurement of the shaft voltages and the neutral voltage. This machine was dynamically modelled with the finite element package FLUX 2D™. The following faults were then both simulated and demonstrated and their results compared:

1. No failure;
2. Inter-turn short-circuit of one ninth of the excitation winding;
3. Inter-turn short-circuit of one pole of the excitation winding;
4. Eccentricity of 3 mm in a 4 mm air-gap (static eccentricity)

In all of the above situations, the generator was unloaded.

Any differences observed between the simulation and the demonstration were explained and it was found that the analysis of shaft voltage and neutral voltage were enough to differentiate a single fault. Following the success of the experiment with the small 30 kVA machine, a 1300 MW generator was also modelled. It was found that the results cannot be directly carried from one generator to another, as the results depend on the geometry and the electrical connection of the machine. However, the simulations did show that the most common failures such as inter-turn short-circuit in the rotor field winding or static or dynamic eccentricities could be diagnosed. These simulations were verified against physical measurements on 1300 MW generators.

The study by Torlay et al. concluded that a failure on a synchronous generator can be identified by analysing shaft voltages and neutral voltages. It was also found that shaft voltages and neutral voltages are not the only electrical variables modified by failures. It was recommended that the influence of harmonics in the network on shaft voltages should be analysed. However, no evidence of further work could be found.

More recently (June, 2004) Nippes [14] published a paper entitled “Early warning of developing problems in rotating machinery as provided by monitoring shaft voltages and grounding currents”. He noted that in mechanical trains, the source of shaft currents is typically either electrostatic charge build-up or voltage generation from residual magnetism. While on trains having rotating electrical machines, there are

many additional voltage sources for shaft currents. Most sources cause unbalance or asymmetry in the magnetic field such as: shorted turns in the rotor and/or stator winding, shorted rotor/stator core laminations, shorted bearing seal and coupling insulation, uneven air gap, and/or harmonics and transients from power electronics, power supplies or loads as well as low level stator winding faults close to the neutral star connection.

Nippes [14] has stated that condition monitoring using shaft grounding currents and voltages of rotating shafts is effective. The following list of factors influencing shaft grounding currents and voltages is taken from his paper (proven field cases are marked with an asterisk [14]) :

1. Shaft or rotor rubs onto casing or stationary members:
 - (a) Shaft voltage decreases at rub occurrence. *
 - (b) Shaft grounding current increases and increasingly compounds, heavily magnetising the rotating and stationary members. *
 - (c) If no detectable shaft voltage exists initially, very likely one would be generated by the rub, depending upon the type of materials that come into contact.
2. Static charge build-up on the rotating member due to:
 - (a) High liquid or gas velocity.
 - (b) Liquid or gas flow through filters.
 - (c) Turbine saturated steam. *
 - (d) Turbine dry steam under certain conditions. *
 - (e) Fogging or wet compression in gas turbines. *
3. Voltage generation from residual magnetism from:
 - (a) Magnetic particle inspection. *
 - (b) Welding with improper ground return. *
 - (c) Improper demagnetising. *
 - (d) Magnetic bases. *
 - (e) Lightning strike nearby. *
 - (f) Plant electrical faults or ground currents.
 - (g) Compounding of residual magnetism. *

4. Electromagnetic asymmetries in electrical machines:

- (a) Loss of bearing or seal insulation. *
- (b) Loss of coupling insulation. *
- (c) Core lamination shorting. *
- (d) Unequal gap between the stator and rotor. *
- (e) Rotor winding turn shorting. *
- (f) Stator winding loss of a parallel circuit. *
- (g) Stator winding transposition or turn shorting.
- (h) Stator winding faults near wye connection.
- (i) Induction motor broken rotor bars.

5. Voltage harmonics and/or transients induced into electrical machines:

- (a) Variable frequency drives. *
- (b) Pulse-width modulated supplies. *
- (c) Excitation system harmonics. *
- (d) Unbalanced phase loads on generators.
- (e) Rectifier or SCR loads or power supplies.

Nippes has obtained a US patent for his voltage and current monitoring system (VCM) [19].

Despite the evidence supporting the effectiveness of shaft voltage and current monitoring, it is still not a widely used technique. An objective of this research is to gain local expertise and experience with this phenomenon.

2.6 Testing platform

2.6.1 Introduction and goals

While the results found in the literature will be taken into account, they are not detailed enough for the purpose of developing a shaft signal based fault diagnosis system. Such a system is the end objective of Eskom, though a complete or near-complete system is not the objective of this research project. The purpose of this research project is to lay the groundwork for the development of such a system. This

project will include the operation and measurement aspects of a miniature turbo-generator (mini-gen). The primary focus of this research project is to show that one or more synchronous generator faults can or can not be reliably diagnosed from shaft voltages.

Given the existing literature, it is expected that a strong correspondence will be found between shaft voltage waveforms and the type and magnitude of faults present on the generator. From the literature it is clear that the exact form of these waveforms is likely to vary from machine to machine, however it is hoped that certain trends will become apparent. In order to recognise the fault(s) present on the generator various signal processing techniques will have to be employed, such as frequency spectrum analysis.

To summarise, the goals of this research are the following:

1. Implement a measurement system for the test generator.
2. Investigate possible FEM based simulation of the test generator, in order that fault characteristics might be predicted using a simulation of a generator. This is an investigation and the actual use of FEM techniques is not a requirement.
3. Identify a methodology (or lack there-of) that enables the identification of the fault from the shaft-voltage waveform.

The testing platform is broken down into 3 components :

1. Simulation
2. Physical measurements
3. Signal processing

2.6.2 Simulation

It has been previously stated that the exact form of a shaft voltage waveform is likely to differ from machine to machine. It would be desirable if one could predict how a fault would manifest itself in the shaft voltage signal for a particular machine.

To this end, finite element method (FEM) simulations using Ansoft's MAXWELL 2DTM transient solver will be used. The method and results of these simulations will be presented in *Chapter 6*.

It is necessary to use a simulation package capable of performing transient or time stepped simulation in order to know the generated electromotive forces (e.m.f.'s). The 2D transient capability of MAXWELL 2DTM has not, in the past, been fully exploited by the School of Electrical and Information Engineering, and one of the outcomes of this research is to establish expertise in this area.

2.6.3 Physical measurements

This research is motivated by Eskom who would like to implement additional fault detection and diagnosis capabilities for their large turbo-generators. These generators are typically in the 600 MW range, with a 2-pole non-salient rotor operating at 3000 RPM. It is difficult and expensive to perform any kind of experimental testing on full-size units. A miniature turbo-generator, or mini-gen will therefore be designed and constructed.

This mini-gen is to be, as much as possible, a scaled down version of the full-size units. It will incorporate the same slot and winding configuration. The machine will be designed with access and modification in mind and will be specially wound so as to allow the introduction of faults into the rotor. It will also allow for the introduction of arbitrary rotor eccentricity. The requirements, design and final characteristics of the machine is given in *Chapter 5*.

2.6.4 Signal processing

Digital data acquisition cards are capable of recording a very large number of samples at high sample rates. It is the intention of this research to see what advantages can be found in processing an extended capture of many thousands of data points.

A DSPACETM data acquisition and control card will be used. The card is primarily designed for the full implementation of digital control systems, and its full capabilities will not be used here. It will, however, support a data capture of up to 500 000 samples. MATLAB will be used to process the samples, and to produce appropriate graphs.

2.7 Conclusion

Rotating machines, while based on fundamental principles of force, motion and magnetic fields, can be complex in both their construction and nature of failure. However, it is possible to both categorise and document the types of failure and techniques of condition monitoring. This chapter has presented a brief overview of the mechanisms of machine failure and condition monitoring. A background on the proposed technique of shaft signal monitoring and analysis has been given, and it is clear from the prior investigation of others that there is definite value in shaft signals as another source of information when building a comprehensive condition monitoring system for rotating machines in general, and synchronous generators in particular.

The principle goal of this research is to investigate the application of shaft signals to condition monitoring and to establish expertise in the field. This will be accomplished using both simulations and physical measurements. The simulations will be conducted using the MAXWELL 2DTM package from Ansoft and will help to establish expertise in the transient features of the package. Physical measurements will be conducted on a miniature 2-pole synchronous generator which will be designed and constructed for the express purpose of investigating condition monitoring techniques and other aspects of turbo-generator operation and parameters. These measurements will be obtained and processed using relatively modern data acquisition hardware in the form of a PC based DSPACETM data acquisition and control card.

Chapter 3

Measurement system

3.1 Introduction

This research is centred on the measurement of shaft voltage in both a simulated and an experimental environment. Knowledge of the absolute angular position of the shaft was also desired. A signal interface box was designed and constructed to interface a DSPACETM DS1104 data acquisition and processing board to the shaft of the machine under test and to an incremental encoder. This chapter is broken into sections which describe the dual-rail DC power supply, the incremental encoder interface and the shaft voltage interface. Use was also made of commercial differential voltage probes and a Rogowski coil.

3.2 Power supply

3.2.1 Requirements

A DC power supply is required to provide power to both the analogue signal conditioning and interface circuitry as well as to the incremental encoder.

Power supply type : Regulated, dual rail

Voltage output : ± 12 V

Current output : ± 500 mA

3.2.2 Design

A general purpose power supply utilising a transformer, full-wave bridge rectifier and 78 & 79 series voltage regulators was implemented. See *Figure 3.1*.

Considering just the positive rail of the supply: The 7812 requires a minimum drop-out of 3 V to achieve rated load regulation of $\Delta V_O = 12\text{mV}$. The transformer supplies 15 V rms at 500 mA, giving 21 V peak. C1 and C2 smooth the rectified wave and a simple $\delta V = IT/C$ calculation where $I = 0,5\text{ A}$, $C = 4400\ \mu\text{F}$ and $T = 0,01\text{ s}$ gives $\delta V = 1,1\text{ V}$. At a load of 0,5 A, the input to the rectifier should not drop below 19 V which is well within the requirements of the regulator. The same will apply to the negative rail.

U1 and U2 incorporate short-circuit and thermal protection, fuse F1 is used to protect against a transformer fault. R2 and R3 ensure that a minimum bias current always flows through U1 and U2 as their voltage regulation is poor at very low currents. D5 is used as a power-on indicator.

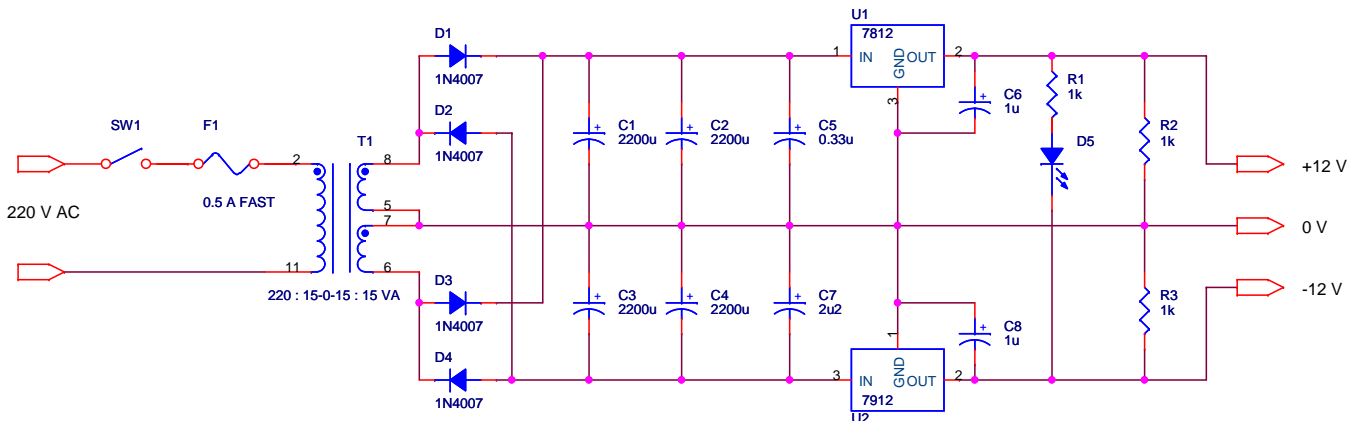


Figure 3.1: Power supply schematic

3.3 Angular position measurement

3.3.1 Requirements

It is difficult to obtain accurate angular position information from a rotating machine in the field. While a once-per-revolution ticker is often utilised to measure average angular velocity, it can not resolve slight perturbations in the velocity between whole revolutions. In addition, a simple ticker is particularly ineffective at

supplying information such as velocity and acceleration when the rotor is spinning at slow speed (e.g. at start-up).

It is thought that an accurate knowledge of the angular position of the rotor may be useful in resolving fault type and position in the machine. Given that an experimental unit is the subject of these measurements, there is freedom to implement an angular position measurement system.

Two models of incremental shaft encoders were used :

Leine & Linde RHI503	Stegmann DG 60 L WSR
Part No: 392911-04	Part No: DGS60-G4A01024
Ser No: 12900388	Ser No: 5W1WC2F00600 - 000266
Supply: 9 – 30 V d.c.	Supply: 9 – 30 V d.c.
Output: 500 ppr HTL	Output: 1024 ppr HTL

In terms of interfacing, these encoders are identical. They require a 9 to 30 V d.c. supply and provide three digital outputs commonly referred to as A (S00 or PHI0), B (S90 or PHI90) and Z (Sref or IDX).

The DSPACE™ DS1104 will accept inputs from two incremental encoders. Its interface however, has different specifications :

DSPACE™ DS1104 encoder interface
 Supply available : 5 V d.c.
 Input: RS422 (differential 0 – 5 V) or
 TTL (single ended 0 – 5 V)

3.3.2 Encoder interface and isolation design

See *Figure 3.2* for the encoder interface schematic. The advantage of this design is that the encoder and its supply are completely isolated from the encoder input on the computer. The encoder is supplied with 24 V obtained by using the +12 V and –12 V rails of the power supply in series. Although 12 V would be sufficient to power the encoder (it requires between 9 and 30 V), the higher voltage resulted in less current drawn by the encoder. In addition, the positive and negative rails are

equally loaded which keeps them symmetrical about the 0 V rail. The single-ended digital outputs from the encoder drive LED's in packaged isolation ICs U2 and U3. R5 – R7 were chosen so that the LED's would be driven at the recommended 10 mA.

The PC side of the interface circuit is powered by the 5 V obtained from the encoder input on the dSPACE™ board, and is only live when the computer is switched on. C1 is a recommended de-coupling capacitor. Pull-up resistors R1 – R4 were chosen to provide a low-impedance for noise-resistant switching and are in the range recommended by the data-sheet. U1 is used to buffer the logic signal and to supply an RS-422 differential signal.

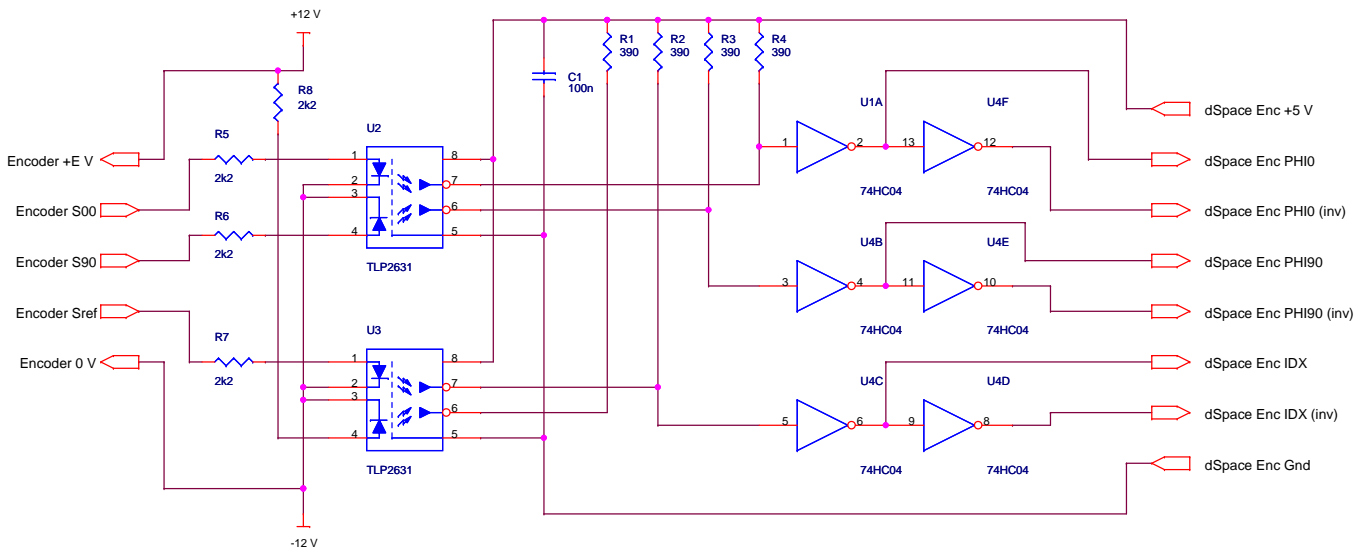


Figure 3.2: Encoder interface schematic

3.4 Shaft voltage measurement

3.4.1 Requirements

The shaft of the test generator is mounted on insulated bearings and grounded at one end; the opposite end of the shaft is left floating. The shaft voltage is measured between the grounded and the floating (or non-grounded) end. An interface circuit was placed between the ADC input of the dSPACE™ DS1104 and the brush riding on the non-grounded end of the shaft.

The shaft voltage interface circuit has three design criteria:

1. High input impedance

2. Low noise and anti-alias filtering
3. Protect the ADC circuitry from an accidental short to live

3.4.2 Design

The input to the circuit is passed through the low current, fast-blow fuse F1. D1 and D2 are connected in a voltage clamping arrangement and should the shaft voltage exceed approximately 10 V above or below ground, D1 and D2 will clamp the signal to ground. If the voltage exceeds 10 V as a result of a serious fault, the high current will blow out the fuse and the remainder of the circuit and PC-side circuitry will be protected.

U2 is an NTE859 quad opamp which was chosen for availability, low-noise and high input impedance, it also exceeds frequency and supply voltage requirements. Note that U2A – U2D and their pins are numbered according to their connection in the physical circuit. U2B is configured as a high-impedance, non-inverting amplifier. R1 sets the input impedance of the circuit to approximately 10 M Ω . U1A, U1C and U1D form a 6 order low-pass Bessel filter. A Bessel filter was chosen as it has a maximally flat group delay across the pass-band, and the preservation of the time domain was deemed important.

The DSPACE™ DS1104 is capable of sampling at 50 kHz therefore the design cut-off frequency was specified as 10 kHz, which is well below the Nyquist frequency of 25 kHz. A 6-pole filter exhibits a roll-off of approximately 120 dB per decade. At Nyquist of 25 kHz, the signal will have been attenuated by 48 dB. This equates to 8 most significant bits of the ADC which will not be affected by aliasing.

An active 3 opamp, 6-pole filter was designed according to the directions and constants described by Horowitz and Hill [20, pp. 275]. This was verified using a linear Spice simulation. Note that the Spice simulation did not take into account the characteristics of the NTE859 being used.

Figure 3.3 is a schematic of the signal conditioning and anti-alias filtering circuit.

3.4.3 Characterisation

Figure 3.4 shows the measured interface gain for a 2 V p-p sine wave. An average of 4.587 was used as a calibration for the recorded shaft voltage.

3.4. SHAFT VOLTAGE MEASUREMENT

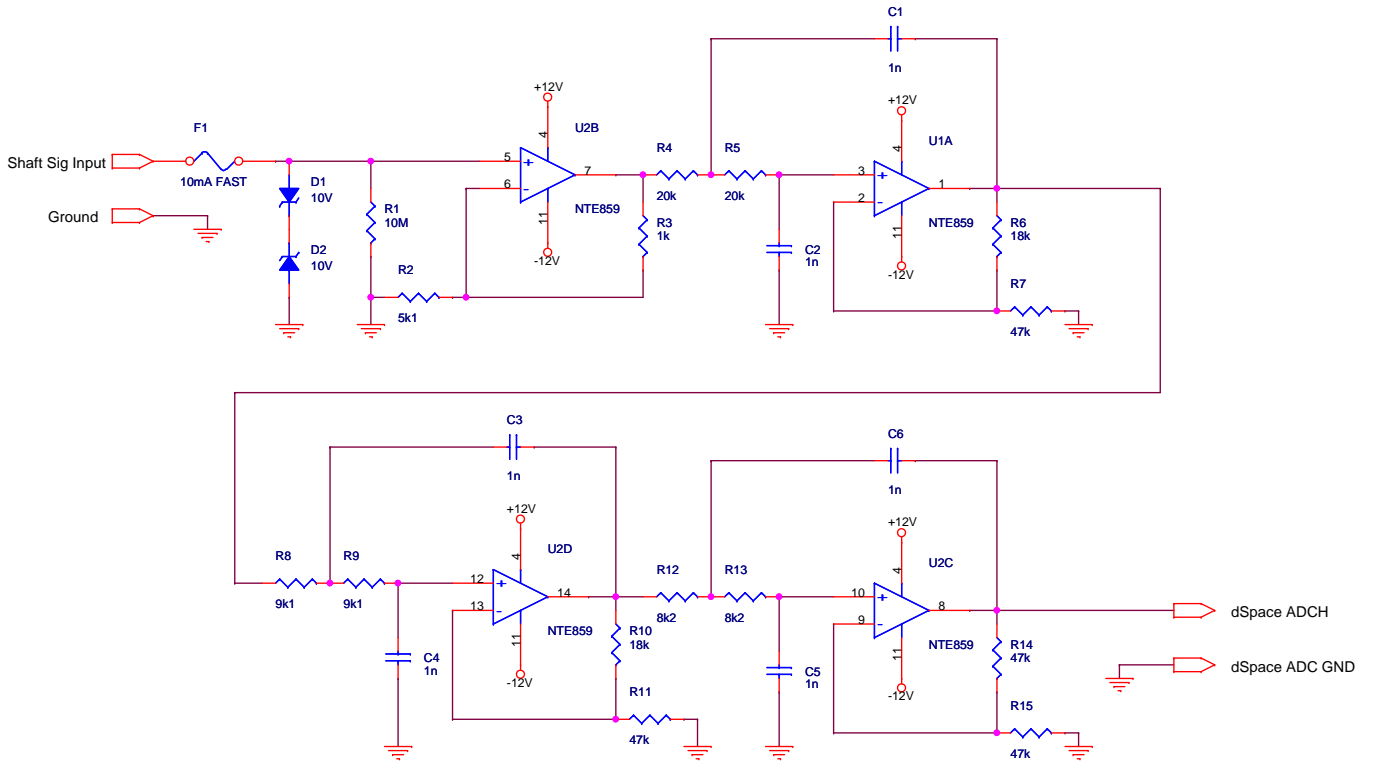


Figure 3.3: Shaft voltage interface schematic

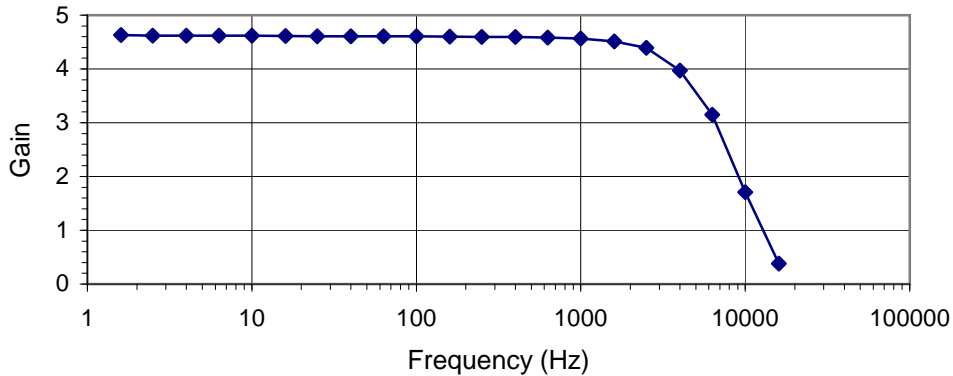


Figure 3.4: Measured interface gain

Note that this is a non-inverting design, and the signal does not get inverted.

The cut-off of the physical interfacing unit is less than 10 kHz. This was deemed to be acceptable since it was found through simulation and testing of the generator that frequencies above 3 kHz are of little interest for shaft eccentricity detection.

A 16-bit ADC channel on the dSPACE™ DS1104 was used. This channel can measure ± 10 V (a range of 20 V). During the course of the measurements the maximum shaft voltage recorded was approximately 3 V p-p. Thus approximately 13 bits of

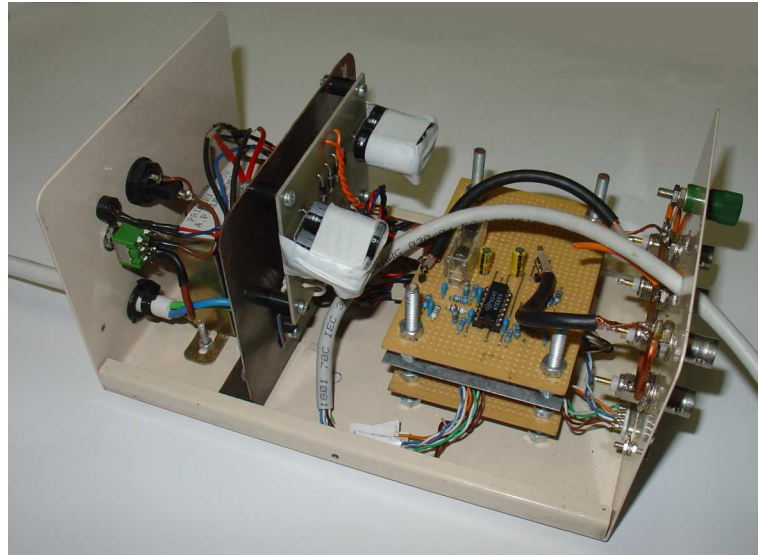


Figure 3.5: Photograph of signal interface box (with cover removed)

resolution were recorded.

Good results in terms of this research were achieved without running into noise problems and the noise floor has not been fully quantified.

3.5 Additional line current and voltage measurements

Additional voltage and current measurements were obtained using commercial 200:1 differential voltage probes and a Rogowski coil. These probes were connected directly to the dSPACE™ DS1104 board using coaxial cables.

3.6 Conclusion

Further details of the layout and connection of the probes to the physical test platform can be found in *Chapter 7* in addition to the presentation and discussion of the measurement results. The interfaces and circuits documented here were found to work well and good results were obtained without further emphasis being given to the noise floor.

The circuits were packaged together in a steel box and the same power supply was

used for both the digital interface circuit and the analogue gain and anti-alias filter. Appropriate smoothing capacitors were used to minimise interference between the two circuits. *Figure 3.5* shows a photograph of the completed signal interface box. Note the additional BNC connectors on the front of the box which were placed there to facilitate filtering of additional channels if necessary.

Chapter 4

Shaft position determination

4.1 Introduction

Shaft voltages (and consequent currents) are a known and generally undesirable feature of rotating machines. Shaft currents can severely damage the bearings over time resulting in machine failure. Shaft voltages and currents are generally higher on larger machines.

Shaft voltages and currents have four primary causes [4] which were expanded on in *Chapter 2*. As previously discussed, shaft voltages are influenced by several characteristics of the machine and they can be used for diagnostic purposes.

In order for shaft voltages and currents to be used for diagnostic purposes a reliable, relatively noise-free signal is required. The importance of the brushes used to ground the shaft (for damage protection) and for signal pick-up is emphasised in almost every paper on the subject of shaft voltage and currents. Because the voltages and currents are relatively small, ordinary carbon brushes do not work because an insulating film builds up between the brush and the shaft. Similar problems occur with solid brushes of other materials [7, 21]. Currently the most effective brushes are of a bristle-type made from gold alloy.

This chapter does not deal with the topic of machine fault diagnosis; rather it presents a technique which will give the position of the shaft from the shaft voltage and a pre-recorded reference signal.

4.2 Experimental setup

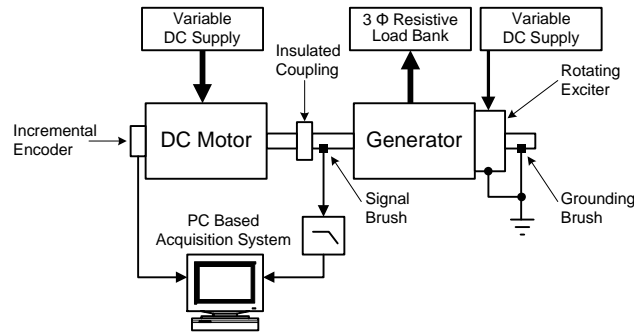


Figure 4.1: Diagram of experimental setup

A standard 400 V salient 4-pole generator with rotating excitor is used. The bearing on the driven side was replaced with an insulated version, insulating the shaft from the case at that end. Two brushes were mounted on the shaft, one at each end. The brush at the insulated end was used to pick up a shaft voltage (signal brush) and the brush at the non-insulated end was used to reliably ground the shaft to the case (grounding brush). The brushes used were manufactured by Sohre Turbomachinery and are of the “shaft riding fibre” type made from a silver/gold alloy.

In addition, a 1024 line rotary incremental encoder was coupled to the shaft. This encoder was used to provide an absolute angular position reference.

A PC based data acquisition system was used to capture the signal from the signal brush and the rotary encoder. The system took care of producing an absolute position from the incremental encoder.

4.3 Measurement system

The measurement system is the same as that discussed in *Chapter 3*. The heart of the system is an acquisition card set up to sample a single ADC input and a single rotary encoder input at 25 kHz. An interface circuit is employed between the acquisition card and the signal brush. This circuit provides a high-impedance input for the signal brush and performs anti-alias filtering, as well as fused protection against an accidental short to live potential.

Using the acquisition card an extended number of points can be captured (at present,

20 seconds of data at 25 kHz). The data is then processed using MATLAB.

The major advantage of the long capture time is the ability to average the data over an extended number of rotational cycles, greatly reducing the noise (compare *Figures 4.3* and *4.4*).

4.4 Algorithm

1. A 20 second capture of the shaft voltage and the absolute shaft position is made. *Figure 4.2* shows a snapshot of the shaft voltage capture with the machine under no load.
2. A plot of the shaft voltage for a single revolution of the machine under no load is produced. The x-axis has a domain of 360 degrees in 0,5 degree increments. Using the absolute position recorded alongside the voltage signal, the voltage signal is averaged over the 20 seconds to produce an almost noise-free signal for a single revolution. This plot becomes the reference plot. In *Figure 4.3* multiple readings at the same absolute position are super-imposed over each other. In *Figure 4.4* these same readings are averaged, producing a noise-free reference signal.
3. A 1 second capture of the shaft voltage and the absolute shaft position is made (the test signal). The absolute position is recorded only for future verification, it is not used in the processing of the second plot. An example time-domain snapshot from the same machines, now running at 90% excitation is show in *Figure 4.6*.
4. The fundamental frequency is found by low-pass filtering the test signal and then looking at the time between peaks. The signal is then averaged using the fundamental frequency. In *Figure 4.5* the no-load signal is averaged over 1 second using the estimated fundamental frequency, and in *Figure 4.7* the same averaging technique is applied to the 90% excitation signal.
5. The averaged test signal is then resampled to have a length of 720 points (the same as the reference signal).
6. Finally, the test signal is “slid” over the reference signal in order to find the point at which the best correlation is obtained. The best correlation is obtained

at the integer offset n when the following sum results in a minimum :

$$\sum_{k=1}^{720} (r(k) - t(k+n))^2 \quad (4.1)$$

(where $r(k)$ is the discrete reference signal and $t(k)$ is the discrete test signal)

4.5 Discussion

In *Figure 4.2* a time-domain snap-shot of a signal recorded with the machine under no-load is shown. The shaft voltage and the absolute position of the shaft were sampled simultaneously and can be seen on the graph. This is a 4-pole machine, with a mechanical rotation of 25 Hz or 1500 RPM. The primary source of the shaft voltage is related to the 50 Hz MMF wave, however, some component of the shaft voltage is related to the mechanical rotation of the machine. This component enables one to distinguish adjacent 50 Hz cycles. Hsu et al. have commented on the fact that the voltage signal is symmetrical about a mechanical rotation, but not an electrical rotation [15].

The advantage of averaging over multiple mechanical cycles can be seen by comparing the super-imposed plot in *Figure 4.3* with the averaged version of the same data in *Figure 4.4*. The purpose of the technique given earlier is to be able to determine shaft voltage position without a permanently connected encoder, hence an averaged plot of the same data, this time using an estimate of the fundamental frequency, is shown in *Figure 4.5*.

The machine was then run with a small resistive load and at 90% excitation current. A different plot of the shaft-voltage was recorded, as shown in *Figure 4.6*. Note that the signal is still affected by mechanical asymmetries and is cyclic over a mechanical revolution. This signal was averaged over one second using an estimated fundamental frequency and not the recorded shaft position.

Finally the averaged test signal was shifted until an optimum correlation was found with the recorded reference signal. These two signals are plotted on the same axes in *Figure 4.8*.

For verification purposes, the absolute shaft position recording was kept alongside the test signal while the test signal was averaged and shifted. It is plotted on the

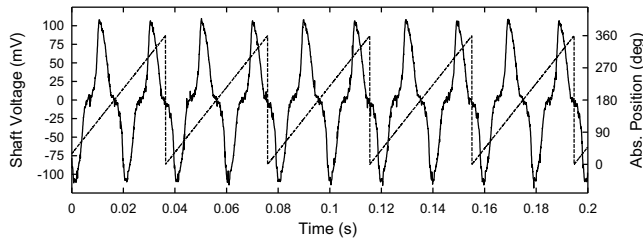


Figure 4.2: Time domain plot of the recorded shaft signal and the shaft absolute position

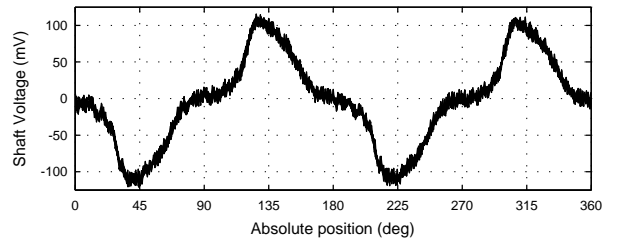


Figure 4.3: Super-imposed plot of shaft signal cycles, referenced against the shaft position

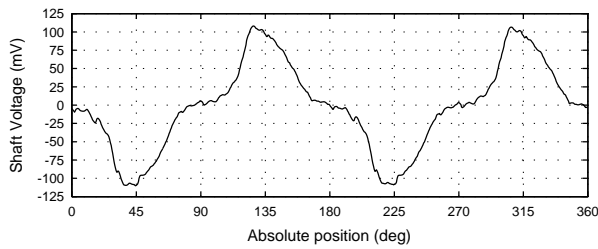


Figure 4.4: Averaged plot of shaft signal cycles over 20 s, referenced using shaft position recording

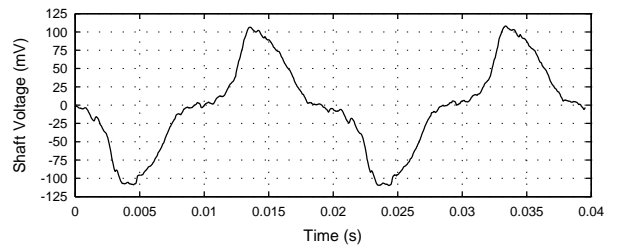


Figure 4.5: Averaged plot of shaft signal cycles over 1 s, referenced using an estimated fundamental frequency

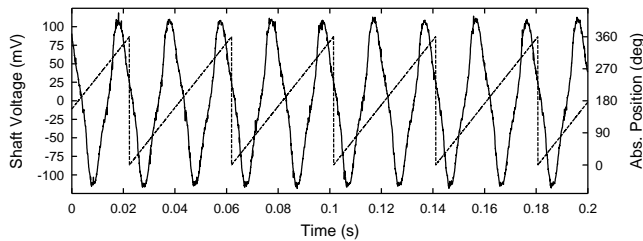


Figure 4.6: Time domain plot of a signal recorded at 90% excitation

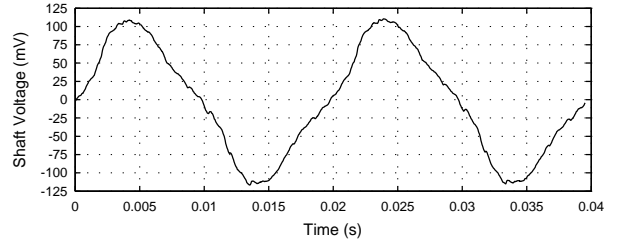


Figure 4.7: Averaged plot of 90% excitation shaft signal. Averaged over 1 s, referenced using an estimated fundamental frequency

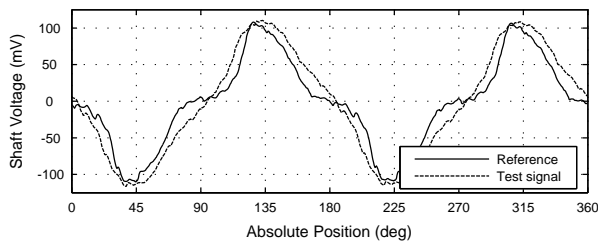


Figure 4.8: The reference plot and the 90% excitation plot after correlation with each other

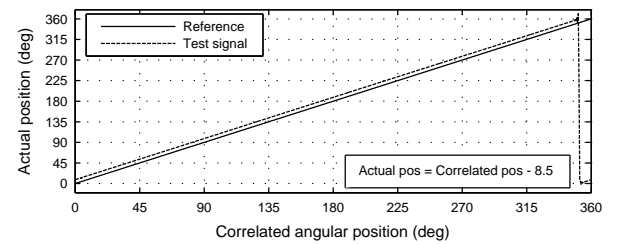


Figure 4.9: Estimated shaft position versus actual shaft position

same axes with the estimated shaft position in *Figure 4.9*. This plot shows that the estimated shaft position is within 8,5 degrees of the actual shaft position.

This process was repeated for different load conditions, 110% excitation and a reduced rotational speed (with 40 Hz output frequency). In the tested cases the estimated shaft position was within 10 degrees of the actual shaft position.

4.6 Conclusion

The shaft voltage waveform, aligned to the angular position of the shaft, is highly consistent and repetitive for the same loading and excitation conditions. A change in load does not greatly distort the waveform. A change of 10% of the excitation field for a constant load produces substantial distortion of the waveform, primarily through the increase or decrease of a 3rd harmonic.

It is possible to determine the shaft position from a shaft voltage measurement given that a reference signal is available. Even in the extreme case of a decreased excitation field, the position of the shaft could be determined to within 10 degrees.

Chapter 5

Mini-gen design

5.1 Introduction

Large turbo generators are typically 2-pole 3000 RPM units with a large air-gap. This is quite unlike commercially available generators for small commercial or industrial use which typically have 4 or more poles and have a comparatively much smaller air-gap. A machine similar to the large units, but which is small enough to be tested and run in the university's laboratory facilities was designed and manufactured.

This chapter presents the requirements of this miniature turbo-generator, its design and a selection of relevant technical drawings and finally its measured operating characteristics.

5.2 Generator requirements

For this and future projects there are 4 fault types of interest:

1. Displaced air-gap (static eccentricity).
2. Excitation current containing harmonics.
3. Shorted turns at different points in the rotor winding.
4. Earth faults on the rotor winding.

In order to implement these, and possibly future faults on the machine the following requirements were decided on. These are grouped into 3 categories:

1. Experimental and modification capability.
2. Similarity to a full-sized turbo-generator.
3. Economic use of off-the-shelf components (e.g. stator sections)

5.2.1 Experimental capability

The miniature generator's purpose is to enable measurements to be made of different conditions imposed on it. The following points list the broad mechanical and electrical requirements in order for the machine to be useful to this and future projects.

- Easy access for measurements, assembly and disassembly. This enables the introduction of faults into the windings, specifically the rotor winding.
- Adjustment of rotor to stator relative position in order to investigate air-gap eccentricity. This is accomplished by fixing the bearing pedestals to a bed-plate, thus the rotor is fixed relative to the bed-plate. The stator is mounted to supporting pillars on the bed-plate either through round holes which locate it correctly and precisely, or with a combination of oblong holes which enable its position relative to the rotor to be shifted in the 2 horizontal dimensions. Shims enable its position to be adjusted in the vertical dimension if desired.
- Insulated bearings for controlled grounding and the measurement of shaft voltages and currents.
- Outboard slip rings for static excitation. This will give control over the excitation current and enable inclusion of harmonics.
- Finished landings on the shaft for specialised gold brushes which will be used to ground the shaft and/or take voltage measurements.
- Option to replace the slip-rings with a rotating-rectifier type exciter in the future.
- The unit must be as enclosed as possible to reduce electrical noise.

5.2.2 Similarity to full-sized machine

In order for the results obtained from the mini-gen to be as applicable as possible to the turbo-generators used by Eskom, the machine needs to have similar characteristics:

- Non-salient, 2-pole, 3000 RPM design.
- Distributed concentric field windings on the rotor.
- Rotor to be machined from solid bar.
- Inclusion of damper-bars on the rotor.
- Open stator slots.

5.2.3 Economic decisions

- A conventional LV induction motor stator is used with open-slots. The stator is therefore a stock item which does not require special tooling for manufacture.
- Windings will not be VPI'ed (Vacuum Pressure Impregnated) to reduce cost and to enable future modification.

5.3 Generator design

5.3.1 General

The requirement to design a miniature version of a large 600 MW turbo-generator presents numerous difficulties. In engineering it is not possible to scale a design by merely reducing all dimensions by a fixed scaling factor. As one obvious example the power output is proportional to the volume of the active material while the heat dissipation is proportional to the surface area.

In this project the small unit also has to be manufactured by a conventional motor manufacturer. Obviously cost was an important consideration.

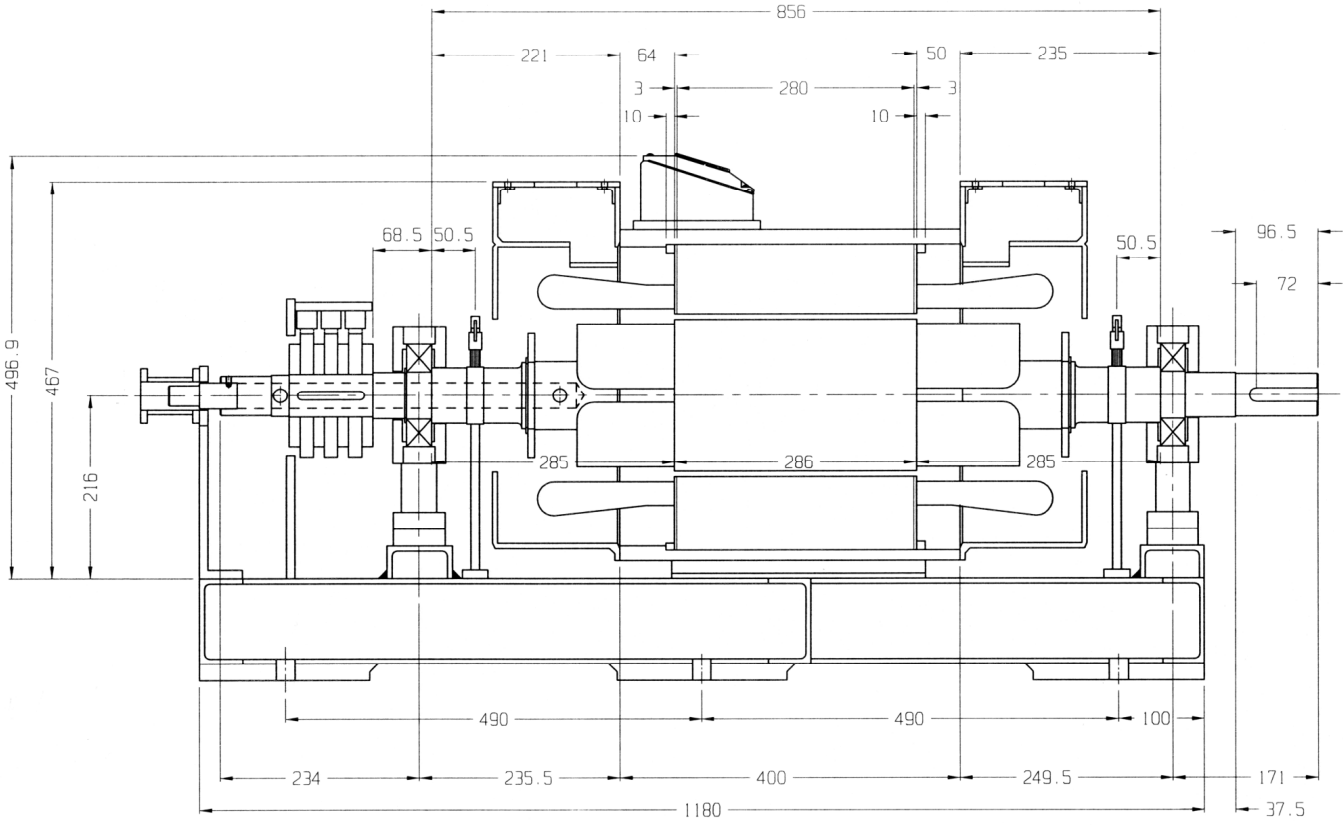


Figure 5.1: Assembly diagram of mini-gen

5.3.2 Constructional features

A conventional LV induction motor stator was used as the basis for the design except that open stator slots were used as on a full sized turbo-generator. It was also not considered wise to keep to the same ratio of rotor diameter to core length as this would present constructional difficulties. The small diameter would make a stator of great length difficult to wind.

The rotor would be machined from solid as on a full sized unit and the slots would be milled to form a non-salient pole synchronous machine. The stator and rotor slotting were the same as the full sized unit. The air-gap dimension on a full sized unit is very large but it was considered prudent to initially set the rotor diameter to give a smaller air-gap and to allow the rotor outside diameter to be machined at a later stage if it was considered of value to the research.

Unlike the full sized unit, the shaft critical speed is well above the operational speed as presently designed. If at a later stage, it is considered desirable to run through the first critical speed, the shaft can be machined to weaken it.

The bearings would be pedestal mounted on a bed-plate. The stator would be mounted with special features so that the air-gap could be distorted in different ways and the effect on the signals observed. The rotor would have outboard slip-rings for the excitation current but at a later stage thus could be replaced by an AC exciter with rotating rectifiers. Landing areas at both ends of the shaft would be provided for the voltage signal. Special gold-bristle brushes would be used to avoid any problems with the contact drops experienced with conventional carbon brushes.

5.3.3 Design

Due to the unusual requirements there were no accepted design procedures that could be followed. Since the stator was of conventional design, existing computer induction motor design software was initially used to obtain the stator winding

This stator design was then used with a proprietary synchronous design package called RMXPRTM. This was only able to design conventional salient pole rotors and this was accepted to provide an initial value for the excitation amp-turns. This design package enables a model of the machine to be prepared for finite element software (MAXWELL 2DTM) from the same software house. The FEM model was analysed.

The model was then modified manually so that the actual cross section of the non-salient pole machine could be analysed.

On the basis of this arrangement, the design values were passed on to the manufacturer.

5.4 Final specification

A full depiction of the machine can be seen in *Figure 5.1*.

5.4.1 Stator

The winding will be a simple mush wound and will basically be a 340 V winding. On the test bed the voltage can be increased to 380 V to allow the effects of saturation

to be examined. See *Figure 5.2* for a photograph of the stator laminations set in the case but without windings.

Core length	280 mm
No. of slots	48
Wire size	1,8 mm
Wires in parallel	6
Pitch	1 – 17
Conductors per slot	6
Parallel circuits	2
Connections	Star

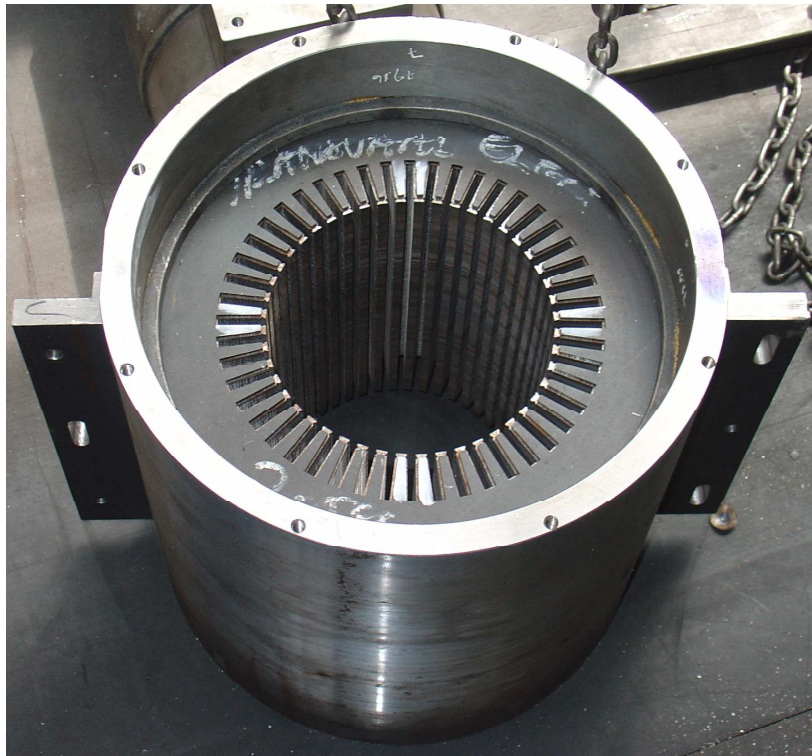


Figure 5.2: Photograph of the stator before winding

5.4.2 Rotor

The rotor is machined from solid bar. The initial size will give an air-gap of 6 mm but the design will allow the rotor to be machined down to enlarge the air-gap to 12 mm without damaging the coils.

No. of slots	32 (16 per side)
Slot size	36 mm × 5 mm
Coil size	30 mm × 5 mm
Coils	Concentric wound in situ
No. of turns	10
Wire size	4 mm × 1,8 mm
All turns in series	

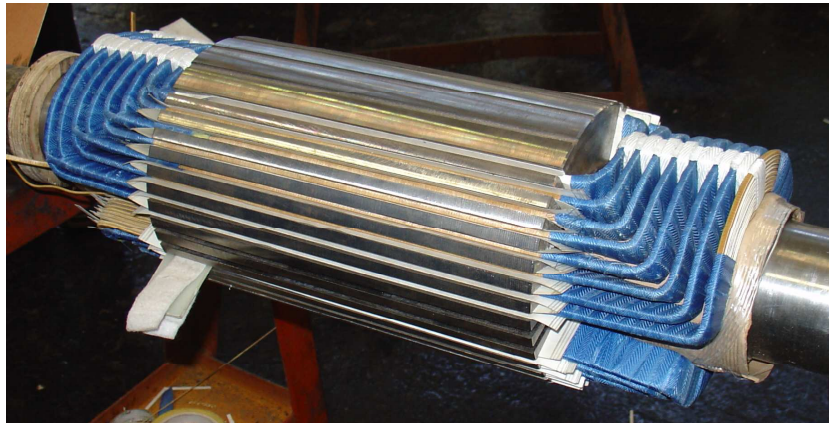


Figure 5.3: Photograph of the rotor in the process of winding

Figure 5.3 is a photograph of the rotor in the process of being wound. Once the windings were complete, damper bars were added to the slots and bound by a copper ring on each end. The whole rotor was then wrapped in resi-glass. Note the exposed wire insulation on the near side of the rotor winding, this is to facilitate the addition of a rotor inter-winding short, or ground fault.

5.5 Operating characteristics

5.5.1 Measured winding resistances

Table 5.1: Mini-gen winding resistances

Red – Blue	53,6 mΩ
Blue – Yellow	53,6 mΩ
Yellow – Red	53,0 mΩ
Rotor (excl. brushes)	457 mΩ
<i>Resistances measured at 23 °C</i>	

The three terminals on the mini-gen were coloured red, blue and yellow. See *Table 5.1*.

5.5.2 Open and short-circuit tests

Due to the unusual design and very large air-gap, the operating point of the machine is best determined from the empirical test results. The open circuit characteristic is shown in *Figure 5.4* and the short circuit in *Figure 5.5*.

The operating point of the machine is chosen to be 340 V and is generated with a field current of 62 A.

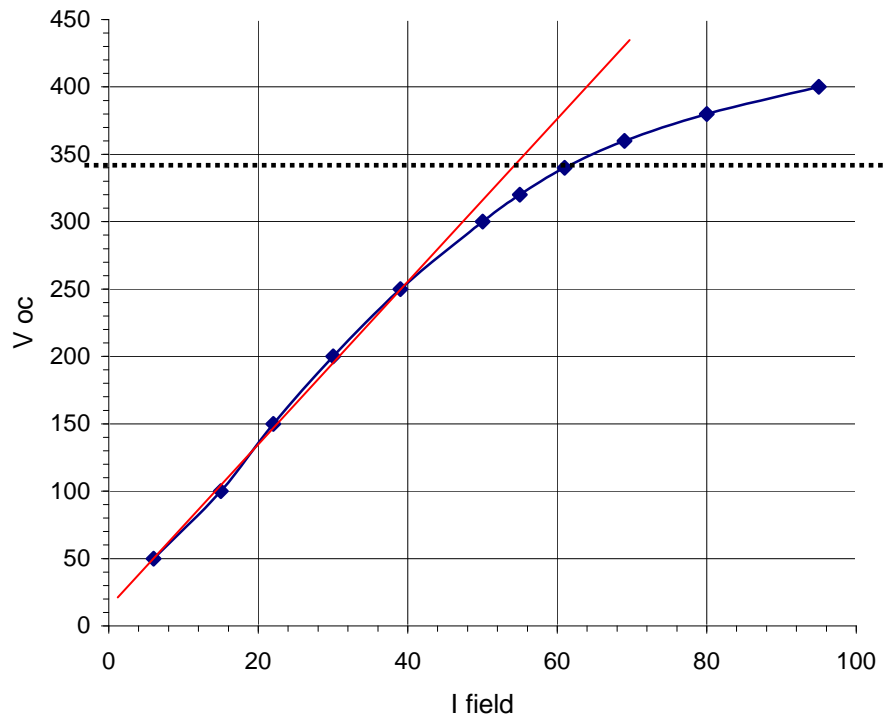


Figure 5.4: Open circuit characteristic of the mini-gen

5.5.3 Rotor temperature rise

Table 5.2 gives the approximate temperature rise of the rotor windings during 25 minutes of operation. The resistance of rotor winding was calculate using V/I . The

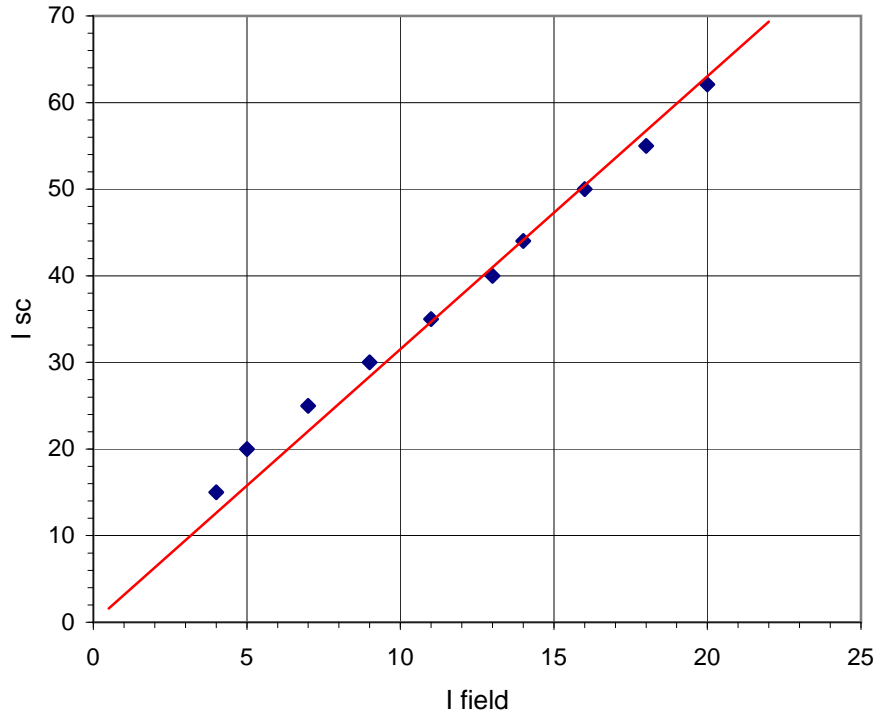


Figure 5.5: Short circuit characteristic of the mini-gen

Table 5.2: Temperature rise of the rotor during no-load operation

Time (minutes)	V field (V)	I field (A)	R winding (Ohms)	T rotor (deg C)
0	33	64	0.516	23.3
5	36	64	0.563	46.8
10	39	64	0.609	70.2
15	40	64	0.625	78.0
20	42	64	0.656	93.6
25	44	64	0.688	109.3

temperature of the winding was calculated using *Equation 5.1*.

$$\frac{R_{\text{HOT}}}{R_{\text{COLD}}} = \frac{234,5 + T_{\text{HOT}}}{234,5 + T_{\text{COLD}}} \quad (5.1)$$

Given the fast and linear temperature rise it is clear that this machine cannot be run for longer than 20 or 25 minutes. The primary source of heating is the rotor and this cannot be avoided. Fortunately, the measurements required for this research could be obtained during short runs of less than 10 minutes each. Should future research require more extended runs a larger, more powerful cooling system could be used. The use of dry-ice could also be considered.

5.6 Conclusion

The requirements for the experimental mini-gen were given, the mini-gen must be small enough to be tested and modified in the Universities machines laboratory, it must be as similar to a full size 600 MVA turbo-generator as possible and it must be cost-effective. These objectives were achieved through the use of a mixture of RMXprt™ and MAXWELL 2D™ to determine the dimensioning and approximate current capability of the machine.

Once completed, open and short-circuit tests were conducted on the mini-gen and their results are presented. From a current generation point of view, the generator's performance is satisfactory. With the present cooling arrangement the mini-gen exceeds its operating temperature within 20 minutes. This is unfortunate and can be attributed to the very high rotor current required to create the required flux in what is a disproportionately large air-gap. This is part of the trade-off between a machine which resembles a turbo-generator four orders of magnitude larger than itself and a machine which operates effectively at its own power level.

Chapter 6

Mini-gen simulation

6.1 Introduction

At the inception of this research project it was thought that simulating shaft voltage waveforms for real machines was not possible, and that much greater emphasis would be placed on the processing of measured waveforms from the test unit.

This has been found to be entirely not true. 2-D transient simulations of a rotating machine can indicate expected shaft voltage waveforms for different fault types. The scope of this research project was limited to static eccentricity, and this has been used to demonstrate the feasibility of simulations for fault diagnosis and condition monitoring.

This chapter is broken down into several sections :

- Modelling of the test generator using MAXWELL 2DTM from Ansoft.
- The strategy which was followed for performing the simulations, given that a single simulation took approximately 20 hours to complete.
- The results from the many simulations performed. This section addresses the areas of interest and the questions which were asked and answered in a simulated environment before performing the tests on the miniature turbo-generator.
- Computing observations and recommendations which briefly discusses those components of a computer thought to most influence simulations performed

with MAXWELL 2DTM and recommendations for the purchase of new computers.

6.2 Modelling

6.2.1 Simulation types

MAXWELL 2DTM is capable of solving a wide range of field-type problems including static electric fields, static magnetic fields, time-varying magnetic fields, time varying electric fields, DC conduction currents, AC conduction currents and thermal problems.

This project is solely concerned with magnetic modelling of a generator and there are two types of simulation which were utilised:

1. Magnetostatic
2. Transient magnetics

For either simulation type, the model to be simulated is drawn in two dimensions, either cartesian (XY plane) or axisymmetric (RZ plane). This is illustrated in *Figure 6.1*.

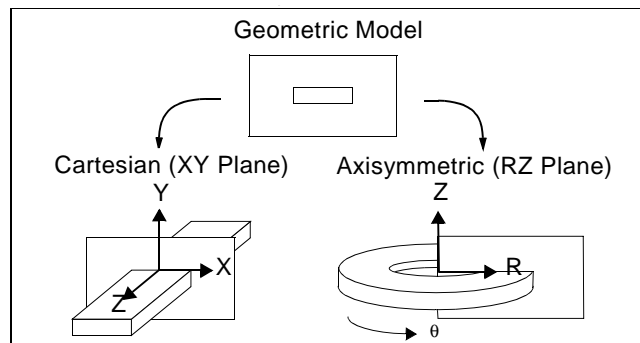


Figure 6.1: Possible drawing geometries for MAXWELL 2DTM models [1]

All models were drawn in the cartesian plane. The drawing represents a cross-section of the model, it is assumed that the model extends to plus and minus infinity in the Z direction (i.e. end-effects are ignored). Current flows exclusively in the Z direction, with no component in either X or Y. Flux flows exclusively in the X and

Y directions with no component in the Z direction. This means that one does not need to place insulation between conducting objects in the model (such as a steel rotor and the rotor winding) as current is assumed to not flow in the XY plane. However, laminated steel must be *modelled as having zero conductance*, because it is physically insulated against current in the Z direction!

For static solutions the depth of the model, for the purpose of quantities, is normalised to one metre. Quantities in the XY plane (such as flux) are per-metre. When performing a transient simulation the physical depth of the model has to be given – end-effects are still ignored and the given depth is used to scale various quantities in order to calculate e.m.f. in the defined windings. If the laminated steel (such as that used for the stator) is not given a zero conductance the transient solver will calculate large eddy currents in the laminations.

Magnetostatic modelling was used to verify the flux in the air-gap of the machine.

Transient magnetic modelling was used far more extensively to model the generator with a rotating rotor and to find generated voltages (most notably that on the shaft). When drawing the model, a transient model requires a “band” object. Objects outside the band are stationary while objects inside move according to the parameters laid down in the setup.

See *Figure 6.2* for the model used. Note the band object which is the circle between the rotor and stator.

6.2.2 Drawing the model

MAXWELL 2D™ provides a simple but functional geometric editor. While geometries can be imported from external formats produced by CAD packages it is recommended that the model be redrawn from scratch with the Maxwell editor. This is because Maxwell relies on “closed objects” and does not permit object overlap (an object can be totally enclosed inside another object, in which case the perimeter of the inner object forms the boundary between the two, as one would expect). When importing a model from an external file, two points which look like they are identical, may not be at a sub-millimetre level and Maxwell won’t regard the object as closed.

When using the editor, good use should be made of the “Boolean” functions which let you subtract, intersect and union one object with another. There are also pow-

erful tools to duplicate an object along an arc (to create stator slots for example) and other types of duplication. These features, combined with the boolean actions enable repetitive structures to be quickly and accurately created. A boolean action generally results in the creation of a new object. The old objects do still exist, they just lose their “visible” and “model object” status, it may be desirable to use the edit menu to select and then delete them permanently.

Arcs (such as a circle) are represented as multiple straight-line segments and the number of segments can be edited. Special care should be given to the number of segments used to represent an arc after boolean operations have been performed on an object, as the results can be unexpected!

By default, successive objects are labelled “objectXX” where “XX” is a sequential number. It is recommended that suitable names be given to all objects in the drawing as this will greatly simplify the later tasks of material, boundary and source assignments. Note that when an object is duplicated the editor is reasonably intelligent about how it names and numbers the resultant new objects and this feature should be exploited. Of course sensible colouring is also recommended.

6.2.3 Choosing materials

The material selection which was finally used for the majority of simulations was relatively basic. Although the actual B-H curve for the stator steel was used (see *Figure 6.4*), the general steels available in MAXWELL 2DTM did not make a noticeable difference to the shaft voltage. Note that when trying other steels as the laminations it was important to set their conductivity to zero.

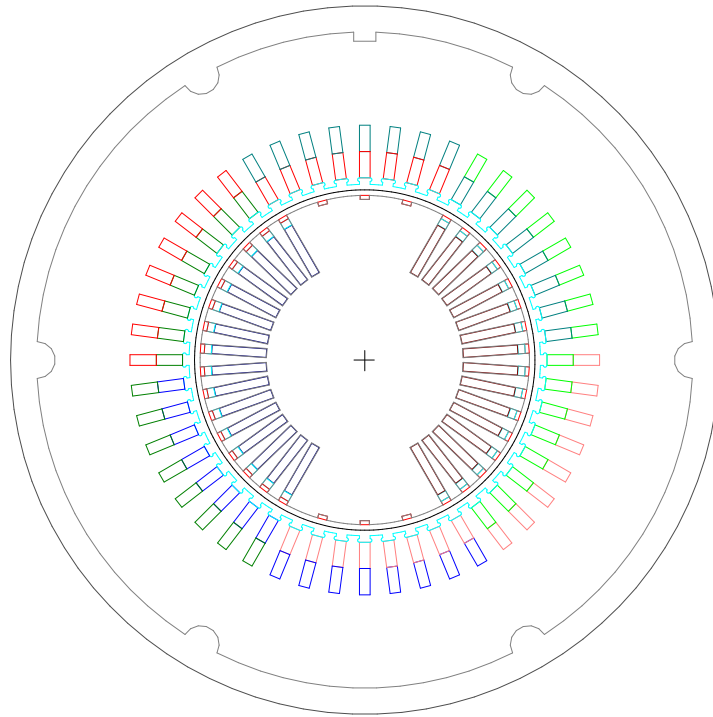


Figure 6.2: MAXWELL 2D™ model of the mini-generator

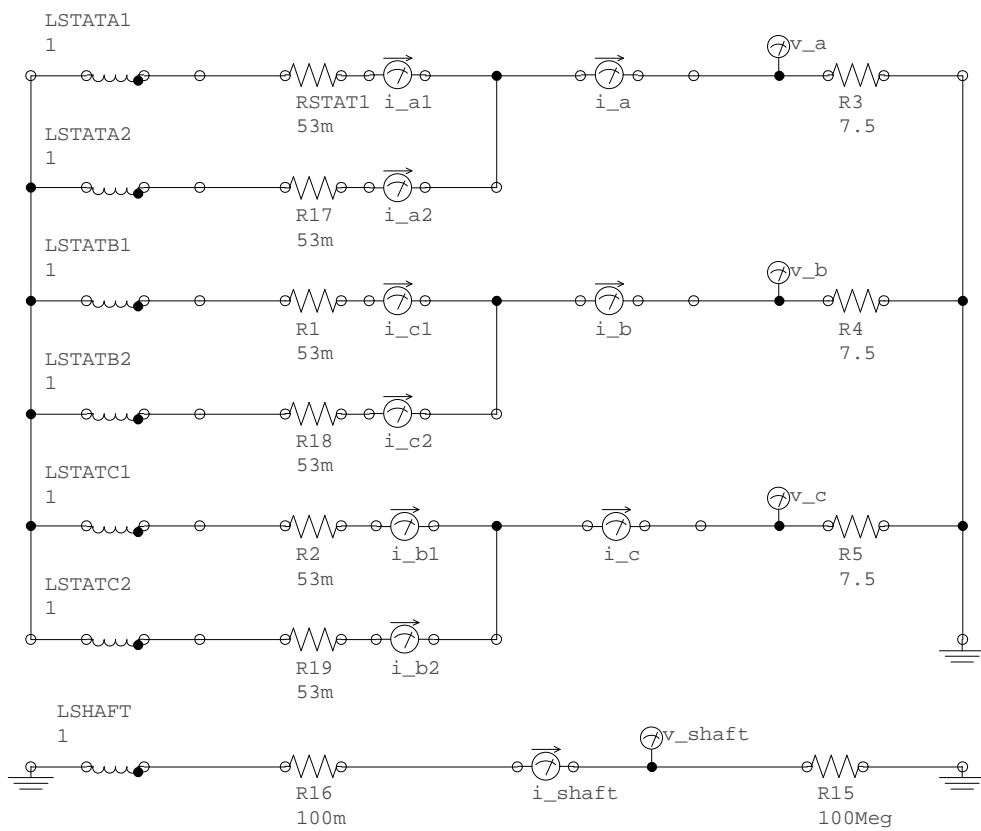


Figure 6.3: MAXWELL 2D™ model external circuit for stator and shaft

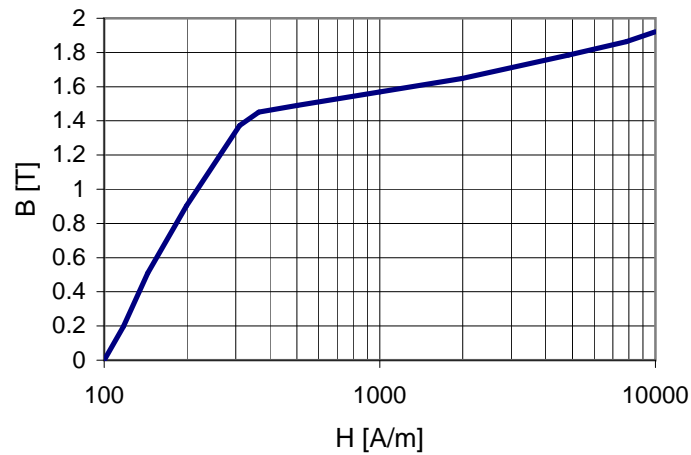


Figure 6.4: B-H curve for laminated steel M400

The materials used for the different components in the model are as follows:

Band	vacuum
Casing	steel_1008
RotCoils	copper
RotDamp (damper bars)	copper
RotPack (packing under damper bars)	vacuum
RotorCore	steel_1008
StatCoils	copper
StatInner (air-gap)	vacuum
StatOuter (the stator)	steelM400 (see <i>Figure 6.4</i>)
background	vacuum

6.2.4 Setting up boundaries and sources

Setting up the boundaries is different for the static and transient cases. This is also where adjustments to excitation and loading are made.

There are many types of boundaries and sources and these are well (though perhaps a bit obscurely) documented in the online help. Only the source types used in these simulations will be presented.

Static simulation

The static simulations assumed an open-circuit stator (i.e. no current in the stator coils). Only 3 sources were required :

- Balloon : A balloon source is special, it is typically the very outer boundary of the model and tells the solver that it should assume that this space extends to infinity with no additional sources.
- Positive rotor coils : A solid current source made up of all the rotor coil objects on the positive current side. A total current value is entered and this is the total current flowing in a single rotor coil object - not all of them selected together! This is different to what was expected.
- Negative rotor coils : The same as for the positive rotor coils except that a negative current value is entered.

Transient simulation

The transient simulation is capable of attaching an external circuit to the windings, this feature was used extensively to obtain shaft voltage and other voltage readings.

Sources were assigned to each stator coil group, the damper windings, the rotor windings and the shaft itself :

- Balloon : This is the same as for a static simulation, see above.
- Stator coil groups : Each group was designated as an externally connected stranded source. There is an option to choose between stranded and solid, the difference is that in the stranded case the current is evenly distributed within the object (as for an individually insulated stranded conductor) and in the solid case a non-uniform current distribution within the object will be assumed and calculated. The total number of turns is entered for the group and this was set as 24.
- Damper bars : These are designated as a “passive end-connected conductor”. The end resistance between conductors as set at $0,002 \Omega$ and the inductance between adjacent conductors as 0 H. It was found that the damper bars did not have a significant effect on the shaft voltage under steady-state operating conditions and giving an accurate inductance was of little importance.

- Rotor Winding : The windings were grouped together and assigned a DC voltage source of 30 V. Total number of turns was set to 160 with a winding resistance of $0,5 \Omega$.
- Shaft : The shaft and the outer casing of the model were designated as a solid single turn winding with an external connection. This enables the easy measurement of shaft voltage.

“External connection” refers to a connection made between the winding and an external circuit. For each time-step of the transient solution the fields and inductances in the magnetic model are solved, this is then passed across to a circuit which is solved using an internal spice solver.

The external circuit used is shown in *Figure 6.3*. This circuit represents the parallel and star connection of the windings as found on the physical unit. The internal resistances of $53 \text{ m}\Omega$ are as measured. A load resistance of $7,5 \Omega$ is a full-load value. The shaft circuit is similarly configured, except that it is assumed to be open circuit and $100 \text{ M}\Omega$ is used as the load resistance. Voltages and currents from the probes indicated are recorded for each time step, and are compared to the physical measurements.

6.2.5 Setting up executive parameters

Executive parameters were not used for static simulations.

When setting up a transient simulation the only option under executive parameters is core loss. The core loss parameters of the stator were entered, but the simulation output was not used.

6.2.6 Setting up the solution

This is the final step before running the simulation. For transient simulations it is broken into two parts: Options and Motion Setup.

Motion setup defines what parts of the model are stationary and which parts are moving. This is done by defining the band object, an object inside which everything is assumed to be moving. There is great flexibility in defining how the non-stationary objects move, and inertia, damping and external forces can be taken into account.

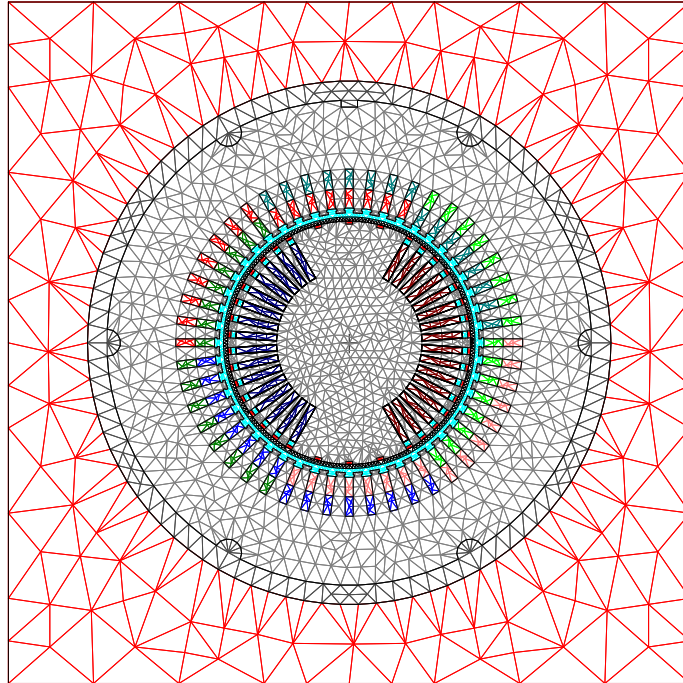


Figure 6.5: Mini-generator model mesh

Damping and external forces can be defined as functions of other available simulation parameters such as time and position. Such transients were, however, not of interest in this work and the rotor objects in the model were set to rotate at a constant 3000 RPM with no consideration given to inertia, damping or other parameters. The solver does produce torque data, which is the torque required to spin the rotor at the fixed angular velocity.

Of key importance when setting up the solution options is defining the mesh. MAXWELL 2DTM uses triangles exclusively in its meshing and solving algorithms. A static simulation is capable of refining the mesh in multiple passes until an error value is reduced below a set threshold. A transient simulation, however, does not refine the mesh during simulation and it is therefore important that the mesh be of sufficient density to achieve accurate results.

There were initial concerns that the meshing itself would introduce anomalous artifacts into the results and care was taken to get a similar mesh density for the different simulations, though it was eventually concluded that this is not the case. Many of the initial models were meshed by simply requesting an initial mesh and then refining the various objects to achieve a greater mesh density. Better meshing was later achieved by seeding the mesh, for which several algorithms are available.

Mesh density is to a large extent subjective and the results and error output from the simulation will typically indicate the success of the mesh. The online help goes into more detail on refining of the mesh and the solver algorithms used.

See *Figure 6.5* for a typical mesh employed in these simulations. It is likely that this mesh is not optimal as emphasis was given to an accurate rather than a quick solution.

Additional parameters in the solver setup for a static simulation were largely left as their default values. The parameters available for a transient simulation were more important:

- Time Step : For most of the simulations this was set to give five steps per stator slot. $48 \text{ slots} \times 5 = 240$ steps in a revolution, the machine was set to spin at 3000 RPM giving a period of 0,02 s, giving a Time Step of $\frac{0,02}{240}$ s. This value was adjusted and different numbers of steps per tooth, including non-integer multiples were tried. Interestingly, the primary harmonics did not change.
- Stop Time : This was set to 10 periods, or 0,2 s. Typically the first one or two periods were markedly different because of the starting transient, thereafter the simulation output settled in a steady-state. This initial transition period was disregarded when analysing the output. Multiple steady-state periods were simulated in order to later perform a high-resolution FFT on the information.
- Model Depth : This serves primarily as a linear scaling factor for the calculated voltages and was set to the actual depth of the magnetic circuit. Initially stacking factor of the laminations was not taken into account. When the depth was corrected with the stacking factor the output voltages showed a proportionate decrease as expected. However, it was the change in output, rather than the absolute magnitudes which was of interest; in order to keep simulations comparable, the model length was left without the stacking factor correction.
- Save Fields : One-dimensional information such as the output voltages and currents are automatically saved for every time step. This option allows one to save complete two-dimensional field information for selected time steps. This allows the fields to be analysed at different values of rotor position. MAXWELL 2DTM uses primarily text files for all its data output, and when it comes to the 2D field plots these files can be very large (approx. 5 MB per time step),

therefore only a few strategic time steps during the steady-state period of the simulation were saved. As an aside, the field post-processor can produce an animation of the changing fields as the model changes with time.

6.3 Areas to investigate

The questions it was hoped that would be answered through the use of 2D transient simulations are as follows:

1. Initial simulation related questions:
 - (a) Can MAXWELL 2DTM simulate a machine under transient conditions and provide an indication of the shaft voltage?
 - (b) Does the number of steps in a revolution significantly affect the shaft voltage?
 - (c) Can linear approximations of the model materials be used?
2. Fault diagnosis related questions:
 - (a) What effect does a static eccentricity have on the shaft voltage?
 - (b) What effect does machine output loading have on the shaft voltage?
 - (c) What effect does reduced excitation current have on the shaft voltage?
 - (d) What effect does reduced angular velocity have on the shaft voltage?
3. Once it was established that static eccentricity was manifested repeatedly in the same fashion (namely an increase in the 5th harmonic), the effect of machine geometry was queried:
 - (a) What effect does the existence of damper bars have on the shaft voltage?
 - (b) What effect does a reduced number of stator slots have on the shaft voltage?

Once the physical attributes and geometry of the machine was completed to a satisfactory degree, care was taken to modify the simulation set-up as little as possible in order to be able to identify the cause and effect relationship between the shaft voltage waveform and the “cause” under test. This care was extended to the fineness of the mesh and a note was made of the number of triangles in each object, and whenever the model was changed the mesh was refined to the same point.

Rigorous attention was given to the colouring and naming of various geometrical objects as well as the naming of all electrical measurements. The various simulations were arranged in a set file and directory structure, this facilitated the use of MATLAB scripts to process and compare different simulation results.

6.4 Data analysis technique

Various forms of analysis were looked at including Fourier, short-time Fourier and wavelets. Traditional FFT analysis proved to be effective at identifying a static eccentricity condition. The process followed is as follows:

- Window the sample with a hanning window.
- Pad the data with zeros up to the nearest 2^x length.
- Perform an FFT on the windowed, padded data.
- If a power spectrum is required then square the output data.
- If normalised data is required (typical) then the data is scaled such that the maximum point has a value of 1.
- If a dB scale is required then a $10 \log ()$ is applied to a power spectrum, or $20 \log ()$ to a magnitude spectrum

In almost all cases the FFT output was normalised in some way. Where the same type of measurement, but of several experiments was compared the normalisation was applied to all the measurements together, so as not to lose perspective of the relative magnitudes between experiments.

6.5 Results

6.5.1 Usefulness of transient simulations

Using the model and external circuit shown in *Figures 6.2* and *6.3*, the node voltage graphs shown in *Figures 6.6* and *6.7* were produced.

Other graphs that can be plotted from the simulation data include:

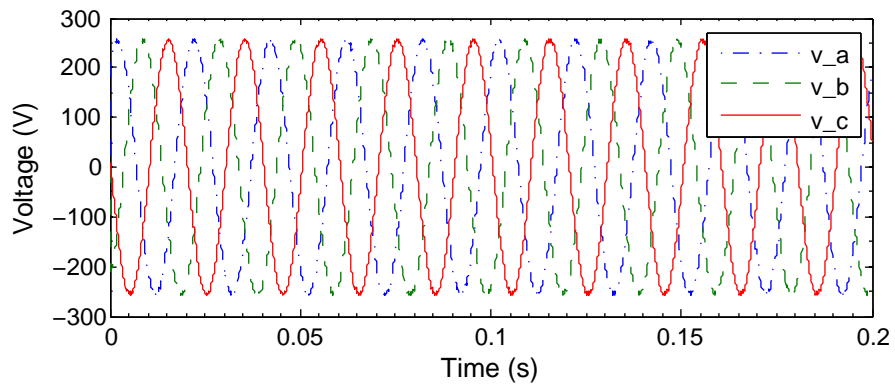


Figure 6.6: Output node voltages relative to ground

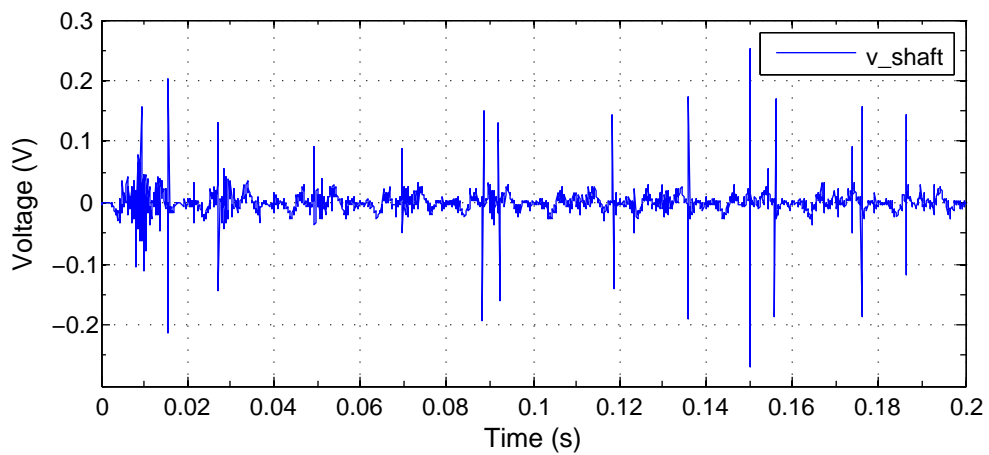


Figure 6.7: Shaft voltage relative to ground

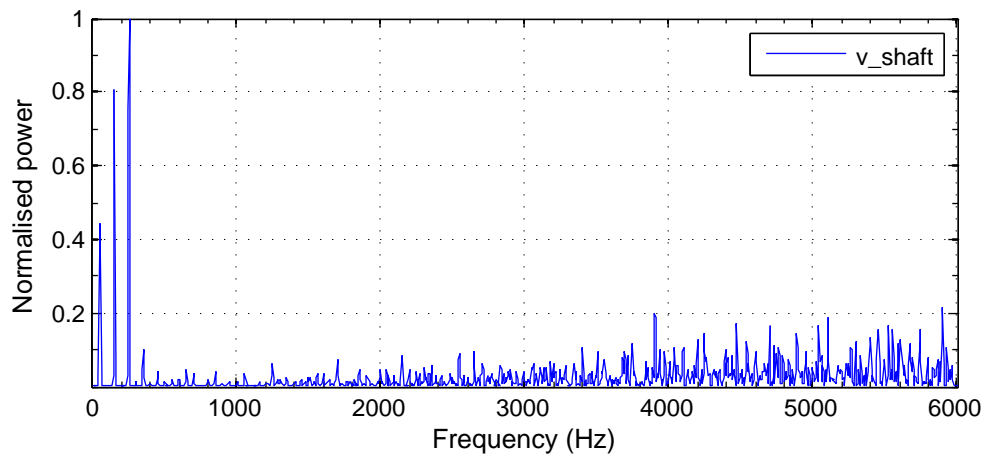


Figure 6.8: Shaft voltage frequency spectrum

Torque ; Power Loss ; Back EMF ; Flux Linkage ; Winding Current ;
 Bar Current ; Bar Voltage ; Position ; Speed ; Branch Current ;
 Node Voltage (plotted in *Figures 6.6* and *6.7*) ; Error ; Core Loss

It is clear from the non-regular peaks in the shaft voltage graph (see *Figure 6.7*) that the simulation is not perfect. Remember that the model is perfectly symmetrical (well, as perfect as finite numerical precision will allow) and one expects a reasonably regular and periodic waveform. The spikes are therefore most likely due to numerical inconsistencies such as loss of information due to finite precision, or because of local minima or similar problems in the numerical solution of simultaneous equations.

In *Figure 6.8* the normalised power spectrum of the shaft voltage is plotted. Three very distinct frequency peaks can be seen at 50 Hz, 150 Hz and 250 Hz (the first, third and fifth harmonics). The fifth harmonic in particular is later found to be highly dependant on the static eccentricity.

It can be concluded that the MAXWELL 2DTM transient solver is capable of modelling a shaft voltage. In *Chapter 7* physical measurements are presented, and the simulations are found to compare favourably with them.

6.5.2 Influence of steps per revolution

Several models with different eccentricities were drawn and simulated. One of the models, with a 0,5 mm offset was simulated with 240 steps in a revolution and then again with 100 steps. 100 steps is also a non-integer multiple of the 48 slots (whereas 240 results from 5 steps per slot). The comparison between the two can be seen in *Figure 6.9*.

For 240 steps per revolution, the Nyquist frequency is approximately 6 kHz while for 100 steps it is 2,5 kHz. Both plots are drawn with range of 0 – 2,5 kHz for comparison.

From these plots it can be concluded that 100 steps per revolution is sufficient to qualify changes in the frequency spectrum due to eccentricity. In addition, having an integer, or an non-integer multiple of the number of stator slots is not important.

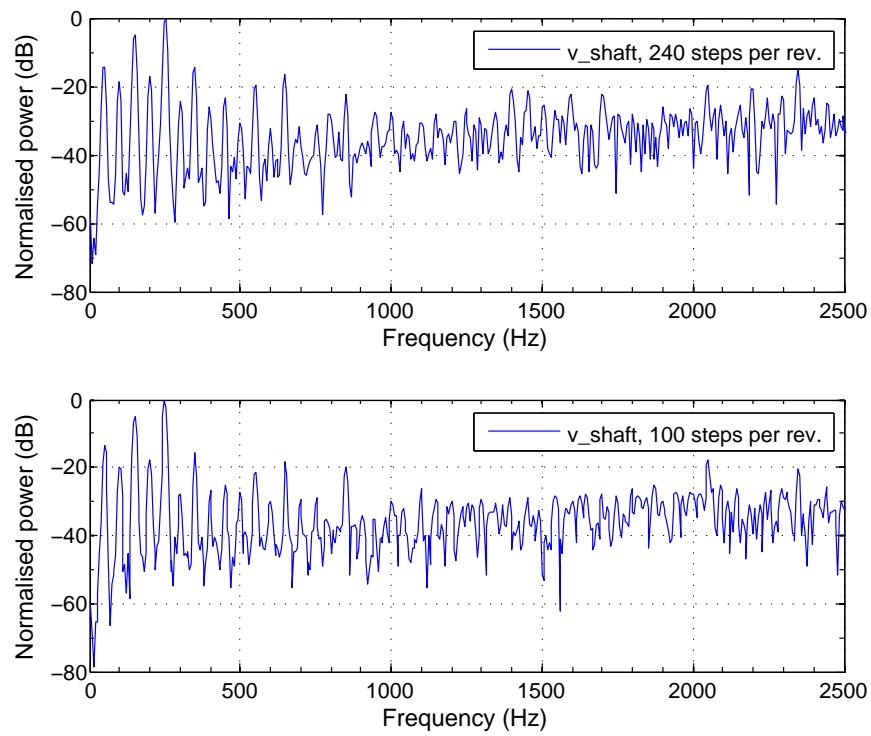


Figure 6.9: Comparison of shaft voltage frequency power spectrums

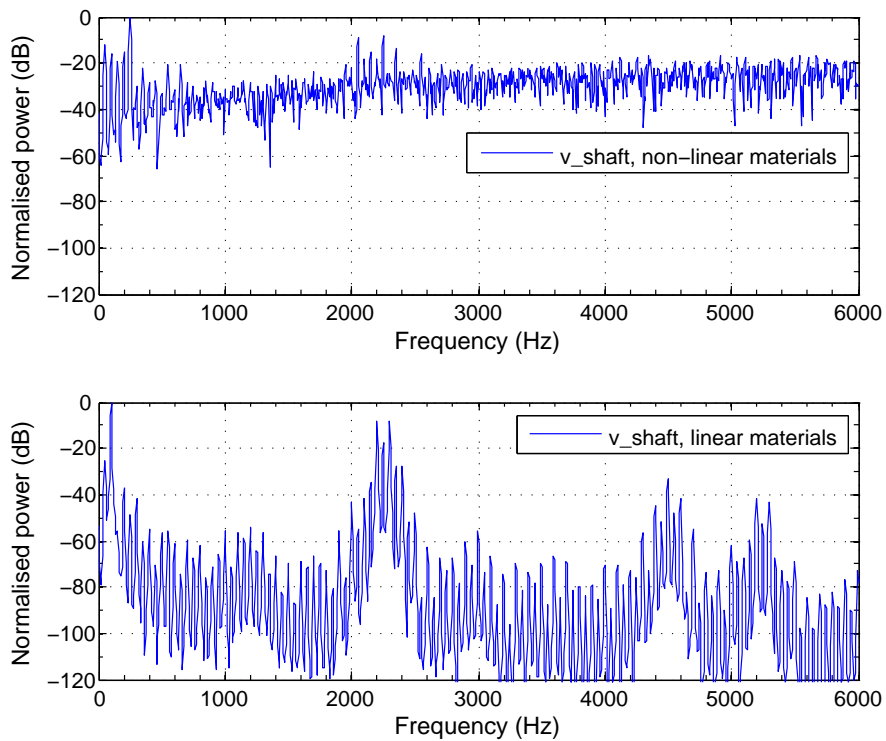


Figure 6.10: Comparison of shaft voltage frequency power spectrums for linear vs non-linear materials

6.5.3 Feasibility of using linear approximations of materials

A 5 mm eccentricity had been simulated normally with non-linear materials. An operating point on the B-H curve of those materials was chosen and their magnetic properties were changed to the chosen linear μ_r .

All output waveforms produced by the linear model were grossly different to the non-linear one. See *Figure 6.10* for a comparison of the power spectral plot for the two cases. It is possible that a better operating point could be chosen, but the savings in computation time did not warrant the time needed to find that operating point and the added risk of unnecessary errors; especially when considering that different loading and excitations were also simulated, each of which would have required the finding of a reliable operating point.

6.5.4 Affect of static eccentricity on shaft voltage

Six different models were simulated, each was identical in the following respects:

- Rotational speed : 3000 RPM
- Ending time : 0,2 s (10 full rotations of the rotor)
- Number of steps per revolution : 240
- Excitation current : 60 A
- Star-connected load resistance (per phase): 7,5 Ω
- Nearly identical mesh density

The following eccentricities were simulated :

0 mm • 0,25 mm • 0,5 mm • 2,5 mm • 5 mm

In *Figure 6.14* the relative frequency power spectrums of the shaft voltage for different eccentricities is plotted. Of interest is the 5th harmonic at 250 Hz which increases significantly as the static eccentricity increases. The purpose of the physical measurements presented in *Chapter 7* is to verify this finding.

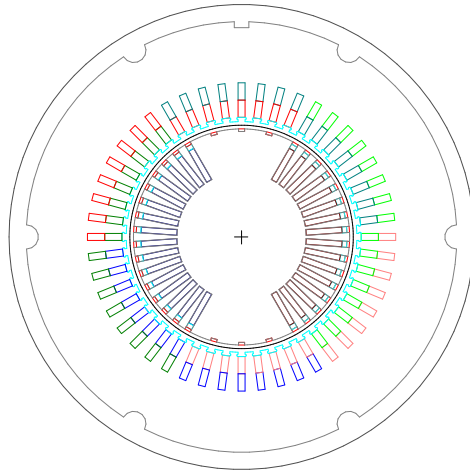


Figure 6.11: Model of the generator with no eccentricity

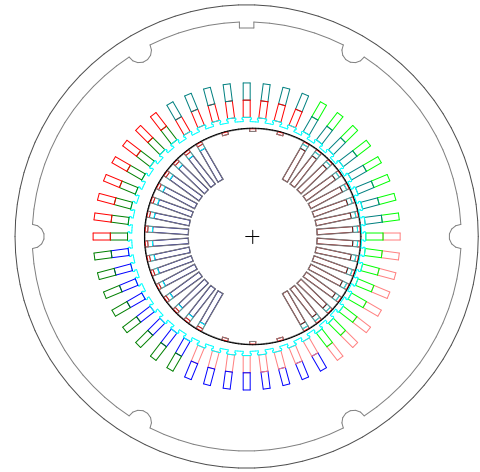


Figure 6.12: Model of the generator with 5 mm of eccentricity

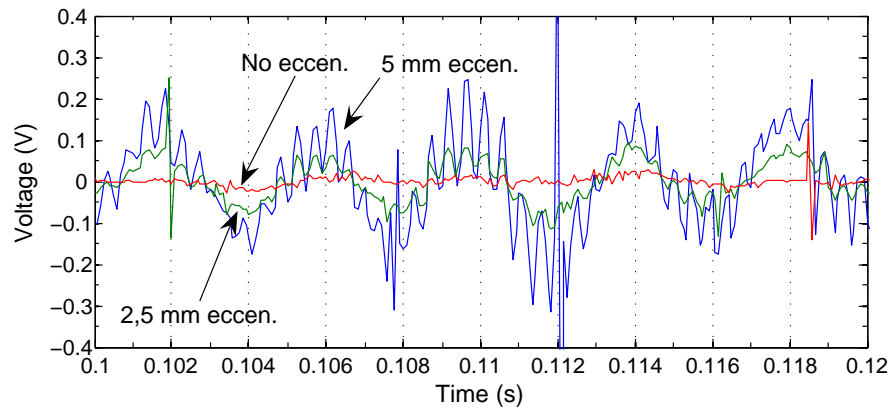


Figure 6.13: Time domain plot of shaft-voltage at full load for different simulated eccentricities

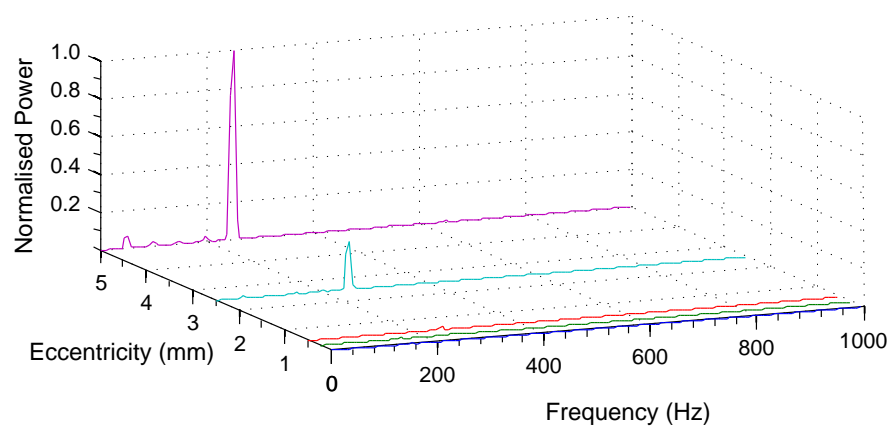


Figure 6.14: Relative frequency spectrum of shaft-voltage at full load for different simulated eccentricities

6.5.5 Affect of machine output loading on shaft voltage

Three different loading conditions were simulated for both a no-eccentricity and a 2,5 mm eccentricity condition. Each was identical in the following respects:

- Rotational speed : 3000 RPM
- Ending time : 0,2 s (10 full rotations of the rotor)
- Number of steps per revolution : 240
- Excitation current : 60 A
- Nearly identical mesh density

Because of the large air-gap the regulation of the machine is very good. *Table 6.1* shows the simulated RMS phase output voltages (*star*) for a constant excitation current of 60 A and different loads with no eccentricity. *Table 6.2* shows the simulated RMS shaft voltage for the same excitation current and loads with no eccentricity. *Table 6.3* shows the simulated RMS shaft voltage but with a 2,5 mm eccentricity.

Figures 6.15 and *6.16* are comparative illustrations of the shaft power spectrum with eccentricities of 0 mm and 2,5 mm respectively. In each case the spectrum of the three cases was normalised to the maximum of any of the three.

From the simulations it appears the machine loading is of little consequence to the shaft voltage. This is in agreement with the physical measurements as documented in *Chapter 7*.

6.5.6 Affect of reduced excitation current on shaft voltage

The rotor winding excitation current was reduced from 60 A to 40 A. Simulations were then performed with no eccentricity and an eccentricity of 2,5 mm. Each was identical in the following respects:

- Rotational speed : 3000 RPM
- Number of rotations : 10 full rotations of the rotor
- Number of steps per revolution : 240

Table 6.1: Phase output voltage (RMS) with different loads and no eccentricity

Full load (7,5 Ω per phase (<i>star</i>)) :	181,04 V
Half load (15 Ω per phase (<i>star</i>)) :	181,65 V
No load (100 M Ω per phase (<i>star</i>)) :	182,17 V

Table 6.2: Shaft voltage (RMS) with different loads and no eccentricity

Full load (7,5 Ω per phase (<i>star</i>)) :	0,0127 V
Half load (15 Ω per phase (<i>star</i>)) :	0,0113 V
No load (100 M Ω per phase (<i>star</i>)) :	0,0116 V

Table 6.3: Shaft voltage (RMS) with different loads and 2,5 mm eccentricity

Full load (7,5 Ω per phase (<i>star</i>)) :	0,0487 V
Half load (15 Ω per phase (<i>star</i>)) :	0,0485 V
No load (100 M Ω per phase (<i>star</i>)) :	0,0476 V

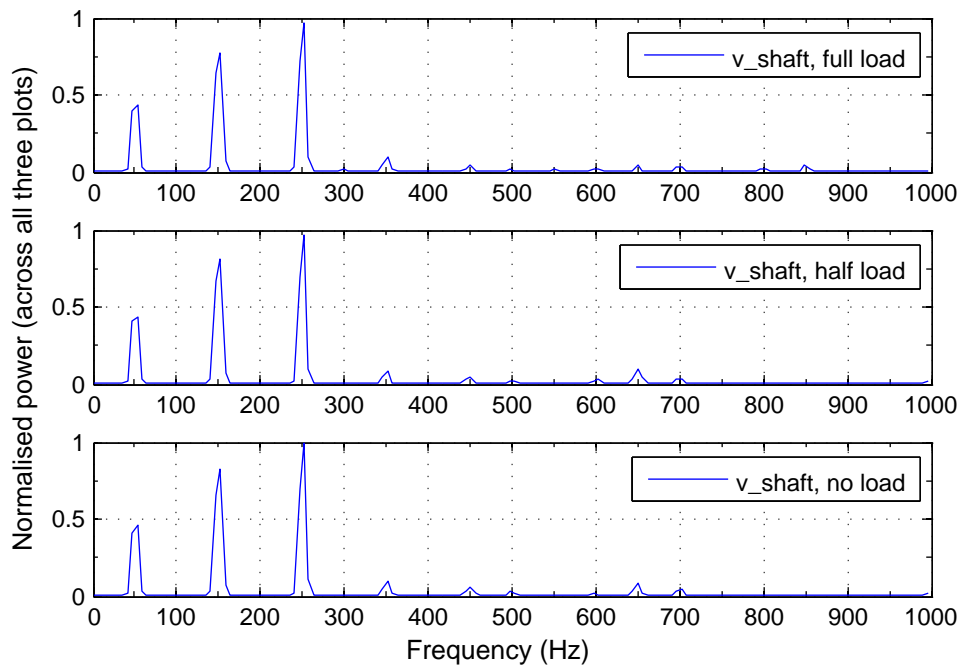


Figure 6.15: Comparison plot of shaft voltage power frequency spectrum for different load conditions with **no eccentricity**

- Star-connected load resistance (per phase): 7,5 Ω
- Nearly identical mesh density

The lower excitation current results in both reduced terminal output voltage (*Table 6.4*) and a large reduction in the shaft voltage (*Table 6.5*). This is also true when an eccentricity of 2,5 mm is introduced (*Table 6.6*).

Figures 6.17 and *6.18* are comparative illustrations of the shaft power spectrum with eccentricities of 0 mm and 2,5 mm respectively. In each case the spectrum of the two cases was normalised to the maximum of any of the two.

From the simulations it is clear that a reduced excitation current greatly reduces the shaft voltage, as expected. However, it can be seen that the fifth harmonic still increases relative to the other significant harmonics.

6.5.7 Affect of reduced angular velocity on shaft voltage

The angular velocity of the shaft was reduced by 20% from 3000 RPM to 2400 RPM. Simulations were then performed with no eccentricity and an eccentricity of 2,5 mm. Each was identical in the following respects:

- Number of rotations : 10 full rotations of the rotor
- Number of steps per revolution : 240
- Excitation current : 60 A
- Star-connected load resistance (per phase): 7,5 Ω
- Nearly identical mesh density

The slower rotation does result in a lower output phase voltage. *Table 6.7* shows the simulated RMS phase output voltages (*star*) for a constant excitation current of 60 A with different shaft rotation speeds. *Table 6.8* shows the simulated RMS shaft voltage for the same excitation current with no eccentricity at the different speeds. *Table 6.9* shows the simulated RMS shaft voltage but with a 2,5 mm eccentricity.

Figures 6.19 and *6.20* are comparative illustrations of the shaft power spectrum with eccentricities of 0 mm and 2,5 mm respectively. In each case the spectrum of the two cases was normalised to the maximum of any of the two.

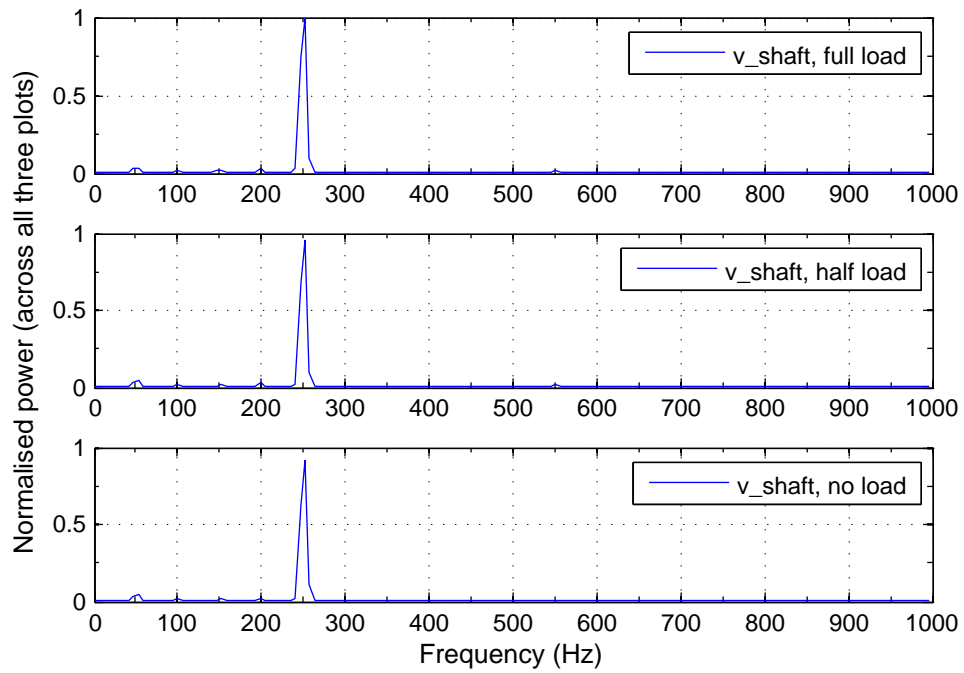


Figure 6.16: Comparison plot of shaft voltage power frequency spectrum for different load conditions with **2,5 mm eccentricity**

Table 6.4: Phase output voltage (RMS) with different excitation currents and no eccentricity

Full excitation (60 A) :	181,04 V
Reduced excitation (40 A) :	132,25 V

Table 6.5: Shaft voltage (RMS) with different excitation currents and no eccentricity

Full excitation (60 A) :	0,0127 V
Reduced excitation (40 A) :	0,000858 V

Table 6.6: Shaft voltage (RMS) with different excitation currents and 2,5 mm eccentricity

Full excitation (60 A) :	0,0487 V
Reduced excitation (40 A) :	0,00370 V

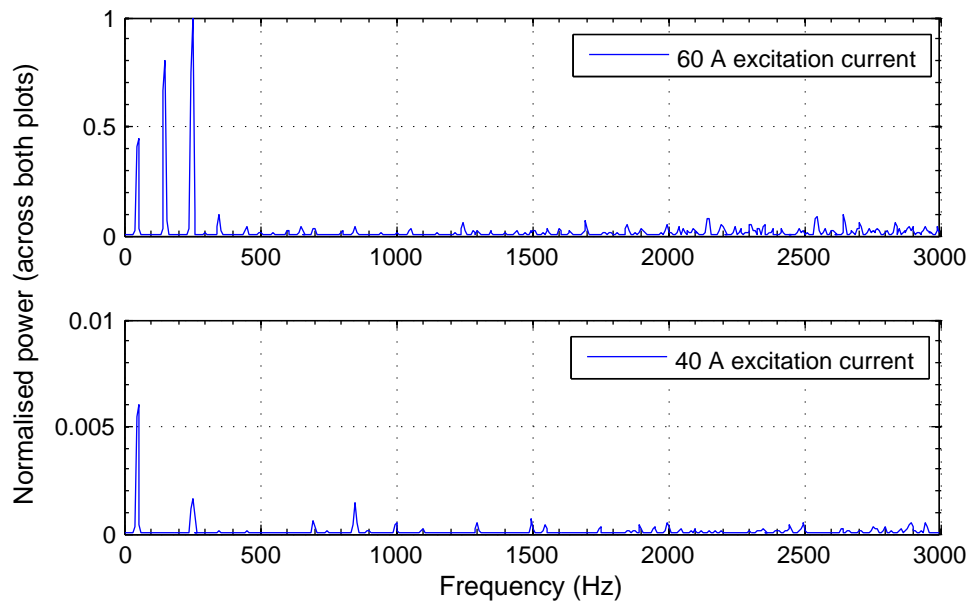


Figure 6.17: Comparison plot of shaft voltage power frequency spectrum for different excitation currents with **no eccentricity**

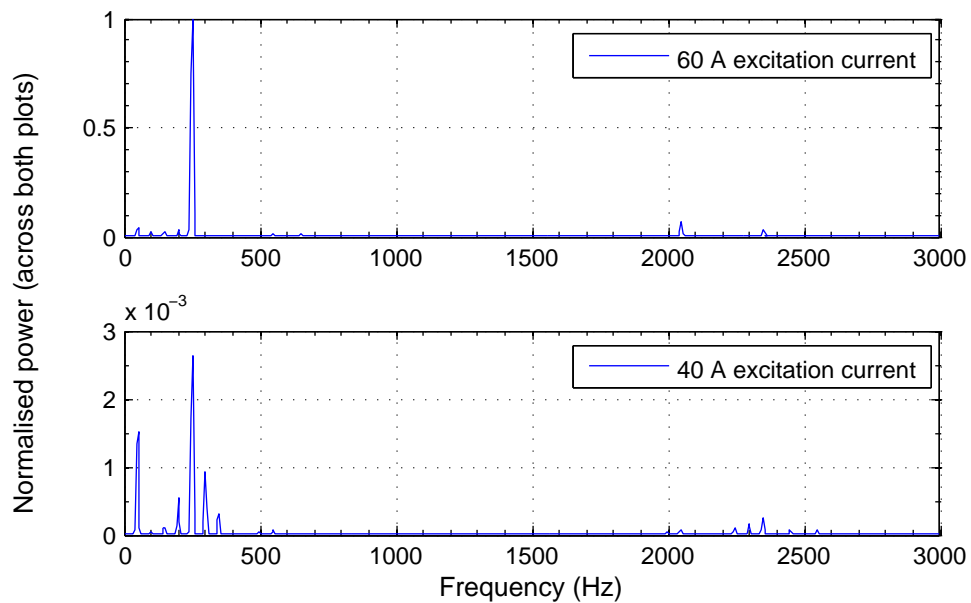


Figure 6.18: Comparison plot of shaft voltage power frequency spectrum for different excitation currents with **2,5 mm eccentricity**

From the simulations it is clear that a slower rotational speed results in lower voltages on both the stator windings and the shaft, this is as expected. At 3000 RPM the first harmonic is at 50 Hz, while at 2400 RPM the first harmonic is at 40 Hz. The relative magnitudes of the harmonics, however, remains constant.

6.5.8 Affect of damper bars on shaft voltage

Although the machine spins at synchronous speed and theoretically there should not be currents in the damper bars, the simulations show that there is current flowing in the bars (see *Figure 6.21*). In order to investigate whether or not this influenced the shaft voltage a model was created where the material properties of the damper bars were set to either vacuum (for those bars present in rotor slots) or to the same steel as the rotor (for those bars not in rotor slots).

The model without damper bars was simulated without eccentricity and then with a 5 mm eccentricity. These results are compared against those from the simulations using damper bars. The difference in the damper bars is the only difference between the two simulations.

- Rotational speed : 3000 RPM
- Number of rotations : 10 full rotations of the rotor
- Number of steps per revolution : 240
- Excitation current : 60 A
- Star-connected load resistance (per phase): 7,5 Ω
- Nearly identical mesh density

Excluding the damper bars has very little influence on the RMS magnitude of the phase output or shaft voltages (*Tables 6.10* and *6.11*, this is not surprising given the plot in *Figure 6.22*). The flux density which is normal to the air-gap is nearly identical for the two cases. However, *Figure 6.24* shows that with no eccentricity the relative magnitudes of the power spectrum harmonics is different between the two cases.

With a 5mm eccentricity the results are very different. The RMS magnitude of the shaft voltage is much greater for the excluded damper bar case as seen in *Table 6.12*

Table 6.7: Phase output voltage (RMS) with different rotational speeds and no eccentricity

Full speed (3000 RPM) :	181,04 V
80% speed (2400 RPM) :	144,85 V

Table 6.8: Shaft voltage (RMS) with different rotational speeds and no eccentricity

Full speed (3000 RPM) :	0,0127 V
80% speed (2400 RPM) :	0,00928 V

Table 6.9: Shaft voltage (RMS) with different rotational speeds and 2,5 mm eccentricity

Full speed (3000 RPM) :	0,0487 V
80% speed (2400 RPM) :	0,0409 V

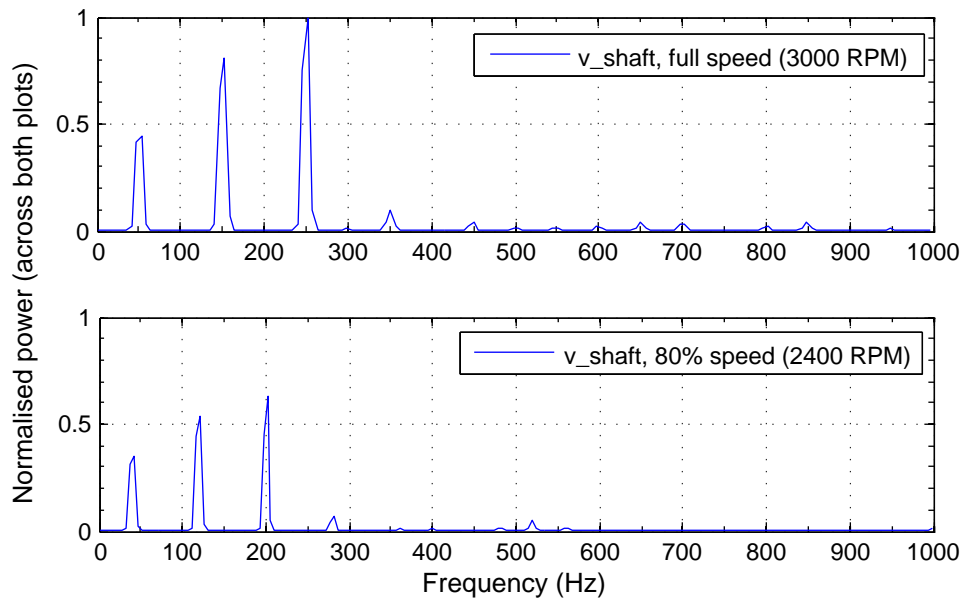


Figure 6.19: Comparison plot of shaft voltage power frequency spectrum for different rotational speeds with **no eccentricity**

and *Figure 6.25*. More than that, the dominant 45th and 47th harmonics at 2250 and 2350 Hz are unique to this experiment.

Given that the damper bars are in parallel with and therefore coupled with the shaft, it is expected that they would influence the shaft voltage. They also influence the torque one would need to apply to the machine to maintain a rotational speed of 3000 RPM as shown in *Figure 6.23*. This indicates that synchronous machines with damper bars will exhibit greater vibration when the rotor is eccentric than machines without damper bars.

One possible explanation for the high-end harmonics in the shaft voltage when the damper bars are excluded is that if the bars are included, they shield the shaft from those high harmonics and the harmonics manifest as circulating currents within the bars themselves.

6.5.9 Affect of stator slot count on shaft voltage

In all the cases discussed above, there is a clear increase in the fifth harmonic when the rotor is made eccentric and this increase is roughly proportional to the level of eccentricity. The question which is now asked, is whether a change to the stator geometry will effect this phenomenon.

The stator model was modified to have one fewer slot per coil group, resulting in 6 fewer slots. Both the tooth and the slot width were modified evenly around the stator to accomplish this. Previously the stator had 48 slots, this experiment was conducted with a 42 slot stator. A 48 slot model is shown in *Figure 6.26* and the new 42 slot model is shown in *Figure 6.27*. The new model was simulated without eccentricity and with a 4 mm eccentricity in order to investigate whether or not the eccentricity on this slightly different geometry would manifest in an increase in the 5th harmonic as previously observed.

A comparison between the power spectrum of the shaft voltage for the two cases is shown in *Figure 6.27*. It can be clearly seen that the 5th harmonic increases significantly for a 4 mm air-gap. It can therefore be concluded that a small variation in the number of stator slots does not influence which harmonic is significant in the diagnosis of a static eccentricity.

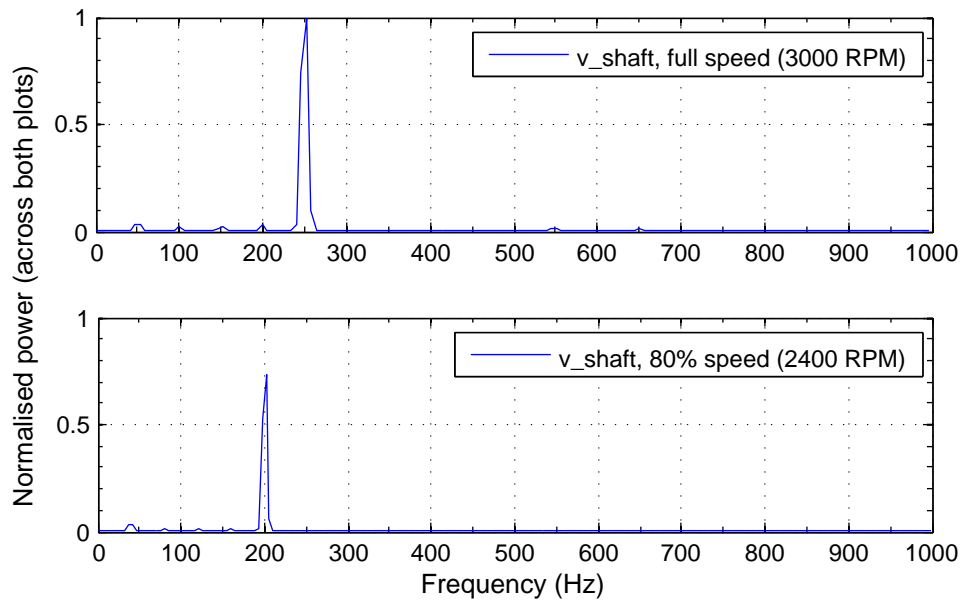


Figure 6.20: Comparison plot of shaft voltage power frequency spectrum for different rotational speeds with **2,5 mm eccentricity**

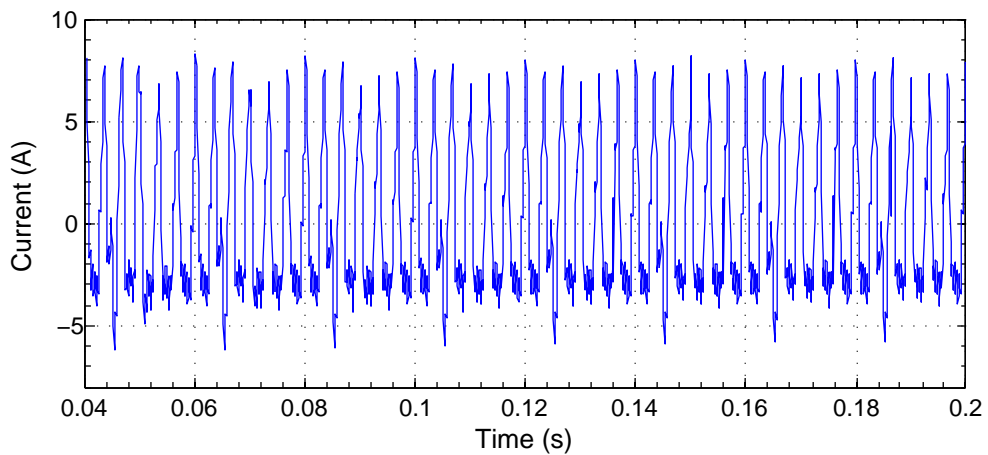


Figure 6.21: Time domain plot of the bar currents for the full load model with no eccentricity

Table 6.10: Phase output voltage (RMS) with and without damper bars (no eccentricity)

With damper bars :	181,04 V
Without damper bars :	182,20 V

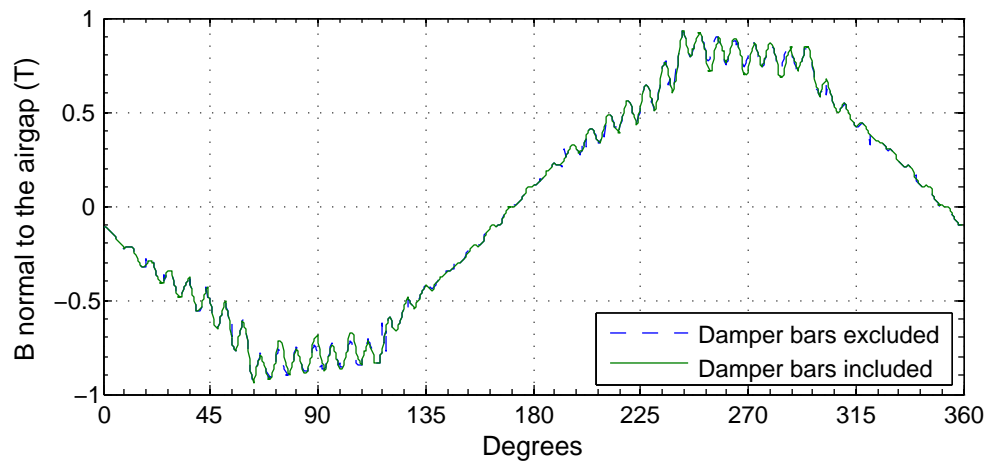


Figure 6.22: Flux density normal to the air-gap for the full load model with no eccentricity

Table 6.11: Shaft voltage (RMS) with and without damper bars (no eccentricity)

With damper bars :	0,0127 V
Without damper bars :	0,0123 V

Table 6.12: Shaft voltage (RMS) with and without damper bars (5 mm eccentricity)

With damper bars :	0,112 V
Without damper bars :	0,230 V

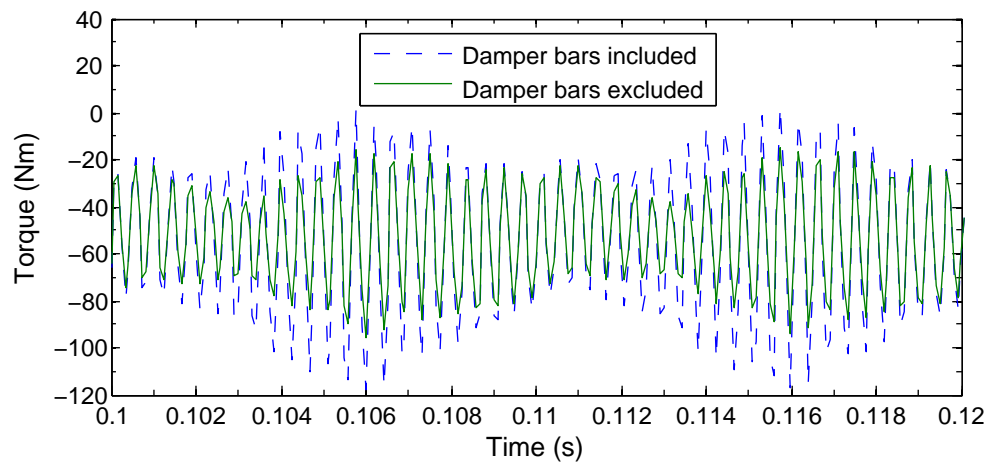


Figure 6.23: Time domain plot of the rotor torque with a 5 mm eccentricity

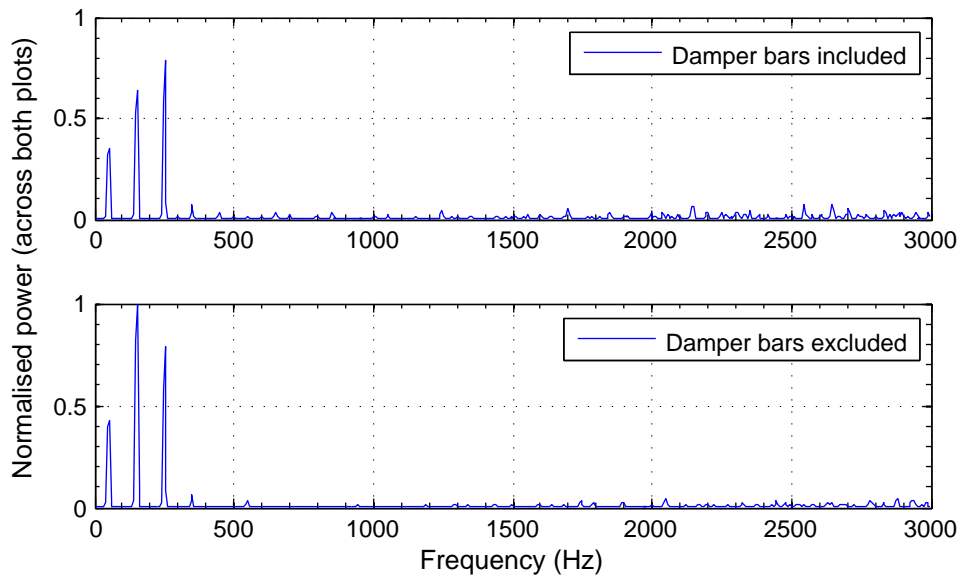


Figure 6.24: Comparison plot of shaft voltage power frequency spectrum for simulations with and without damper bars (**no eccentricity**)

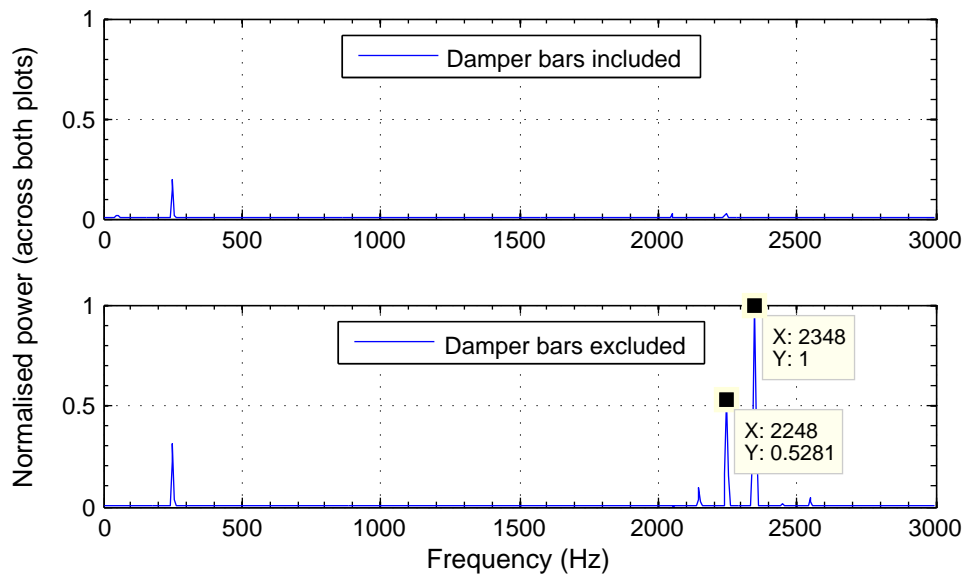


Figure 6.25: Comparison plot of shaft voltage power frequency spectrum for simulations with and without damper bars (**5 mm eccentricity**)

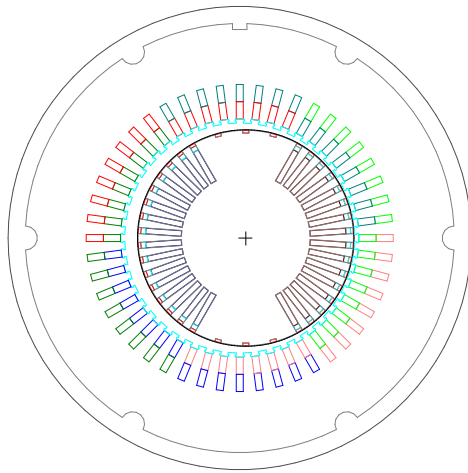


Figure 6.26: Model of the 48 slot generator with 5 mm of eccentricity

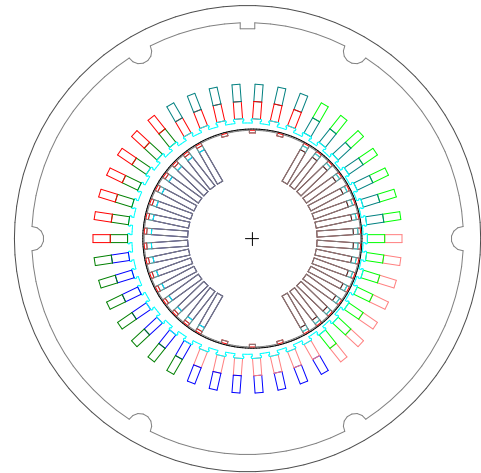


Figure 6.27: Model of the 42 slot generator with 4 mm of eccentricity

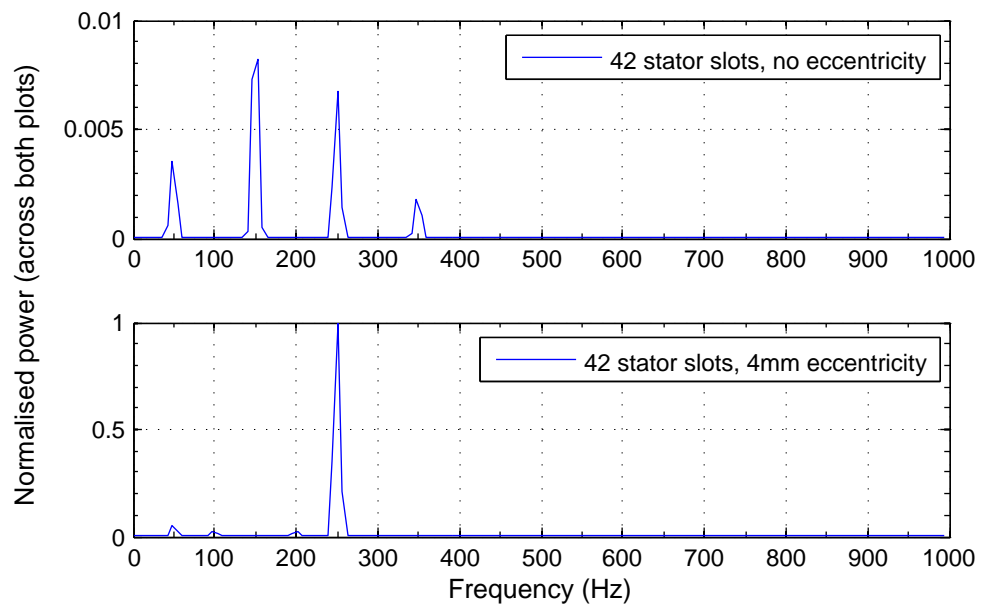


Figure 6.28: Comparison plot of shaft voltage power frequency spectrum for no eccentricity and 4mm eccentricity of a machine with a 42 slot stator

6.6 Computing observations and recommendations

A single simulation took, on average, 20 hours on a single processor 32-bit Intel Pentium 4 2.8 GHz with 512 MB of RAM. RAM utilisation was low and the simulation process alone did not make use of disk based virtual memory.

An FEM simulation involves converging a large set of non-linear simultaneous equations. This makes an FEM problem difficult to decompose into a form that can be run in a cluster environment¹. It is certainly impossible to solve a single problem in a cluster environment with the current release of MAXWELL 2D™ from Ansoft. Support for such an environment has to be coded into the engine at a very low level, and is intertwined in the program's design. This is changing with the increasing affordability and popularity of dual-core processors or multiple processor based machines. The latest release of MAXWELL 3D™ includes support for dual-core and multiple processor systems, however, cluster support is still not available. The bottle-neck in the simulation process appeared to be the processor, with it seeing extended 100% utilisation, it is therefore worthwhile to obtain as high an instruction rate as possible. Note that a faster clock rate does not necessarily indicate a higher instruction rate. AMD advertises that their processors can do more with fewer clocks than Intel processors. It is not the objective of this report to quantify or to substantiate such claims, only that the buyer be aware of them when making a purchasing decision.

Engineering maths is typically performed using 64-bit floating point numbers. At the time of writing, 32-bit processors still power the majority of workstations, including the workstation on which the simulations were run. This too, is changing, and workstation level 64-bit processors are available and are seeing far more widespread use. Microsoft Windows 64-bit has also been recently released. There are definite penalties incurred for performing maths and manipulating 64-bit numbers on a 32-bit processor. It is therefore recommended that in future, any machine which is intended to perform simulations or other heavy maths processing be equipped with a 64-bit processor as a matter of course.

The memory requirements of a 2-D simulation were modest, and 512 MB was more than adequate, however, memory access speed will affect the speed of simulation. It is therefore recommended that preference be given to fast, or low-latency memory rather than a large quantity of slower memory. According to Ansoft, 3-D simulations

¹A computer cluster is made up of more than one computer connected in a network. All computers in the cluster are put to work to solve a single problem, typically with a central machine administering the whole process

require far larger quantities of RAM and this must be taken into account if 3-D simulations are likely to be performed.

6.7 Conclusion

To summarise, the following questions were posed in *Section 6.3*, here they are repeated with their conclusions:

1. Initial simulation related questions:

- (a) *Can MAXWELL 2DTM simulate a machine under transient conditions and provide an indication of the shaft voltage?*

MAXWELL 2DTM is clearly capable of simulating transient conditions and producing a shaft voltage measurement.

- (b) *Does the number of steps in a revolution significantly affect the shaft voltage?*

It was concluded that 100 steps per revolution is sufficient to qualify changes in the frequency spectrum due to eccentricity. In addition, having an integer, or a non-integer multiple of the number of stator slots is not important.

- (c) *Can linear approximations of the model materials be used?*

All output waveforms produced by the linear model were grossly different to the non-linear one. It is possible that a better operating point could be chosen, but the savings in computation time did not warrant the time needed to find that operating point and the added risk of unnecessary errors; especially when considering that different loading and excitations were also simulated, each of which would have required the finding of a reliable operating point.

2. Fault diagnosis related questions:

- (a) *What effect does a static eccentricity have on the shaft voltage?*

In the simulations the 5th harmonic of the shaft voltage showed a marked increase when a static eccentricity was introduced. This is encouraging as it provides evidence that the shaft voltage is affected by changing running conditions and that the change to the shaft voltage can be predicted using simulations.

- (b) *What effect does machine output loading have on the shaft voltage?*

From the simulations it appears that the machine loading is of little consequence to the shaft voltage, this is in agreement with the physical measurements as documented in *Chapter 7*.

- (c) *What effect does reduced excitation current have on the shaft voltage?*

From the simulations it is clear that a reduced excitation current greatly reduces the shaft voltage, as expected. However, it can be seen that the fifth harmonic still increases relative to the other significant harmonics.

- (d) *What effect does reduced angular velocity have on the shaft voltage?*

From the simulations it is clear that a slower rotational speed results in lower voltages on both the stator windings and the shaft, this is as expected. At 3000 RPM the first harmonic is at 50 Hz, while at 2400 RPM the first harmonic is at 40 Hz. The relative magnitudes of the harmonics, however, remains constant.

3. Once it was established that static eccentricity was manifested repeatedly in the same fashion (namely an increase in the 5th harmonic), the effect of machine geometry was queried:

- (a) *What effect does the existence of damper bars have on the shaft voltage?*

Removing the damper bars in the simulation at a large eccentricity had the effect of increasing the rms magnitude of the shaft voltage. In addition, high frequency peaks appeared in the spectrum at the 45th and 47th harmonics. One possible explanation for these high-end harmonics is that if the bars are included, they shield the shaft from those high harmonics and the harmonics manifest as circulating currents within the bars themselves. The origin of the harmonics is deemed to be the 48 slots in the stator.

- (b) *What effect does a reduced number of stator slots have on the shaft voltage?*

It is concluded that a small variation in the number of stator slots does not influence which harmonic is significant in the diagnosis of a static eccentricity.

Chapter 7

Mini-gen measurements

7.1 Introduction

This chapter presents the measurements obtained from the miniature generator. The purpose of the experiments which were conducted was to verify the feasibility of using transient FEM simulations, specifically with the Ansoft MAXWELL 2DTM package, to predict changes in the shaft voltage for a static eccentricity (and ultimately other faults as well).

7.2 Experimental set up

The experimental setup is presented in *Figure 7.1* and a photo is shown in *Figure 7.2*. A variable speed drive is used to drive a 2-pole induction motor. It is important that the input frequency to the induction machine can be varied in order to compensate for increased slip when the load is increased. The induction motor is coupled to the mini-gen with an insulated flexible coupling. Note that the selection of the coupling is quite important – if the coupling makes use of black rubber then the rubber is mostly likely impregnated with carbon making it conductive. A resistance as low as $400\ \Omega$ was measured across a large tyre type coupling. The actual power being supplied to the induction motor was not of interest, but a digital voltmeter was placed to measure the line voltage at the induction motor's inputs in order to monitor the supplied voltage and the supplied frequency. The mini-gen excitation current was supplied through slip-rings on the non-driven end (NDE), a separate DC generator powered by a synchronous motor was used to supply the DC current. A series resistance and a DC voltmeter were used to monitor the current while another



Figure 7.2: Photograph of the coupled miniature turbo-generator and 2-pole induction motor

DC voltmeter was used to measure the voltage at the slip-ring brushes. In order to have full control over the load placed on the mini-gen an auto-transformer was used between the mini-gen output terminals and a 3-phase resistive load-bank. The auto-transformer is star connected and has a maximum phase current rating of 30 A, which limited the load that could be placed on the generator.

A DSPACE™ DS1104 data acquisition and control card was used to capture 5 channels of analogue input and one digital incremental encoder input. This card is installed in a PC and the data is captured to RAM before being saved to the PC's hard-drive. The DSPACE™ platform allows for sophisticated screen based interfaces to be created, and this was put to use in order to display real-time quantities such as the rotational speed of the generator and the rms output voltage and current.

The shaft voltage was measured using two gold-alloy bristle brushes sprung mounted on either side of the shaft (see *Figures 7.2* and *7.3*), the brush on the NDE was grounded. The shield of a coax cable was connected to ground at the same point, the inner of the coax was connected to the brush on the driven end (DE). The cable was then connected to the high-impedance and protected input of the interfacing unit (see *Section 3.4* in *Chapter 3*). The interface unit and the PC were powered through an isolation transformer and care was taken not to introduce any ground loops. The incremental encoder is intrinsically isolated from the shaft and was connected to the digital level-shifting input on the interface unit. The filtered shaft voltage output from the interface unit was connected with a coax cable to ADCH1 on the DSPACE™ card while the digital encoder output was connected to ENC1 on the

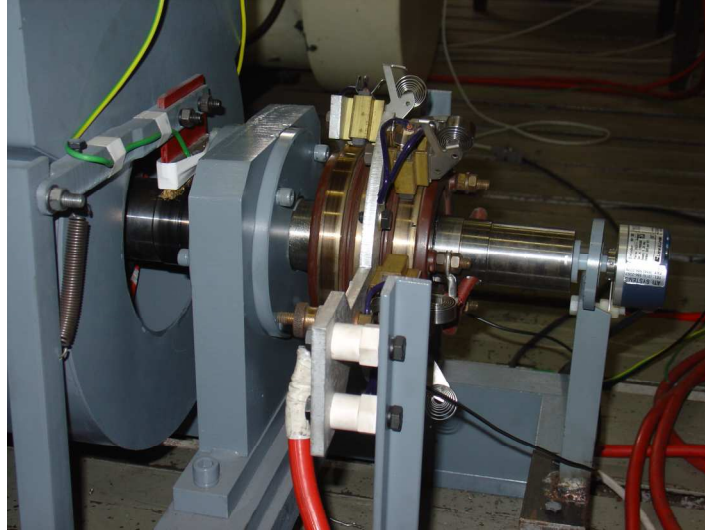


Figure 7.3: Closeup of the NDE shaft brush, slip rings and incremental encoder

DSPACE™ card.

Additional mini-gen output terminal voltages were captured using 200:1 differential voltage probes and single line current was captured using a 10 mV/A Rogowski unit.

Table 7.1: DSPACE™ channel connections

Encoder input Ch 1 :	Shaft mounted incremental encoder
ADCH1 (16-bit) :	Shaft voltage
ADCH5 (12-bit) :	Red (+ve) – Yellow (-ve) line voltage
ADCH6 (12-bit) :	Yellow (+ve) – Blue (-ve) line voltage
ADCH7 (12-bit) :	Blue (+ve) – Red (-ve) line voltage
ADCH8 (12-bit) :	Red line current

7.3 Eccentricity adjustment

The design of the mini-gen is such that the rotor remains fixed to the bed-plate via the bearing pedestals. It is possible to move the stator and misalign it relative to the rotor, creating a static eccentricity. This can be done without disturbing the machine coupling. In order to move the stator, one bolt from each side of the stator needs to be removed (the bolt on the one side can be seen to missing in *Figure 7.4*). The remaining four bolts are loosened and an overhead crane is used to very slightly lift the stator off its mounting, the stator can then be relatively easily man-handled into an eccentric position. When all six bolts (three on each side) are



Figure 7.4: Closeup of a stator mounting bracket, showing the oblong locating holes and removable shim

inserted the stator is centred without eccentricity. In addition, the shims can be changed, removed or boosted to allow for the introduction of a vertical eccentricity.

The mini-gen has a 6 mm air-gap, however it is unwise to attempt much more than a 3 mm eccentricity because the rotor is wrapped in a layer of resi-glass of uncertain thickness, and it is not desirable for this to rub against the stator!

7.4 Experiments

The primary goal is to verify whether or not the shaft voltage power spectrum will behave in a similar fashion to the simulations. The simulations were performed with numerically perfect symmetry, while the physical machine is not geometrically perfect and could have been effected by any of a number of manufacturing processes including welding (which can result in residual magnetism), machining error (it is known that one slot on the rotor was gouged at the first attempt to cut it) and other unintended or unavoidable byproducts of machine manufacture.

- Check the noise floor by obtaining a measurement at no load, no excitation.
- Take the generator up to 50 A on no-load and take a reading
- Take the generator to rated output voltage (340 V line) on no load and take a reading.

- Take the generator to 70 A with no-load and take a reading
- Bring the generator back to rated output voltage (at 62 A) and apply a 15 A (line) load, keeping the output voltage constant.
- Apply a 30 A (line) load, keep the output voltage constant.

Measurements were taken with the following eccentricities :

- 0 mm (all six bolts inserted)
- +0,65 mm
- +1,9 mm
- -3,1 mm

Where the negative indicates a horizontal eccentricity in the opposite direction.

7.5 Measured results

7.5.1 No Eccentricity

Table 7.2 presents the mini-gen output rms line voltage and the rms shaft voltage. This gives a clear indication of whether the shaft voltage was increasing or decreasing. These are all true rms values, as the shaft voltage in particular deviates quite significantly from a regular first harmonic sinusoid.

The most important result relevant to the diagnosis of static eccentricity is that in the case of no eccentricity, the shaft voltage rms magnitude does not vary greatly with loading when the output voltage is held constant.

Figure 7.5 is a plot of the shaft voltage using the recorded absolute angular position as a reference. This plot uses the technique detailed in *Chapter 4*. The periodicity and the harmonic content of the waveform can be seen. The high frequency ripple is attributed to the stator teeth.

Figure 7.6 shows the dominant frequency components in the shaft voltage.

Table 7.2: Measured rms voltages for no eccentricity

No load	<i>line (rms)</i>	<i>shaft (rms)</i>
No excitation :	9,95 V	0,0063 V
50 A excitation :	293,34 V	0,0455 V
Rated line voltage :	339,87 V	0,0775 V
70 A excitation :	364,18 V	0,0741 V

Half load		
Rated line voltage :	339,84 V	0,0777 V

Full load		
Rated line voltage :	342,03 V	0,0788 V

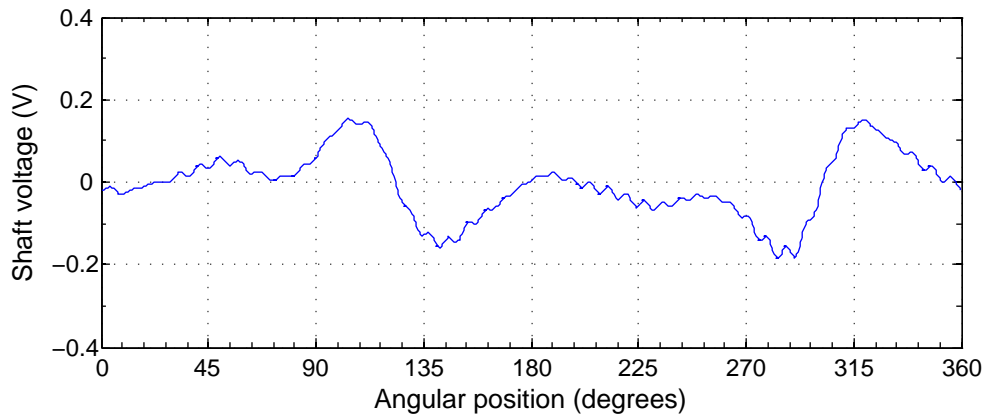


Figure 7.5: Position referenced average shaft voltage for no eccentricity and full load

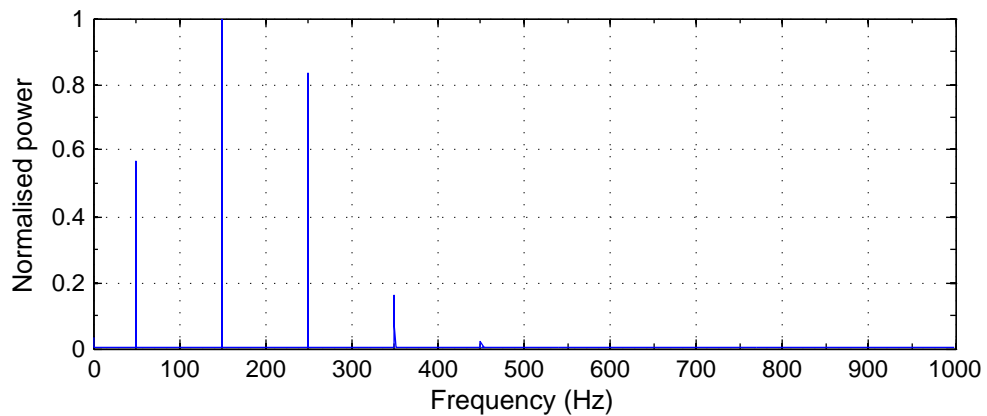


Figure 7.6: Normalised power spectrum of the shaft voltage for no eccentricity and full load

Table 7.3: Measured rms voltages for +0,65 mm eccentricity

No load	<i>line (rms)</i>	<i>shaft (rms)</i>
No excitation :	9,74 V	0,0039 V
50 A excitation :	300,90 V	0,0514 V
Rated line voltage :	339,55 V	0,0848 V
70 A excitation :	361,56 V	0,0844 V

Half load		
Rated line voltage :	341,14 V	0,0872 V

Full load		
Rated line voltage :	341,01 V	0,0879 V

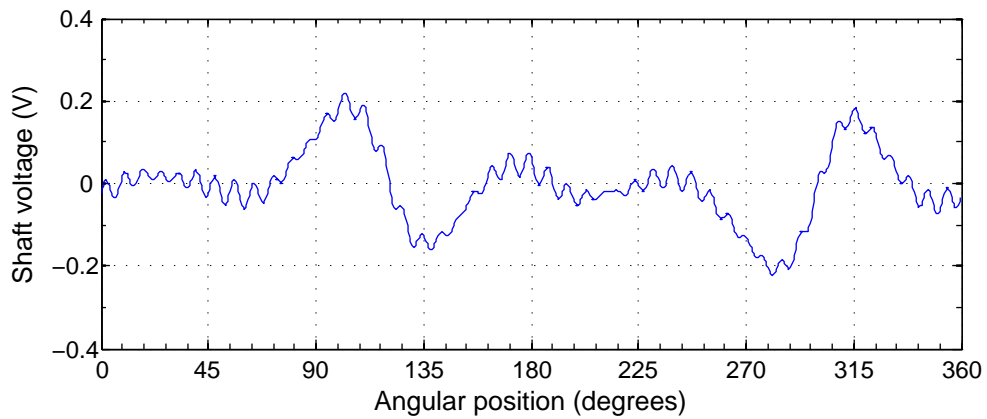


Figure 7.7: Position referenced average shaft voltage for +0,65 mm eccentricity and full load

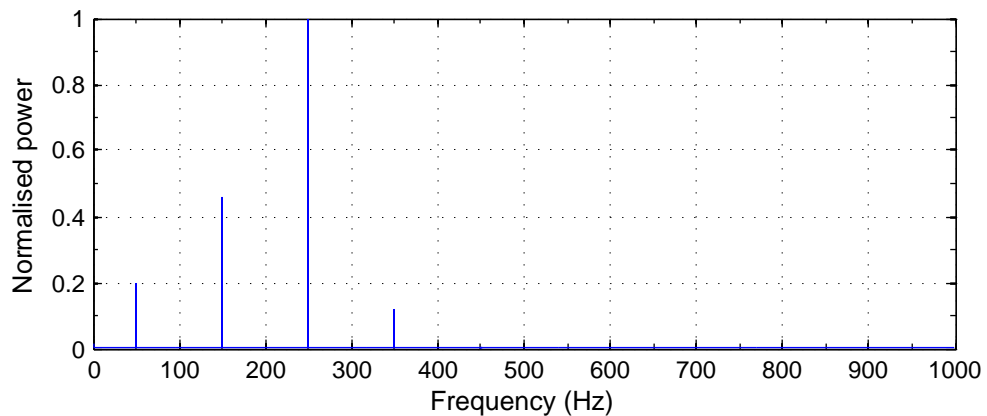


Figure 7.8: Normalised power spectrum of the shaft voltage for +0,65 mm eccentricity and full load

7.5.2 +0,65 mm eccentricity

A slight eccentricity of 0,65 mm was introduced and the same quantities as presented for the non-eccentric case are presented in *Table 7.3*, *Figures 7.7* and *7.8*.

The rms value of the shaft voltage has increased, and again there is only a small increase in the magnitude between the loaded and unloaded cases.

The power spectrum plot in *Figure 7.8* shows a substantial increase in the relative magnitude of the fifth harmonic when compared to the no eccentricity power spectrum in *Figure 7.6*.

7.5.3 +1,9 mm eccentricity

This is the highest eccentricity tested in the positive direction and the results are shown in *Table 7.4*, *Figures 7.9* and *7.10*.

The rms value of the shaft voltage has further increased while different loading still does not result in a substantial difference between the rms magnitudes. The fifth harmonic is now clearly visible in *Figure 7.9* and the ripple due to the stator teeth has also increased. The power spectrum plot in *Figure 7.10* illustrates the much-increased relative magnitude of the fifth harmonic.

7.5.4 -3,1 mm eccentricity

The stator was adjusted so as to reverse the orientation of the eccentricity. This is the largest eccentricity tested, and the same illustrations as before are given in *Table 7.5*, *Figures 7.11* and *7.12*.

Table 7.5 demonstrates the already established trend that an increase in eccentricity results in an increase in the rms value of the shaft voltage. Further, the loading of the generator is found not to have a significant impact on the rms magnitude of the shaft voltage.

The fifth harmonic is once again dominant in *Figure 7.12*, though curiously the first harmonic has increased in relative magnitude.

Table 7.4: Measured rms voltages for +1,9 mm eccentricity

No load	<i>line (rms)</i>	<i>shaft (rms)</i>
No excitation :	9,58 V	0,0048 V
50 A excitation :	294,29 V	0,0731 V
Rated line voltage :	340,70 V	0,1250 V
70 A excitation :	360,23 V	0,1289 V

Half load		
Rated line voltage :	339,78 V	0,1278 V

Full load		
Rated line voltage :	339,63 V	0,1311 V

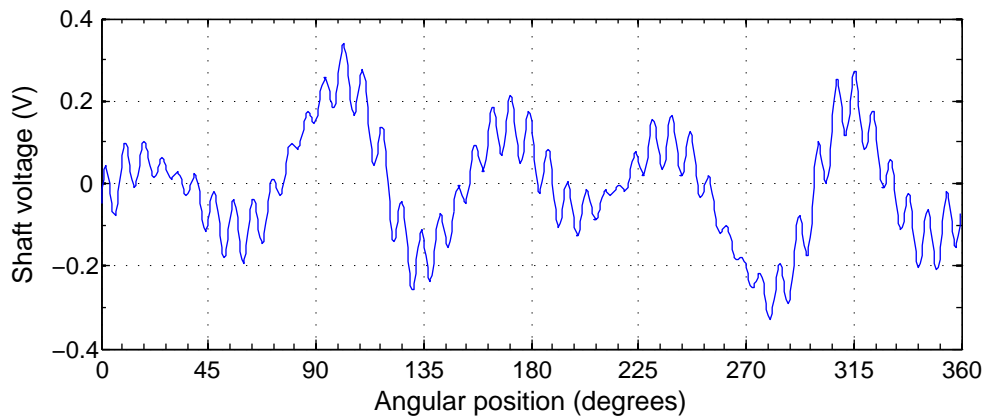


Figure 7.9: Position referenced average shaft voltage for +1,9 mm eccentricity and full load

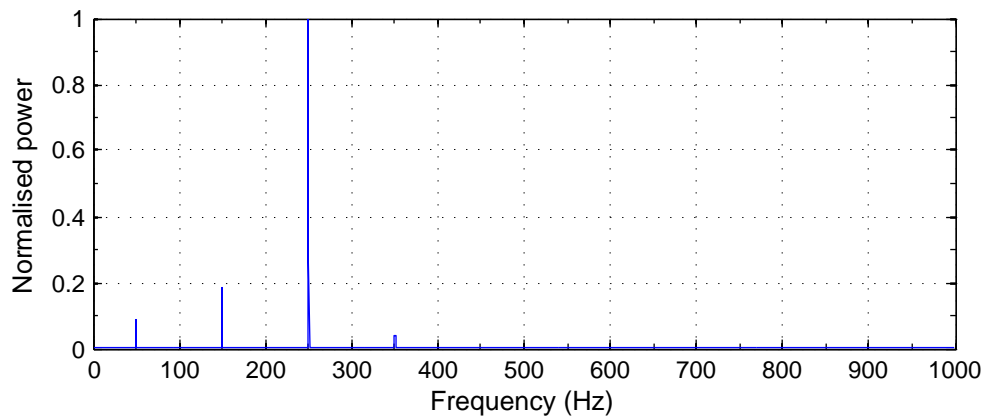
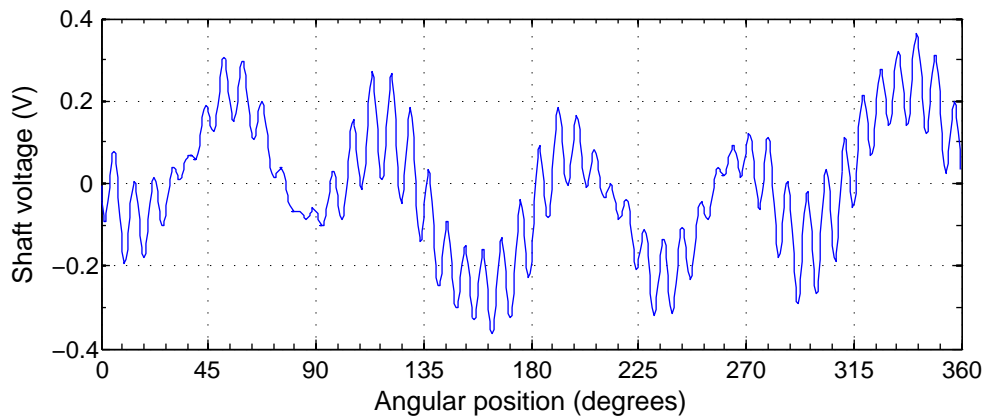
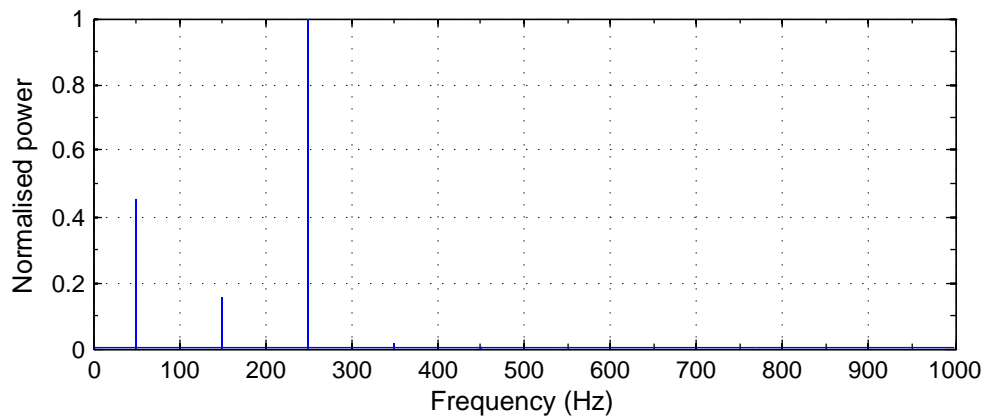


Figure 7.10: Normalised power spectrum of the shaft voltage for +1,9 mm eccentricity and full load

Table 7.5: Measured rms voltages for $-3,1$ mm eccentricity

No load	<i>line (rms)</i>	<i>shaft (rms)</i>
No excitation :	9,61 V	0,0073 V
50 A excitation :	296,11 V	0,0998 V
Rated line voltage :	341,49 V	0,1458 V
70 A excitation :	362,30 V	0,1537 V
Half load		
Rated line voltage :	340,70 V	0,1493 V
Full load		
Rated line voltage :	339,87 V	0,1534 V

Figure 7.11: Position referenced average shaft voltage for $-3,1$ mm eccentricity and full loadFigure 7.12: Normalised power spectrum of the shaft voltage for $-3,1$ mm eccentricity and full load

7.5.5 Waveform comparison

What is interesting is to now compare the relationship of shaft voltage waveform to the absolute shaft position, for the different eccentricities.

In *Figure 7.13* the shaft voltage waveform for the two positive eccentricities are laid one on another. It should be noted that the phase remains unchanged when simply increasing the eccentricity in a radial direction.

This is not the case in *Figure 7.14* where the shaft voltage waveforms from two eccentricities, one in a positive direction and the other in the radially opposite negative direction, are laid one on another. The one waveform is phase shifted 180° for the other, as one would expect. This observation leads to the possibility of developing a method to determine the direction of the shaft eccentricity from the relative phase of the harmonics.

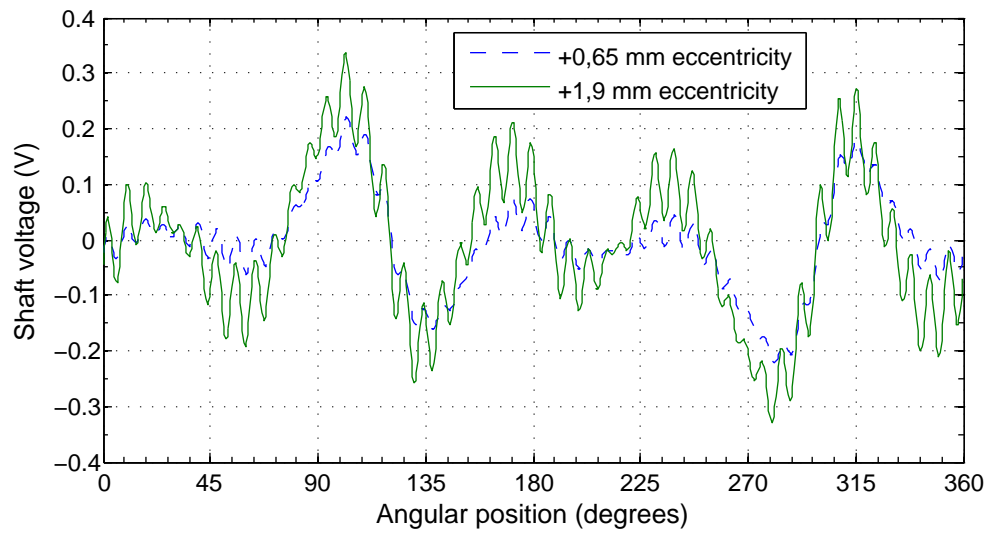


Figure 7.13: Position referenced average shaft voltage for +0,65 mm and +1,9 mm eccentricity at full load

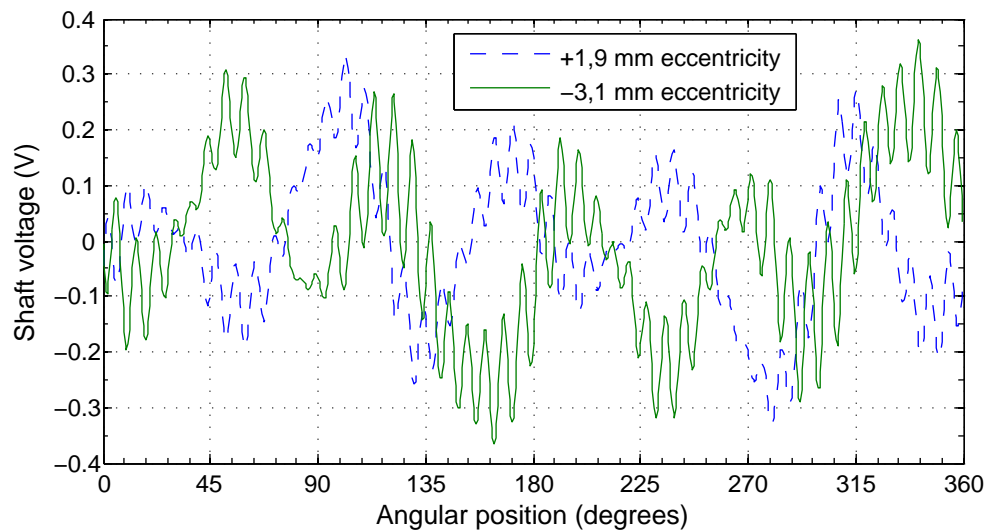


Figure 7.14: Position referenced average shaft voltage for +1,9 mm and -3,1 mm eccentricity at full load

7.6 Conclusion

The simulations in *Chapter 6* gave strong theoretical evidence of a static eccentricity influencing the shaft voltage by way of an increased fifth harmonic. This has been found to be entirely the case. Of further interest is the relative phase difference in the shaft voltages measured when the eccentricity is first in one direction and then in the opposite direction. This could possibly be used to determine the orientation of a shaft misalignment. Given that shaft voltages can be successfully captured, analysed and used to determine a simple fault such as static eccentricity, it is possible the further work in this field could provide a suite of techniques for diagnosing several different faults.

Chapter 8

Conclusion

8.1 Outcomes

After presenting a background to machine fault types and condition monitoring techniques, *Section 2.6* in *Chapter 2* gave the goals of this research project as follows:

1. Implement a measurement system for the test generator.
2. Investigate possible FEM based simulation of the test generator, in order that fault characteristics might be predicted using a simulation of a generator. This is an investigation and the actual use of FEM techniques is not a requirement.
3. Identify a methodology (or lack there-of) that enables the identification of the fault from the shaft-voltage waveform.

An effective measurement system has been developed and tested. Using the DSPACE™ DS1104 as its platform, it enables the capture of shaft voltage, additional probe measurements and the absolute angular position of the shaft. The measurement system is composed of three circuits: a power supply circuit, an anti-alias, amplifier and protection circuit for measuring the shaft voltage and a level shifter and isolator circuit for the incremental encoder used to measure the absolute shaft position. See *Chapter 3*.

Prior to the completion of the experimental mini-gen, experiments were conducted on a 4-pole synchronous generator and it was found that the shaft voltage waveform is periodic about a mechanical revolution and can be used to determine the angular position of the shaft. In order to do this, an extended capture of the shaft voltage

is required. An averaging technique is then used to determine a clean periodic waveform. See *Chapter 4* and [2].

The design of the experimental mini-gen was undertaken by Mr Alan Meyer and the design itself was not a primary concern of this research project, though naturally the mini-gen itself is central to the physical measurement of shaft signals under fault conditions. The design, specifications and operating characteristics are presented in *Chapter 5*. A key objective in the design of the mini-gen was to approximate the physical characteristics of a large 600 MVA turbo-generator. One of these characteristics is a large air-gap. The generator was operated at approximately 20 kW with an output voltage of 340 V and a rotor excitation current of 62 A. The very high excitation current was necessitated by the disproportionately large air-gap, and with the current cooling system the rotor exceeds safe operating temperatures in 20 minutes.

When this project was conceived it was doubtful whether a shaft voltage could be simulated, and hence the success of FEM simulations was not a required outcome. This notion has been turned on its head, so to speak! Multi-step/transient simulations using MAXWELL 2D™ were found to be highly capable of simulating shaft voltage for the fault type of interest (namely static eccentricity). Simulations were used to not only predict shaft voltage as a result of static eccentricity, but also as a result of different physical geometries and rotor-bar inclusion and exclusion. See *Chapter 6*.

This led to a methodology for the identification of static eccentricity. It was observed in simulations that a static eccentricity resulted in an increase of the 5th harmonic in the shaft voltage. This was verified with physical measurements on the completed experimental mini-gen. See *Chapter 7*.

8.2 Recommendations for future research

This project has formed the first step in what is hoped to be a new avenue of research and research-capability in the School of Electrical and Information Engineering at Wits University. Some recommendations for future research in the field of shaft signals and of synchronous generator condition monitoring are outlined below.

- Create a portable instrument which can be taken out into the field. It is important to capture as long a sample period as possible in order to perform

averaged time-domain analysis.

- Obtain full design details of the stators and rotors as employed at one or two of Eskom's power stations and arrange to perform measurements there on a regular basis.
- Perform transient simulations of faults on both the mini-gen and the full-size units and compare both averaged time domain and frequency domain.
- Execute further faults on the mini-gen and compare with mini-gen simulations. The fault of immediate interest is a rotor shorted-turn.
- By taking into account additional components attached to a full size turbo-generator shaft (essentially just the steam turbine), consider what signal components are as a result of the turbine, and what is as a result of the electrical generator.
- Can phase and magnitude of the shaft voltages be predicted by maths of feasible complexity, without resorting to an FEM model?
- Patents and papers already exist for the use of shaft voltage and current as a diagnostic tool. However, the focus is typically on simply observing medium to long term trends in the waveform. There is room for the use of FEM simulation as a predictive tool of how a particular fault in the machine will manifest. The shaft measurements are then compared against this in a time, frequency, or perhaps other domains such as short-time frequency or wavelet.

References

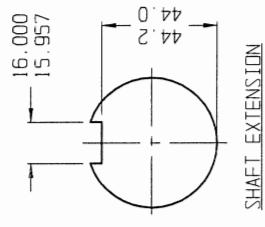
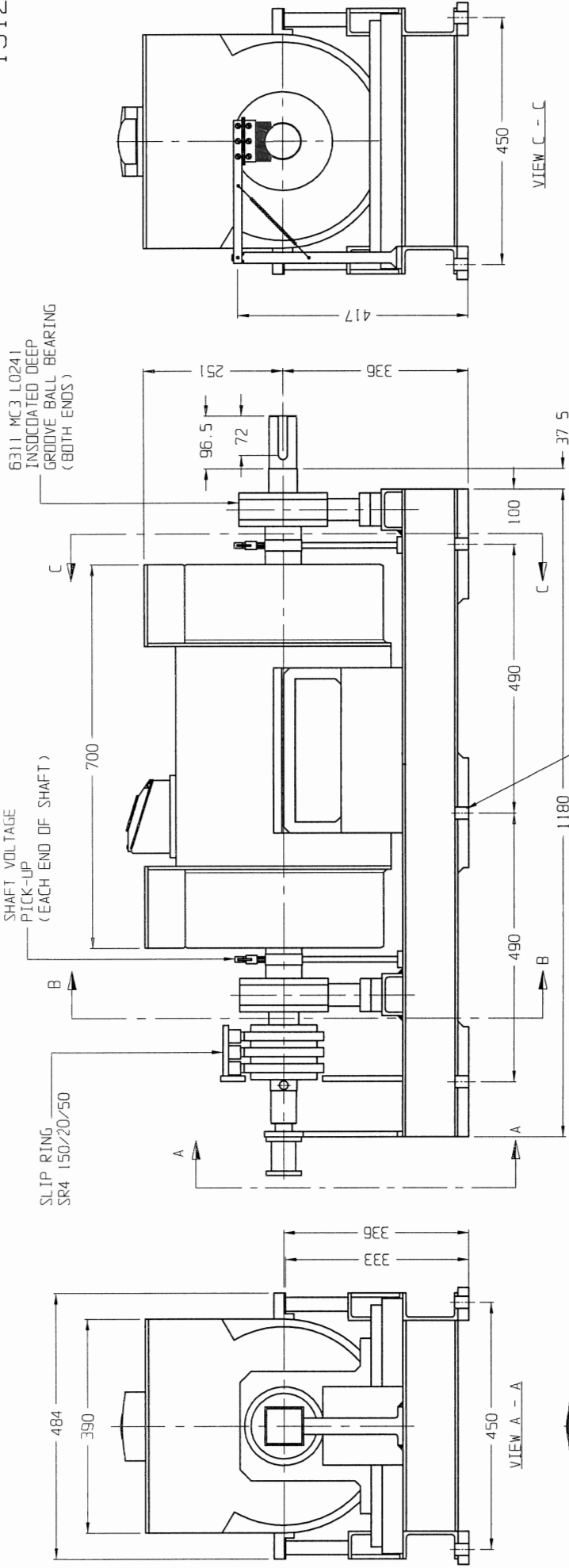
- [1] Ansoft Corporation. *Maxwell 2D Version 11 - Online Help*, 2005.
- [2] Simon J. Hoffe, Alan S. Meyer, and Willie A. Cronje. Determination of shaft position from shaft voltage on a synchronous generator. In *Proc. IEEE SDEMPED '05*, pages 291–294, Vienna, Austria, Sep 2005.
- [3] Peter J. Tavner and James Penman. *Condition Monitoring of Electrical Machines*. Research Studies Press Ltd, John Wiley & Sons Inc., Chichester, West Sussex, England, 1987.
- [4] Peter Vas. *Parameter Estimation, Condition Monitoring, and Diagnosis of Electrical Machines*. Oxford University Press, 1993.
- [5] P. L. Alger and W. Samson. Shaft currents in electric machines. *AIEE Trans.*, pages 235–245, Feb 1924.
- [6] C. Ammann, K. Reichert, R. Joho, and Z. Posedel. Shaft voltages in generators with static excitation systems – problems and solution. *IEEE Trans. Energy Conversion*, 3(2):409–419, Jun 1988.
- [7] Michael J. Costello. Shaft voltages and rotating machinery. *IEEE Trans. Energy Conversion*, 29(2):419–426, Mar 1993.
- [8] S. P. Verma, R. S. Girgis, and R. J. Fleming. Shaft potentials and bearing currents in modern turbogenerators: Damages and means of prevention. In *Spring Meeting of the Canadian Electrical Association*, Toronto, Ontario, Mar 1981.
- [9] Sang Bin Lee, Gerald Kliman, Manoj Shah, Dongwook Kim, Tony Mall, Kutty Nair, and Mark Lusted. Experimental study of inter-laminar core fault detection techniques based on low flux core excitation. In *Proc. IEEE SDEMPED '05*, pages 163–171, Vienna, Austria, Sep 2005.
- [10] FAG. Mounting of ball and roller bearings. FAG Bearing Company South Africa (Pty) Ltd. Booklet code 1695 E/65/1/9a/1.

- [11] Doyle Busse, Jay Erdman, Russel J. Kerkman, Dave Schlegel, and Gary Skibinski. System electrical parameters and their effects on bearing currents. *IEEE Trans. Ind. Applicat.*, 33(2):577–584, Mar 1997.
- [12] Olivier Chadebec, Viet Phuong Bui, Pierre Granjon, Laure-Line Rouve, Nicholas Le Bihan, and Jean-Louis Coulomb. Rotor fault detection of electrical machines by low frequency magnetic stray field analysis. In *Proc. IEEE SDEMPED '05*, pages 191–196, Vienna, Austria, Sep 2005.
- [13] Raymond Ong, J. H. Dymond, and R. D. Findlay. A comparison of techniques for measurement of shaft currents in rotating machines. *IEEE Trans. Energy Conversion*, 12(4):363–367, Dec 1997.
- [14] Paul I. Nippes. Early warning of developing problems in rotating machinery as provided by monitoring shaft voltages and grounding currents. *IEEE Trans. Energy Conversion*, 19(2):340–345, Jun 2004.
- [15] John S. Hsu and Jan Stein. Effects of eccentricities on shaft signals studied through windingless rotors. *IEEE Trans. Energy Conversion*, 9(3):564–571, Sep 1994.
- [16] John S. Hsu and Jan Stein. Shaft signals of salient-pole synchronous machines for eccentricity and shorted-field-coil detections. *IEEE Trans. Energy Conversion*, 9(3):572–578, Sep 1994.
- [17] Jean-Éric Torlay, Chantal Corenwinder, Alain Audoli, Joël Hérigault, and Albert Foggia. Shaft voltage analysis: A new generator diagnostic tool. In *Proc. ICEM '98*, pages 396–401, Sep 1998.
- [18] Jean-Éric Torlay, Chantal Corenwinder, Alain Audoli, Joël Hérigault, and Albert Foggia. Analysis of shaft voltages in large synchronous generators. In *Proc. IEEE IEMDC '99*, pages 607–609, May 1999.
- [19] P. I. Nippes. Shaft voltage current monitoring system for early warning and problem detection. U. S. Patent 6,460,013, Oct 1 2002.
- [20] Paul Horowitz and Winfield Hill. *The Art of Electronics*. Cambridge University Press, second edition edition, 1989.
- [21] S. A. Higgins. Shaft earthing brush comparison carried out on eskom's generators. In *Iris Rotating Machine Conference*, San Antonio, Texas, Jun 2002.

Appendix A

Minigen drawings

19125



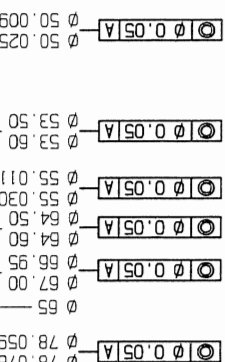
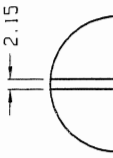
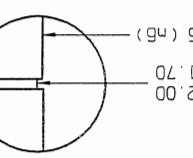
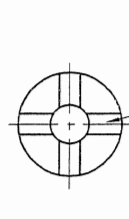
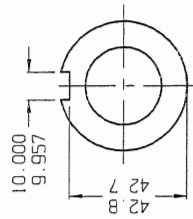
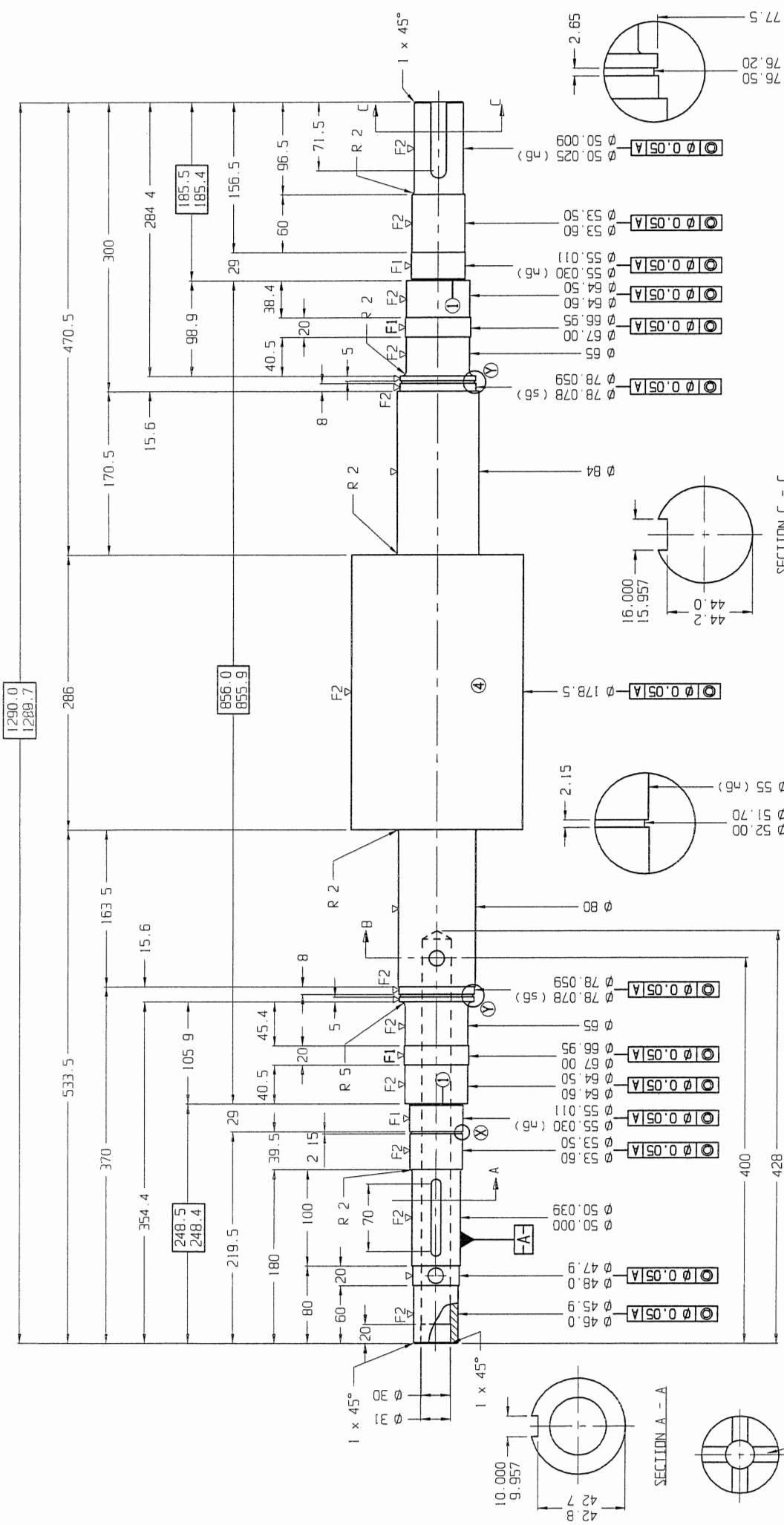
APPROVED

<p>Trans Vaal Electric (pty. ltd.)</p> <p>THIS DRAWING IS THE EXCLUSIVE PROPERTY OF TRANSSAAL ELECTRIC AND MAY NOT BE REPRODUCED BY , OR PASSED ON TO ANY THIRD PARTY , EXCEPT WITH THE PERMISSION OF THE COMPANY</p>		<p>FINISH SYMBOL μm 0 001mm</p> <table border="1"> <thead> <tr> <th>μm</th> <th>FINISH DESCRIPTION</th> </tr> </thead> <tbody> <tr> <td>F1 0.3</td> <td>GRIND OR EQUAL</td> </tr> <tr> <td>F2 0.8</td> <td>SMOOTH MACHINE</td> </tr> <tr> <td>F3 1.6</td> <td>MEDIUM MACHINE</td> </tr> <tr> <td>F4 3.2</td> <td>ROUGH MACHINE</td> </tr> </tbody> </table> <p>SCALE: 1 T S IF IN DOUBT ASK</p>		μ m	FINISH DESCRIPTION	F1 0.3	GRIND OR EQUAL	F2 0.8	SMOOTH MACHINE	F3 1.6	MEDIUM MACHINE	F4 3.2	ROUGH MACHINE	<p>FLAMEPROOF PATH THESE SURFACES MUST BE FREE FROM TOOLMARKS AND BURRS</p>		<p>OUTLINE DIMENSIONS</p> <p>TYPE 15460 A</p> <p>EXPERIMENTAL</p> <p>MINI-GENERATOR</p>	
μ m	FINISH DESCRIPTION																
F1 0.3	GRIND OR EQUAL																
F2 0.8	SMOOTH MACHINE																
F3 1.6	MEDIUM MACHINE																
F4 3.2	ROUGH MACHINE																
REV	DESCRIPTION	CHKD	DATE	<p>DRAWN BY: M. R. (CHKD) APPR</p> <p>DATE 07/10/2004</p> <p>19125</p>													

19086

MATERIAL:
709 M 40 (EN 19T)

O.D. = 180 L = 1300



2 - HOLES
DRILL Ø 16 THRU'
AS SHOWN

SECTION B - B

SECTION C - C

DETAIL X

DETAIL Y

NOTE 1:
A1.6W411 UNDERCUTS

NOTE 2:
BREAK ALL SHARP CORNERS 0.5 x 45°

NOTE 3:
ALL UNSPECIFIED MACHINING F3

NOTE 4:
FOR ROTOR MACHINING SEE DRG 19087

TRANSVAAL ELECTRIC (PTY.) LTD.

THIS DRAWING IS THE EXCLUSIVE PROPERTY OF TRANSVAAL ELECTRIC AND MAY NOT BE REPRODUCED BY OR PASSED ON TO ANY THIRD PARTY EXCEPT WITH THE PERMISSION OF THE COMPANY

FINISH SYMBOL	um	FINISH DESCRIPTION
F1	0.8	GRIND OR EQUAL
F2	1.6	SMOOTH MACHINE
F3	3.2	MEDIUM MACHINE
F4	6.4	ROUGH MACHINE

SCALE: N T S IF IN DOUBT ASK

REV	DESCRIPTION	CHKD	DATE

FLAMEPROOF PATH
THESE SURFACES MUST BE FREE FROM TOOLMARKS AND BURRS

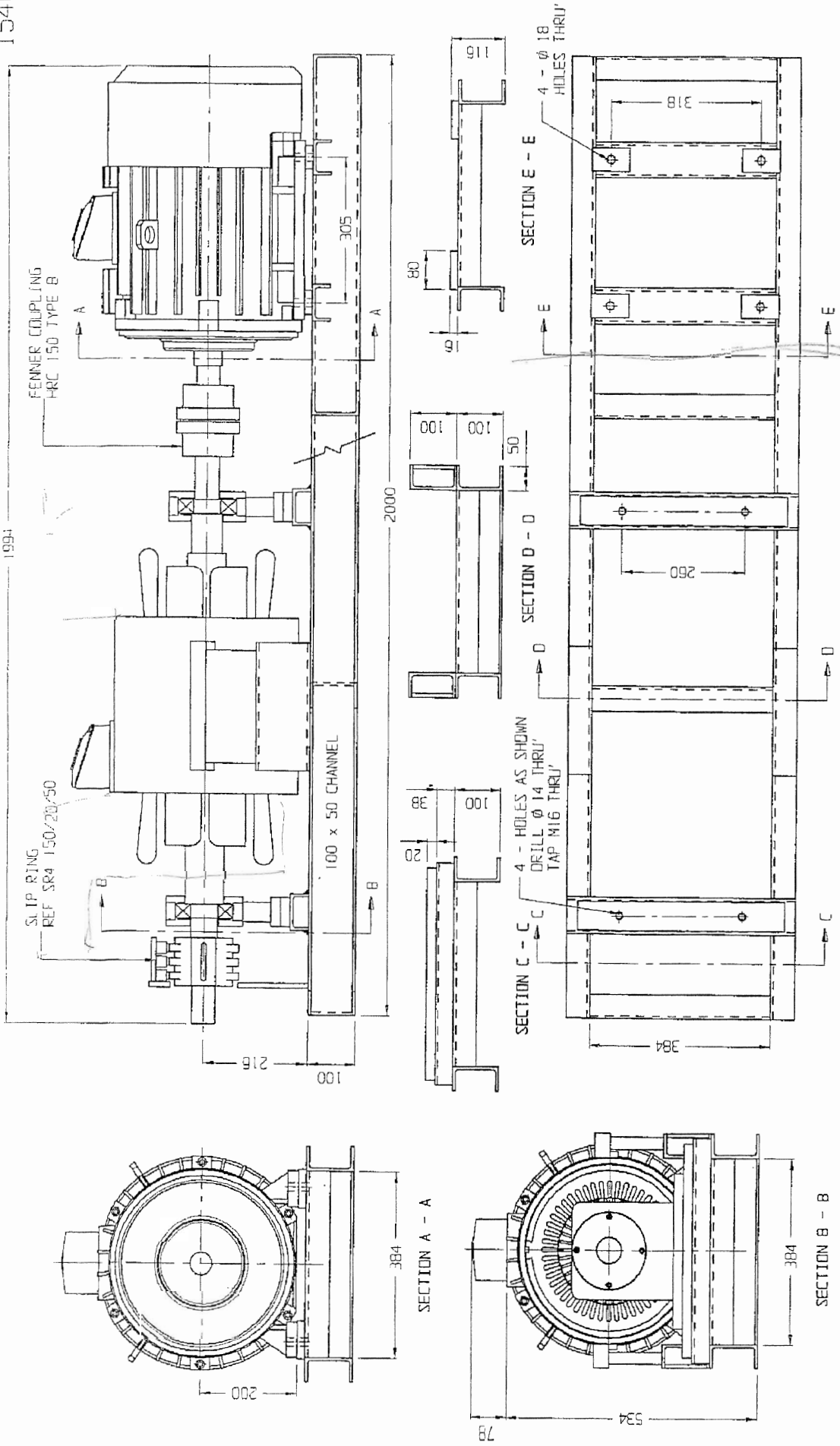
SHAFT & ROTOR MACHINING

TYPE 15460

DRAWN BY: M.R. CHKD: APPR: DATE: 01/10/2004

19086

15460



15460

ALTERNATOR LAYOUT

WITS UNIVERSITY

MOTOR - ALTERNATOR SET

TYPE 15460

DATE 30/06/2004

APPR

CHKD

FLAMEPROOF PATH

THESE SURFACES MUST BE FREE FROM TOOL-MARKS AND BURRS

REV	DESCRIPTION	CHKD	DATE

FINISH SYMBOL in 0.001mm

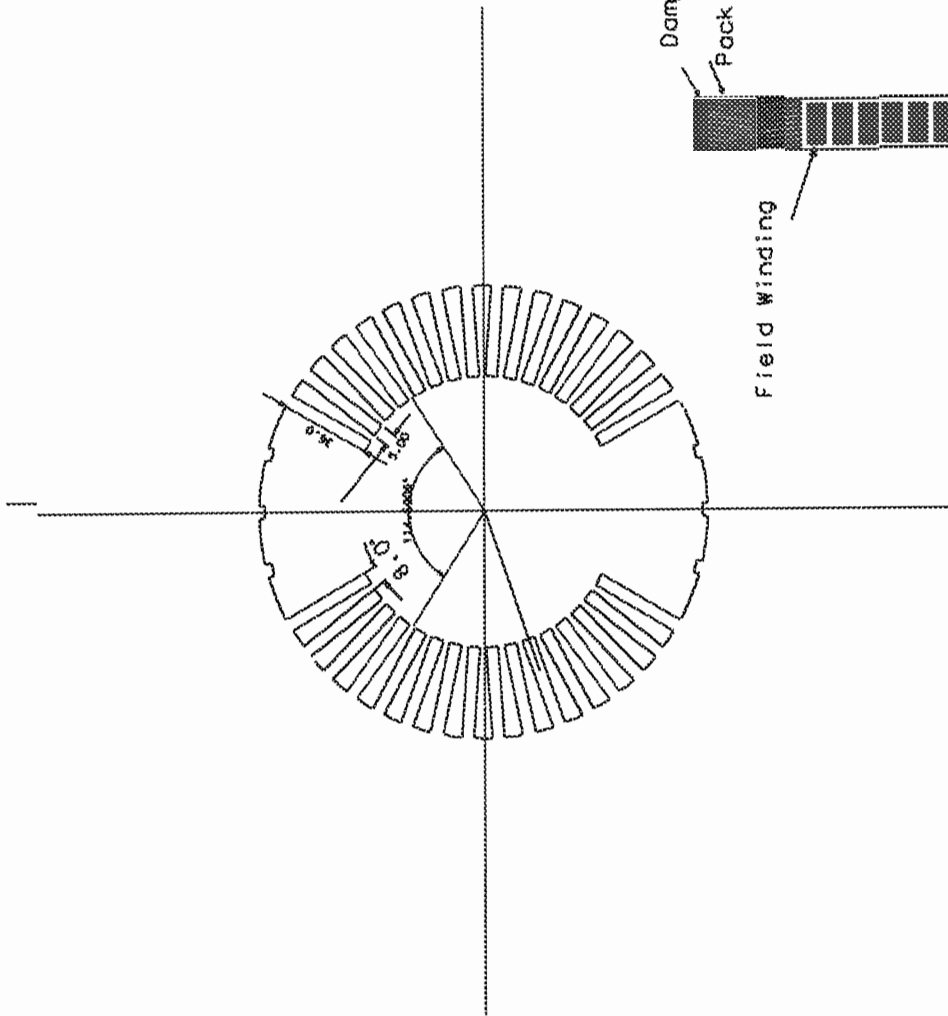
SYMBOL	FINISH DESCRIPTION
F1	GRIND OR EQUAL
F2	SMOOTH MACHINE
F3	REWORK MACHINE
F4	ROUGH MACHINE

SCALE: 1:1 IF NOT INDICATED

TRANSVAAL ELECTRIC (PTY) LTD.

THIS DRAWING IS THE EXCLUSIVE PROPERTY OF TRANSVAAL ELECTRIC AND MAY NOT BE REPRODUCED, COPIED, OR PASSED ON TO ANY THIRD PARTY, EXCEPT WITH THE PERMISSION OF THE COMPANY.

17737



Damper bar

Packing [to allow for enlarging airgap]

Field Winding



STATOR SLOT 1948-T
TOOL No: 321

Appendix B

Matlab source code

B.1 Introduction

The following source code listings are given :

sjh_process_sims.m This script is used to process simulation results. The script must be edited to achieve the desired plots and comparisons on each execution. It makes use of the `sjhspec` and `loaddat` functions (listed below).

sjh_process_measured.m This script is used to process measured results. The script must be edited to achieve the desired plots and comparisons on each execution. It makes use of the `sjhspec` and `loadmeas` functions (listed below).

sjhspec.m This is general purpose function used to generate a frequency spectrum from time domain data. It allows different windows types and lengths to be used as well as options in terms of normalising, decibel scale and others.

loaddat.m This function loads data out of a `.dat` file generated by the Maxwell transient solver.

loadmeas.m This function loads data out of a `.mat` file generated by dSpace from measured signals.

loadsig.m This function produces the same form of output from either a simulation or a measured data file, enabling easy comparison.

ave_data.m This function performs the averages time domain data against a position reference, removing noise and producing a position-periodic signal.

rmssim.m This function calculates the RMS value of a time-domain sample using trapezoidal integration.

B.2 sjh_process_sims.m

```

1 % Process simulated results, by editing this script various simulated
2 % outputs can be lined up next to one another for comparison.
3
4 % PROJECT NAME      mm OFFSET
5 %
6 % gen_norm          0
7 % gen_eccen_3       0.25
8 % gen_eccen_4       0.5
9 % gen_eccen_2       2.5
10 % gen_eccen_cut     4
11 % gen_eccen         5
12
13 %%
14 clear all;
15
16 condition = 'fullload';
17 %condition = 'slowrot';
18 datatype = 'extnl_v';
19 plotparam = 'v_shaft';
20
21 tests = { 'norm', 'eccen_3', 'eccen_4', 'eccen_2', 'eccen' };
22 %tests = { 'norm', 'eccen_4', 'eccen_4_lores' };
23 numtests = length(tests);
24 Ydata = [ 0; 0.25; 0.5; 2.5; 5];
25 %Ydata = [ 0; 1; 2 ];
26
27 XLabel = 'Freq (Hz)';
28 YLabel = 'Offset (mm)';
29 ZLabel = 'Normalised Power (dB)';
30
31 StopFreq = 3000;
32
33 % Load data out of files
34 clear data;
35 data = cell(numtests,1);
36
37 for ct = [1:numtests]
38     t = char(tests(ct));
39
40     estr = [ 'temp = loaddat(''gen_', ...
41             condition, '/gen_', t, '.pjt/', datatype, '.dat'', 0.04);'];
42     eval(estr)
43
44     estr = [ 'data(ct) = {temp.', plotparam, '};' ];
45     eval(estr);
46     clear temp;

```

```

47 end
48
49 clear estr
50 clear cc c ct t cd d
51
52 %%
53 maxlen = -inf;
54 maxSpan = -inf;
55 minT = inf;
56
57 for i = [1:numtests]
58     T = data{i}(2,1) - data{i}(1,1);
59     minT = min(minT, T);
60     maxSpan = max(maxSpan, T * length(data{i}(:,1)));
61 end
62
63 maxlen = ceil(maxSpan / minT);
64
65 %%
66 window = @hann;
67
68 % Resample all vectors to the same length
69 % but Window them first!
70 for i = [1:numtests]
71     T = data{i}(2,1) - data{i}(1,1);
72     oldlen = length(data{i});
73
74     p = round(oldlen * (T / minT));
75     q = oldlen;
76
77     data{i}(:,2) = data{i}(:,2) .* window(oldlen);
78
79     y = data{i}(:,2);
80     x = data{i}(:,1);
81
82     if p ~= q
83         y = resample(y, p,q);
84         x = linspace(x(1), x(end), length(y))';
85     end
86
87     y = [ y ; zeros(maxlen - length(y),1) ];
88     x = [ x ; [1:1:maxlen - length(x)]' * (x(2) - x(1)) + x(end)];
89
90     data(i) = {[x, y]};
91 end
92
93 %%
94 %figure;
95 %for i = [1:numtests]
96 %    plot(data{i}(:,1), data{i}(:,2));
97 %    hold all;
98 %end
99
100 %%
101 NFFT = 2^ceil(log(maxlen)/log(2));

```

```

102
103 % Convert to frequency data
104 spec_opt.dB = 0;
105 spec_opt.Norm = 0;
106 spec_opt.DCremove = 0;
107
108 clear s; s = cell(numtests,1);
109 clear f; f = cell(numtests,1);
110 for i = [1:numtests]
111     clear st; clear ft;
112     [st ft] = sjhspec(data{i}, spec_opt, @rectwin, NFFT);
113     s(i) = {st};
114     f(i) = {ft};
115 end
116
117 StopIdx = ceil((StopFreq / f{1}(end)) * length(f{1}));
118
119 for i = [1:numtests]
120     s(i) = {s{i}(1:StopIdx)};
121     f(i) = {f{i}(1:StopIdx)};
122 end
123
124
125
126 %%
127 %MAX = -inf;
128 %for i = [1:numtests]
129 %    MAX = max([MAX; s{i}]);
130 %end
131 %
132 %for i = [1:numtests]
133 %    s(i) = {10*log10(s{i} ./ MAX)};
134 %end
135
136 %%
137 x = f{1};
138 y = Ydata(1:numtests);
139 [X,Y] = meshgrid(x,y);
140 Z = zeros(length(y), length(x));
141 for i = [1:numtests]
142     Z(i,:) = s{i};
143 end
144
145 %%
146 fh = figure;
147 mesh(X, Y, Z);
148 axis tight;
149 set (gca, 'XScale', 'lin');
150 h = xlabel(XLabel);
151 set (h, 'Interpreter', 'none');
152 h = ylabel(YLabel);
153 set (h, 'Interpreter', 'none');
154 zlabel(ZLabel);
155 h = title([condition, '.', datatype, '.', plotparam]);
156 set (h, 'Interpreter', 'none');

```



```

157 colormap hsv
158 colorbar
159
160 %%
161 figure;
162 plot3(X', Y', Z');
163 axis tight;
164 set (gca, 'XScale', 'lin');
165 h = xlabel(XLabel);
166 set (h, 'Interpreter', 'none');
167 h = ylabel(YLabel);
168 set (h, 'Interpreter', 'none');
169 zlabel(ZLabel);
170 h = title([condition, '.', datatype, '.', plotparam]);
171 set (h, 'Interpreter', 'none');

```

B.3 sjh_process_measured.m

```

1 % Process measured results, by editing this script various measured
2 % outputs can be lined up next to one another for comparison.
3
4
5 %%
6 clear all;
7
8 experiment = 'eccen2';
9
10 cd(['Z:\', experiment]);
11
12 prefix = [experiment, '.'];
13
14 tests = { 'fl_rv' };
15 %tests = { 'nl_fe_40hz', 'nl_fe_45hz', 'nl_fe_48hz', 'nl_fe', 'nl_fe_52hz', } ;
16 %tests = { 'nl_ne', 'nl_he', 'nl_40e', 'nl_50e', 'nl_fe' } ;
17 %tests = { 'nl_fe', 'fl_fe' } ;
18 Ynum = 3;
19 numtests = length(tests);
20 Ydata = [0:numtests-1]*1+1;
21
22 XLabel = 'Freq (Hz)';
23 YLabel = 'Offset (mm)';
24 ZLabel = 'Normalised Power (dB)';
25
26 StopFreq = 500;
27 PointsLimit = inf;
28
29 % Load data out of files
30 clear data;
31 clear tempX tempY;
32 data = cell(numtests,1);

```

```

33
34 for ct = [1:numtests]
35     t = char(tests(ct));
36
37     load(t);
38
39     estr = [ 'datalen = length(', t, '.X(1).Data);'];
40     eval(estr)
41     datalen = min([datalen PointsLimit]);
42     estr = [ 'data{ct} = zeros(datalen,2);'];
43     eval(estr)
44     estr = [ 'data{ct}(:,1) = ', t, '.X(1).Data(1:datalen);'];
45     eval(estr)
46     estr = [ 'data{ct}(:,2) = ', t, '.Y(Ynum).Data(1:datalen);'];
47     eval(estr)
48     estr = [ 'clear ', t, ',' ];
49     eval(estr);
50 end
51
52 clear estr
53 clear cc c ct t cd d
54
55 %%
56 % Convert to frequency data
57 spec_opt.dB = 0;
58 spec_opt.Norm = 0;
59 spec_opt.DCremove = 1;
60
61 clear s; s = cell(numtests,1);
62 clear f; f = cell(numtests,1);
63 clear st; clear ft;
64
65 for i = [1:numtests]
66     [st ft] = sjhspec(data{i}, spec_opt);
67     s(i) = {st};
68     f(i) = {ft};
69     clear st; clear ft;
70 end
71
72
73 for i = [1:numtests]
74     StopIdx = min(...
75         ceil((StopFreq / f{i}(end)) * length(f{i})),...
76         length(f{i}));
77     s(i) = {s{i}(1:StopIdx)};
78     f(i) = {f{i}(1:StopIdx)};
79 end
80
81
82
83 %%
84 % Normalise and/or convert to dB
85 % MAX = -inf;
86 % for i = [1:numtests]
87 %     MAX = max([MAX; s{i}]);

```

```

88 % end
89 %
90 % for i = [1:numtests]
91 %   s(i) = {10*log10(s{i} ./ MAX)};
92 % end
93
94 %%
95 %% Cutoff lower end
96 % for i = [1:numtests]
97 %   s(i) = {max(s{i}, -100)};
98 % end
99
100
101
102 %%
103 %figure;
104
105 for i = [1:numtests]
106     plot3(f{i}, ones(size(f{i})) .* Ydata(i), s{i});
107     hold all;
108 end
109
110 axis tight;
111 grid on;
112 set (gca, 'XScale', 'lin', 'YTickLabel', [], 'YTickLabelMode', 'Manual');
113 h = xlabel(XLabel);
114 set (h, 'Interpreter', 'none');
115 %h = ylabel(YLabel);
116 %set (h, 'Interpreter', 'none');
117 zlabel(ZLabel);
118 h = title('Measured Data');
119 set (h, 'Interpreter', 'none');
120
121 for i = [1:numtests]
122     text(0,Ydata(i),0, [prefix, tests{i}, '  '], 'HorizontalAlignment', 'right', 'Interpreter', 'none');
123 end

```

B.4 sjhspec.m

```

1 function [s,f]=sjhspec(dat, options, window, NFFT)
2 %function [s,f]=sjhspec(dat, options, windows, NFFT)
3 %
4 % Where dat is a 2 column matrix (time and signal)
5 % Returns spectrum in s and frequency in f
6 %
7 % This is a configurable frequency spectrum calculator, depending on the
8 % options it can remove the DC component, normalise the output, plot the
9 % output in dB and produce a power spectrum. The window used and the length
10 % of the FFT window are also configurable. It is used extensively by many
11 % other data processing scripts.
12

```

```

13 opt.DCremove = 1;
14 opt.Norm = 1;
15 opt.dB = 1;
16 opt.Power = 1;
17
18 if ~exist('options', 'var')
19     options = opt;
20 else
21     if isfield(options, 'DCremove')
22         opt.DCremove = options.DCremove;
23     end
24
25     if isfield(options, 'Norm')
26         opt.Norm = options.Norm;
27     end
28
29     if isfield(options, 'dB')
30         opt.dB = options.dB;
31     end
32
33     if isfield(options, 'Power')
34         opt.Power = options.Power;
35     end
36 end
37
38
39 if nargin==0
40     error('No input vector given');
41 end
42
43 % Get the time vector
44 t = dat(:,1);
45
46 % Find the sampling frequency
47 fs = 1/(t(2) - t(1));
48
49 % Get the data vector
50 y = dat(:,2);
51 datlen = length(y);
52
53 if ~isa('window', 'function_handle')
54     window = @hann;
55 end
56
57 if ~exist('NFFT', 'var')
58     % Get the closest length of a radix 2 FFT
59     NFFT = 2^ceil(log(datlen)/log(2));
60 end
61
62 % Make the window
63 win = window(datlen);
64 %win = ones(datlen, 1);
65
66 %Remove offset
67 if opt.DCremove

```

```

68     dc_offs = mean(y);
69     y = y - dc_offs;
70 end
71
72 %Apply window and pad with zeros to NFFT length
73 y = [ y .* win ; zeros(NFFT - datlen , 1) ];
74
75 Y = fft(y);
76
77 % Only interested in the first half (and a bit) of the FFT
78 Y = Y(1:NFFT/2+2);
79
80 % Get the power spectrum
81 if opt.Power
82     Yout = Y .* conj(Y) / NFFT;
83 else
84     Yout = Y / NFFT;
85 end
86
87 %Normalise the power spectrum to max 1
88 if opt.Norm
89     Yout = Yout ./ max(Yout);
90 end
91
92 %Convert to dB
93 if opt.dB
94     Yout = 10 * log10(Yout);
95 end
96
97 % Create the frequency scale
98 f = [fs * (0:length(Yout)-1) / NFFT]';
99
100 % Assign the spectrum output
101 s = Yout;
102
103 if nargout==0
104     plot(f,s);
105     if opt.dB
106         ylabel('Power Spectrum [dB]');
107     else
108         ylabel('Magnitude');
109     end
110     xlabel('Frequency');
111     grid on;
112 end

```

B.5 loaddat.m

```

1 function [out] = loaddat(fn, skiptime)
2 % function [out] = loaddat(fn, skiptime)
3 %

```

```

4 % Load a .dat file as produced by Maxwell
5
6 out = [ ];
7 if (~exist('fn','var'))
8     disp('You must specify a filename');
9     return
10 end
11
12 if (~exist('skiptime', 'var'))
13     skiptime = [ ];
14 end
15
16 [fid,msg] = fopen(fn, 'r');
17 if fid == -1
18     % Maxwell can compress a project, which basically means compressing
19     % every file and adding a .Z to its extension. The code here
20     % transparently handles this, decompressing data files if need be.
21     % Note that the compress tool from unixutils is required.
22     zfn = [fn '.Z'];
23     [fid,msg] = fopen(zfn, 'r');
24     if fid == -1
25         disp([fn ' not found!']);
26         return
27     end
28
29     fclose(fid);
30     syscmd = 'c:\unixutils\usr\local\wbin\compress -d -c';
31
32     [status,msg] = dos([syscmd ' ' zfn ' >' fn]);
33     if status == 0
34         delete(zfn);
35     else
36         disp(['Decompression failed with status ' int2str(status)]);
37         disp(msg);
38         return;
39     end
40 else
41     fclose(fid);
42 end
43
44
45 [fid,msg] = fopen(fn, 'r');
46 if (fid == -1)
47     disp(['Error loading file ''' , fn, ''']);
48     disp (msg);
49     return
50 end
51
52 % File is now successfully opened, iterate through it pulling the data into
53 % a Matlab structure based on the names stored in the data file.
54 out = [ ];
55 out.title = fgetl(fid);
56 out.xlabel = fgetl(fid);
57 out.ylabel = fgetl(fid);
58

```

```

59 data = [ ];
60
61 while (feof(fid) == 0)
62     tline = fgetl(fid);
63     if tline
64         if any (isstrprop(tline(1), 'alpha'))
65             name = regexp(tline, ' ', '_');
66             estr = [ 'out.', name, ' = data;'];
67             disp(estr);
68             eval(estr);
69             data = [ ];
70         else
71             newentry = [ sscanf(tline, '%g %g', [2 1]) ]';
72             if skiptime
73                 if newentry(1) > skiptime
74                     data = [ data ; newentry ];
75                 end
76             else
77                 data = [ data ; newentry ];
78             end
79         end
80     end
81 end
82
83 % Take care of the case where there's only one unlabeled data set in the
84 % file
85 if length(data) ~= 0
86     disp('out.data = data;');
87     out.data = data;
88 end

```

B.6 loadmeas.m

```

1 function struct = loadmeas(filename, PointsLimit)
2 % function struct = loadmeas(filename, PointsLimit)
3 %
4 % This is a utility function to pull information out of a measured data file
5 % produced by dSpace and put it into a structure which can be manipulated
6 % with Matlab. The frequency spectrum is also calculated and stored in the
7 % structure.
8
9 StopFreq = 3000;
10
11 % Load data out of files
12 clear struct;
13
14 if ~exist('PointsLimit', 'var')
15     PointsLimit = inf;
16 end
17
18

```

```

19 Ynum_pos = 1;
20 Ynum_line = 2;
21 Ynum_shaft = 3;
22
23
24 varname = regexprep(filename, '^(.*/+|)([/])\.[mM][aA][tT]$', '$2');
25 load(filename, varname);
26 estr = [ 'datalen = length(', varname, '.X(1).Data);'];
27 eval(estr)
28 datalen = min([datalen PointsLimit]);
29 estr = [ 'time = ', varname, '.X(1).Data(1:datalen)'';'];
30 eval(estr)
31 estr = [ 'struct.pos = [time, ', varname, '.Y(Ynum_pos).Data(1:datalen)'';'];];
32 eval(estr)
33 estr = [ 'struct.line = [time, ', varname, '.Y(Ynum_line).Data(1:datalen)'';'];];
34 eval(estr)
35 estr = [ 'struct.shaft = [time, ', varname, '.Y(Ynum_shaft).Data(1:datalen)'';'];];
36 eval(estr)
37 estr = [ 'clear ', varname, '; ' ];
38 eval(estr);
39
40 clear time
41 clear estr
42
43 %%
44 % Convert to frequency data
45 spec_opt.dB = 0;
46 spec_opt.Norm = 0;
47 spec_opt.DCremove = 0;
48 spec_opt.Power = 1;
49
50 clear st; clear ft;
51
52 [struct.s struct.f] = sjhspec(struct.shaft, spec_opt);
53
54 StopIdx = min(...
55     ceil((StopFreq / struct.f(end)) * length(struct.f)),...
56     length(struct.f));
57
58 struct.s = struct.s(1:StopIdx);
59 struct.f = struct.f(1:StopIdx);

```

B.7 loadsig.m

```

1 function [data, s, f] = loadsig(type, filename, varargin)
2 % function [data, f, s] = loadsig(type, filename)
3 % where type = "sim" or "meas" and filename is the dat or matlab file
4 %
5 % This utility function will return a consistent Matlab structure for either
6 % measured or simulated data files, allowing easy comparison. It also takes

```



```

7 % care of the Z compression applied to some Maxwell data files.
8
9 StopFreq = inf;
10
11 % Load data out of files
12 clear data;
13 clear f;
14 clear s;
15
16 if strcmp(type, 'sim')
17     [fid,msg] = fopen(filename, 'r');
18     if fid == -1
19         zfilename = [filename '.Z'];
20         [fid,msg] = fopen(zfilename, 'r');
21         if fid == -1
22             disp([filename ' not found!']);
23             return
24         end
25
26         fclose(fid);
27         syscmd = 'c:\unxutils\usr\local\wbin\compress -d -c';
28
29         [status,msg] = dos([syscmd ' ' zfilename ' >' filename]);
30         if status == 0
31             delete(zfilename);
32         else
33             disp(['Decompression failed with status ' int2str(status)]);
34             disp(msg);
35             return;
36         end
37     else
38         fclose(fid);
39     end
40
41     filedata = loadmat(filename, 0.04);
42     data = filedata.v_shaft;
43     clear filedata;
44
45 elseif strcmp(type, 'meas')
46     if nargin == 5
47         Ynum = varargin{4};
48         PointsLimit = varargin{5};
49     else
50         PointsLimit = inf;
51         Ynum = 3;
52     end
53
54
55     varname = regexp(filename, '^(./+|)([~/]+)\.[mM][aA][tT]$', '$2');
56     load(filename, varname);
57     estr = [ 'datalen = length(', varname, '.X(1).Data);'];
58     eval(estr)
59     datalen = min([datalen PointsLimit]);
60     data = zeros(datalen,2);
61     estr = [ 'data(:,1) = ', varname, '.X(1).Data(1:datalen);'];

```

```

62     eval(estr)
63     estr = [ 'data(:,2) = ', varname, '.Y(Ynum).Data(1:datalen);'];
64     eval(estr)
65     estr = [ 'clear ', varname, ';' ];
66     eval(estr);
67
68 else
69     disp('You must give either ''sim'' or ''meas'' for type');
70     return;
71 end
72
73 clear estr
74
75 %%
76 % Convert to frequency data
77 spec_opt.dB = 0;
78 spec_opt.Norm = 0;
79 spec_opt.DCremove = 0;
80 spec_opt.Power = 1;
81
82 clear s;
83 clear f;
84 clear st; clear ft;
85
86 [s f] = sjhspec(data, spec_opt);
87
88 StopIdx = min(...
89     ceil((StopFreq / f(end)) * length(f)),...
90     length(f));
91
92 s = s(1:StopIdx);
93 f = f(1:StopIdx);

```

B.8 ave_data.m

```

1 function [x,y] = ave_data(data1, data2)
2 % function [x,y] = ave_data(data1, data2)
3 % data1 and data2 must be identical length
4 % they are assumed to be two simultaneously sampled signals
5 % data1 would be position, and data2 is signal
6
7 if length(data1) ~= length(data2)
8     disp('data1 and data2 must be the same length!');
9     return;
10 end
11
12 x_len = 720;
13
14 d_len = length(data1);
15 d1_min = min(data1);

```

```

16 d1_max = max(data1);
17
18 dx = (d1_max - d1_min)/(x_len-1);
19 x = [d1_min:dx:d1_max];
20 y = zeros(x_len,1);
21 y_num = y;
22
23 for i = 1:d_len
24     d1 = data1(i);
25     d2 = data2(i);
26
27
28     idx = ((d1-d1_min)/(dx+d1_max-d1_min)) * x_len + 1;
29     near_idx = round(idx);
30
31     y(near_idx) = y(near_idx) + d2;
32
33     y_num(near_idx) = y_num(near_idx) + 1;
34 end
35
36 y = y ./ y_num;
37

```

B.9 rmssim.m

```

1 function rms = rmssim(d)
2 % function rms = rmssim(d) where d is a 2 column matrix with
3 %   time and data in columns 1 and 2 respectively
4 %
5 % Calculate the rms value of time domain data and print it out, for
6 % convenience a root 3 value is also calculated in case it's of interest.
7
8 T = (d(end,1) - d(1,1)) / (length(d)-1);
9 % Using trapezoidal integration:
10 outrms = sqrt(sum(((d(1:end-1,2)+d(2:end,2))/2).^2.*T) / (d(end,1)-d(1,1)));
11
12 % Using left-hand Riemann sum:
13 %outrms = sqrt(sum(d(1:end,2).^2.*T) / (d(end,1)-d(1,1)+T));
14
15 if nargin == 0
16     disp(['RMS = ', num2str(outrms, 12)]);
17     disp(['RMS * sqrt(3) = ', num2str(outrms*sqrt(3), 12)]);
18     disp(['RMS / sqrt(3) = ', num2str(outrms/sqrt(3), 12)]);
19 else
20     rms = outrms;
21 end

```

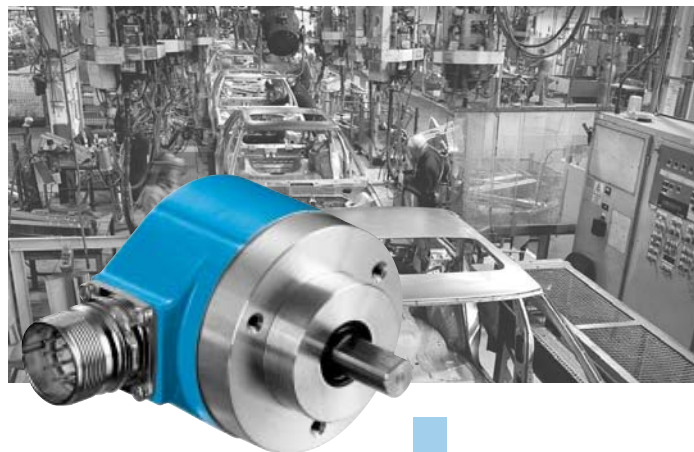
Appendix C

Datasheets

- DGS 60 incremental encoder
- ICPL2631 dual opto-coupler
- NTE859 opamp
- 74HC04 hex inverter
- LM78XX series positive voltage regulator
- LM79XX series negative voltage regulator

DGS 60, DGS 65 and DGS 66: Incremental Encoders for rough environmental conditions

DATA SHEET



Select your individual encoder!
Possible product variants:
6 and 10 mm solid shafts with
servo flange or face mount flange,
through or blind hollow shafts with
connector or cable outlet, TTL or
HTL interface.

Thanks to this wide variety of
products, there are numerous
possible uses, for example in:

- machine tools
- textile machines
- woodworking machines
- packaging machines

**Number of lines
100 to 10,000**
Incremental Encoder

Incremental encoders in the
DGS 60, DGS 65 and DGS 66
series are in use world-wide
under the toughest environmental
conditions.
The rugged construction – up to
IP 67 degree protection – and the
individual adaptation of the
design to the requirements of
the user are the outstanding
features of this series.
Resolutions up to 10,000 lines
are available.

SICK | STEGMANN

**Number of lines
100 to 10,000**
Incremental Encoder

- Servo or face mount flange
- Connector or cable outlet
- Protection class up to IP 67
- Electrical Interfaces
TTL and HTL

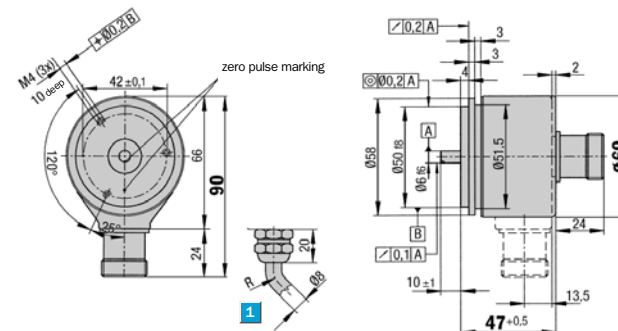


CE

Accessories
Connection systems
Mounting systems

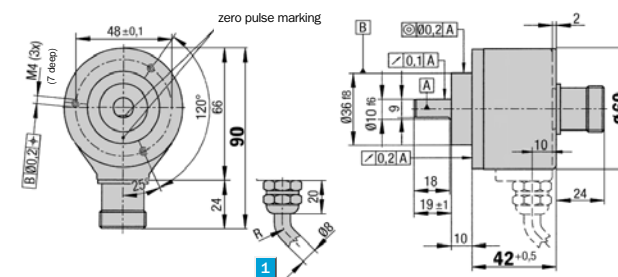
Incremental Encoder DGS 60, face mount and servo flange

Dimensional drawing servo flange



1 R = bending radius min. 40 mm General tolerances according to DIN ISO 2768-mk

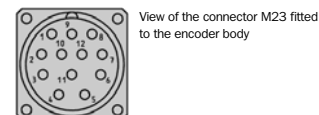
Dimensional drawing face mount flange



1 R = bending radius min. 40 mm General tolerances according to DIN ISO 2768-mk

PIN and wire allocation/cable 11 core

PIN	Signal HTL	Signal TTL	Core colour (cable outlet)	Explanation
1	N. C.	B	black	Signal line
2	N. C.	Sense +	grey	Connected internally to U _s
3	Z	Z	ilac	Signal line
4	N. C.	Z̄	yellow	Signal line
5	A	A	white	Signal line
6	N. C.	Ā	brown	Signal line
7	N. C.	N. C.	orange	N. C.
8	B	B	pink	Signal line
9	Screen	Screen		Housing potential
10	GND	GND	blue	Ground connection
11	N. C.	Sense -	green	Connected internally to ground
12	U _s	U _s	red	Power supply ¹⁾



View of the connector M23 fitted to the encoder body

¹⁾ Potential free to housing
N. C. =
Not Connected

Technical Data		DGS 60		Flange type											
		servo	face m.												
Solid shaft	10 mm														
	6 mm														
Number of lines (Z) per revolution	00100 to 10,000, see order info														
Attention: number of lines > 5000	Only with TTL 4 ... 6V														
Electrical interface	TTL/RS 422, 6-channel														
	HTL/push-pull, 3-channel (A, B, Z)														
Mass ¹⁾	Approx. 0.3 kg														
Moment of inertia of the rotor															
Servo flange	13 gcm ²														
Face mount flange	25 gcm ²														
Measuring step	90°/number of lines														
Reference signal															
Number	1														
Position	90° electr. & logically interlocked with A+B														
Error limits															
100 ≤ Z < 1250	45/Z + 0.054°														
1250 < Z ≤ 10000	45/Z + 0.039°														
Measuring step deviation	45/Z °														
Max. output frequency															
TTL	300 kHz (600 at > 5000 lines)														
HTL	200 kHz														
Max. operating speed ²⁾															
with shaft seal	6,000 min ⁻¹														
without shaft seal	10,000 min ⁻¹														
Max. angular acceleration	5 x 10 ⁵ rad/s ²														
Operating torque															
with shaft seal	1 Ncm														
without shaft seal	0.1 Ncm														
Start up torque															
with shaft seal	1.5 Ncm														
without shaft seal	0.2 Ncm														
Permissible shaft loading															
Servo flange radial/axial	20 N/10 N														
Face mount flange radial/axial	40 N/20 N														
Bearing lifetime	3.6 x 10 ¹⁰ revolutions														
Working temperature range	- 20 ... + 85 °C														
Storage temperature range	- 30 ... + 85 °C														
Permissible relative humidity ³⁾	90 %														
EMC ⁴⁾															
Resistance															
to shocks ⁵⁾	30/11 g/ms														
to vibration ⁶⁾	20/10 ... 2000 g/Hz														
Protection class acc. IEC 60529 ⁷⁾															
Housing side	IP 67														
Flange side	IP 65														
Operating voltage range															
Load current TTL/RS 422, 4 ... 6 V	Max. 20 mA														
TTL/RS 422, 10 ... 30 V	Max. 20 mA														
HTL/push-pull, 10 ... 30 V	Max. 60 mA														
Operating current range at no load															
at 24 V	100 mA														
at 5 V	120 mA														

¹⁾ For an encoder with connector outlet ³⁾ Condensation not permitted ⁵⁾ To DIN EN 60068-2-27
²⁾ At speeds > 6000 rpm the shaft seal must be removed ⁴⁾ To DIN EN 61000-6-2 and DIN EN 61000-6-3 ⁶⁾ To DIN EN 60068-2-6
⁷⁾ With mating connector fitted

Order information see page 5

Contact:

- Australia**
Phone +61 3 9497 4100
1800 33 48 02 – tollfree
E-Mail sales@sick.com.au
- Belgium/Luxembourg**
Phone +32 (0)2 466 55 66
E-Mail info@sick.be
- Brazil**
Phone +55 11 5091-4900
E-Mail sac@sick.com.br
- Ceská Republika**
Phone +420 2 57 91 18 50
E-Mail sick@sick.cz
- China**
Phone +852-2763 6966
E-Mail ghk@sick.com.hk
- Danmark**
Phone +45 45 82 64 00
E-Mail sick@sick.dk
- Deutschland**
Phone +49 (0)21 53 01-250
E-Mail vzdinfo@sick.de
- España**
Phone +34 93 480 31 00
E-Mail info@sick.es
- France**
Phone +33 1 64 62 35 00
E-Mail info@sick.fr
- Great Britain**
Phone +44 (0)1727 831121
E-Mail info@sick.co.uk
- Italia**
Phone +39 011 797965
E-Mail stegmann@stegmann.it
- Japan**
Phone +81 (0)3 3358 1341
E-Mail info@sick.jp
- Korea**
Phone +82-2 786 6321/4
E-Mail kang@sickkorea.net
- Nederlands**
Phone +31 (0)30 229 25 44
E-Mail info@sick.nl
- Norge**
Phone +47 67 81 50 00
E-Mail austefjord@sick.no
- Österreich**
Phone +43 (0)22 36 62 28 8-0
E-Mail office@sick.at
- Polska**
Phone +48 22 837 40 50
E-Mail info@sick.pl
- Schweiz**
Phone +41 41 619 29 39
E-Mail contact@sick.ch
- Singapore**
Phone +65 6744 3732
E-Mail admin@sicksgp.com.sg
- Suomi**
Phone +358-9-25 15 800
E-Mail sick@sick.fi
- Sverige**
Phone +46 8 680 64 50
E-Mail info@sick.se
- Taiwan**
Phone +886 2 2365-6292
E-Mail sickgrc@ms6.hinet.net
- USA**
Phone +1 937-454-1956
E-Mail sales@stegmann.com

More representatives and agencies in all major industrial nations at www.sick.com



SICK AG • Industrial Sensors • Waldkirch • Germany • www.sick.com
 Stegmann GmbH & Co. KG • Donaueschingen • Germany • www.sick-stegmann.de

8 010 302/03-04 - DW/3/2000 • Printed in Germany (0704) • Subject to change without prior notice • The specified product features and technical data do not represent any guarantee • 01_A45ig - 2c m116

ICPL2631
ICPL2630



DUAL CHANNEL, HIGH CMR, VERY HIGH SPEED OPTICALLY COUPLED ISOLATOR LOGIC GATE OUTPUT

APPROVALS

- UL recognised, File No. E91231

DESCRIPTION

The ICPL2630 / ICPL2631 are dual channel optocouplers consisting of GaAsP light emitting diodes and high gain integrated photo detectors to provide 3500Volts_{RMS} electrical isolation between input and output. The output of the detector I.C.'s are open collector Schottky clamped transistors. The ICPL2631 has an internal shield which provides a guaranteed common mode transient immunity specification of 1000V/ μ s minimum. This unique design provides maximum ac and dc circuit isolation while achieving TTL compatibility. The coupled parameters are guaranteed over the temperature range of 0°C to 70°C, such that a maximum input signal of 5mA will provide a minimum output sink current of 13mA (equivalent to fan-out of eight gates)

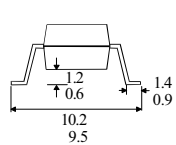
FEATURES

- High speed - 10MBit/s
- High Common Mode Transient Immunity 10kV/ μ s typical
- Logic gate output
- ICPL2631 has improved noise shield for superior common mode rejection
- Options :-
10mm lead spread - add G after part no.
Surface mount - add SM after part no.
Tape&reel - add SMT&R after part no.

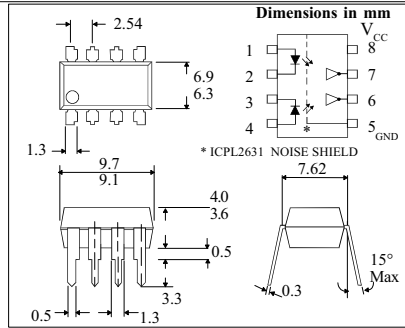
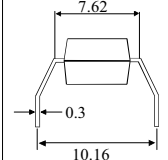
APPLICATIONS

- Line receiver, data transmission
- Computer-peripheral interface
- Data multiplexing
- Pulse transformer replacement

OPTION SM SURFACE MOUNT



OPTION G



ABSOLUTE MAXIMUM RATINGS (25°C unless otherwise specified)

Storage Temperature _____ -55°C to + 125°C
Operating Temperature _____ 0°C to + 70°C
Lead Soldering Temperature (1/16 inch (1.6mm) from case for 10 secs) 260°C

INPUT DIODE

Average Forward Current _____ 15mA (note 5)
Peak Forward Current _____ 30mA (less than 1msec duration)(note 5)
Reverse Voltage _____ 5V (note 5)

DETECTOR

Supply Voltage (V_{CC}) _____ 7V (1 minute maximum)
Output Current (I_O) _____ 16mA (note 5)
Output Voltage (V_O) _____ 7V (note 5)
Collector Output Power Dissipation _____ 60mW

ISOCOM COMPONENTS LTD
Unit 25B, Park View Road West,
Park View Industrial Estate, Brenda Road
Hartlepool, Cleveland, TS25 1YD
Tel: (01429) 863609 Fax : (01429) 863581

ISOCOM INC
1024 S. Greenville Ave, Suite 240,
Allen, TX 75002 USA
Tel: (214) 495-0755 Fax: (214) 495-0901
e-mail info@isocom.com
http://www.isocom.com

ELECTRICAL CHARACTERISTICS ($T_A = 0^\circ\text{C}$ to 70°C Unless otherwise noted)

PARAMETER	SYM	DEVICE	MIN	TYP*	MAX	UNITS	TEST CONDITION
High Level Output Current (note 5)	I_{OH}		2	250		μA	$V_{CC} = 5.5\text{V}, V_O = 5.5\text{V}$ $I_F = 250\mu\text{A}$
Low Level Output Voltage (note 5)	V_{OL}		0.4	0.6		V	$V_{CC} = 5.5\text{V}, I_F = 5\text{mA}$ $I_{OL}(\text{sinking}) = 13\text{mA}$
High Level Supply Current (both channels)	I_{CCH}		14	30		mA	$V_{CC} = 5.5\text{V}, I_F = 0\text{mA}$
Low Level Supply Current (both channels)	I_{CCL}		26	36		mA	$V_{CC} = 5.5\text{V}, I_F = 10\text{mA}$
Input Forward Voltage	V_F		1.55	1.75		V	$I_F = 10\text{mA}, T_A = 25^\circ\text{C}$
Input Reverse Breakdown Voltage	V_{BR}		5			V	$I_R = 10\mu\text{A}, T_A = 25^\circ\text{C}$
Input Capacitance	C_{IN}		60			pF	$V_F = 0, f = 1\text{MHz}$
Temperature Coefficient of Forward Voltage	$\frac{\Delta V_F}{\Delta T_A}$		-1.4			mV/ $^\circ\text{C}$	$I_F = 10\text{mA}$
Input-output Isolation Voltage (note 4)	V_{ISO}		2500	5000		V_{RMS}	R.H. equal to or less than 50%, $t = 1\text{min}, T_A = 25^\circ\text{C}$
Input-output Insulation Leakage Current (note 4)	I_{I-O}			1		μA	R.H = 45% $t = 5\text{s}, T_A = 25^\circ\text{C}$ $V_{I-O} = 3000\text{V dc}$
Resistance (Input to Output) (note 4)	R_{I-O}			10^{12}		Ω	$V_{I-O} = 500\text{V dc}$
Capacitance (Input to Output) (note 4)	C_{I-O}			0.6		pF	$f = 1\text{MHz}$
Input-input Insulation Leakage Current (note 6)	I_{I-I}			0.005		μA	R.H = 45% $t = 5\text{s}, T_A = 25^\circ\text{C}$ $V_{I-O} = 500\text{V dc}$
Resistance (Input to input) (note 6)	R_{I-I}			10^{11}		Ω	$V_{I-O} = 500\text{V dc}$
Capacitance (Input to input) (note 6)	C_{I-I}			0.6		pF	$f = 1\text{MHz}$

* All typicals at $T_A = 25^\circ\text{C}$

RECOMMENDED OPERATING CONDITIONS

PARAMETER	SYMBOL	MIN	MAX	UNITS
Input Current, Low Level	I_{FL}	0	250	μA
Input Current, High Level	I_{FH}	6.3*	15	mA
Supply Voltage, Output	V_{CC}	4.5	5.5	V
Fan Out (TTL Load)	N		8	
Operating Temperature	T_A	0	70	$^\circ\text{C}$

*6.3mA is a guard banded value which allows for at least 20% CTR degradation. Initial input current threshold value is 5.0mA or less

SWITCHING SPECIFICATIONS AT $T_A = 25^\circ\text{C}$ ($V_{CC} = 5\text{V}$, $I_F = 7.5\text{mA}$ Unless otherwise noted)

PARAMETER	SYM	DEVICE	MIN	TYP	MAX	UNITS	TEST CONDITION
Propagation Delay Time to Logic Low at Output (fig 1)(note2)	t_{PHL}			55	75	ns	$R_L = 350\Omega$, $C_L = 15\text{pF}$
Propagation Delay Time to Logic High at Output (fig 1)(note3)	t_{PLH}			45	75	ns	$R_L = 350\Omega$, $C_L = 15\text{pF}$
Common Mode Transient Immunity at Logic High Level Output (fig 2)(note7)	CM_H	ICPL2630 ICPL2631	1000	10000	10000	V/ μs V/ μs	$I_F = 0\text{mA}$, $V_{CM} = 50V_{PP}$ $R_L = 350\Omega$, $V_{OH} = 2V_{min}$.
Common Mode Transient Immunity at Logic Low Level Output (fig 2)(note8)	CM_L	ICPL2630 ICPL2631	-1000	-10000	-10000	V/ μs V/ μs	$V_{CM} = 50V_{PP}$ $R_L = 350\Omega$, $V_{OL} = 0.8V_{max}$.

NOTES:-

- 1 Bypassing of the power supply line is required, with a $0.01\mu\text{F}$ ceramic disc capacitor adjacent to each isolator. The power supply bus for the isolator(s) should be separate from the bus for any active loads. Otherwise a larger value of bypass capacitor (up to $0.1\mu\text{F}$) may be needed to suppress regenerative feedback via the power supply.
- 2 The t_{PHL} propagation delay is measured from the 3.75mA level Low to High transition of the input current pulse to the 1.5V level on the High to Low transition of the output voltage pulse.
- 3 The t_{PLH} propagation delay is measured from the 3.75mA level High to Low transition of the input current pulse to the 1.5V level on the Low to High transition of the output voltage pulse.
- 4 Device considered a two terminal device; pins 1, 2, 3, and 4 shorted together, and pins 5, 6, 7 and 8 shorted together.
- 5 Each channel.
- 6 Measured between pins 1 and 2 shorted together and pins 3 and 4 shorted together.
- 7 CM_H is the maximum tolerable rate of rise of the common mode voltage to assure that the output will remain in a high logic state (ie $V_{out} > 2.0\text{V}$).
- 8 CM_L is the maximum tolerable rate of fall of the common mode voltage to assure that the output will remain in a low logic state (ie $V_{out} < 0.8\text{V}$).

FIG.1 SWITCHING TEST CIRCUIT

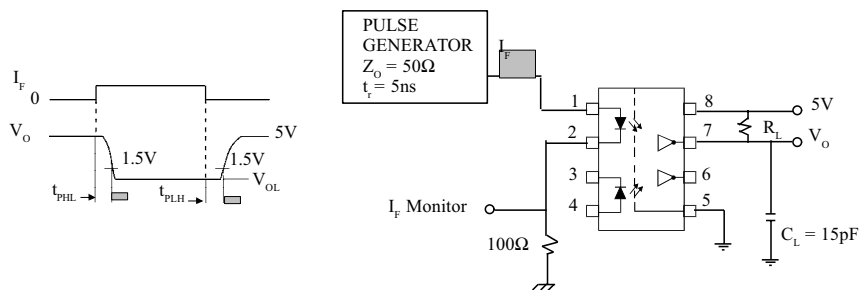
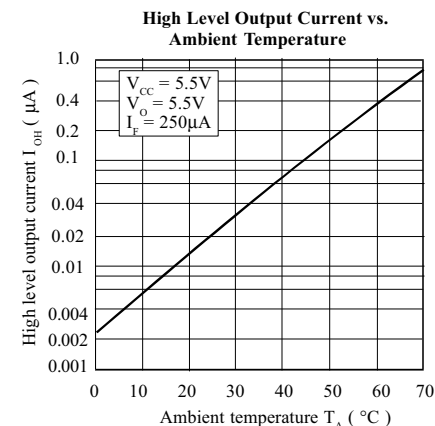
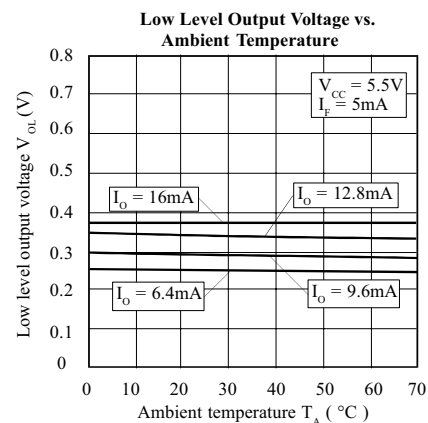
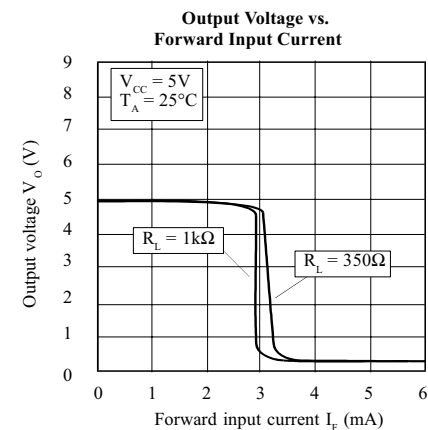
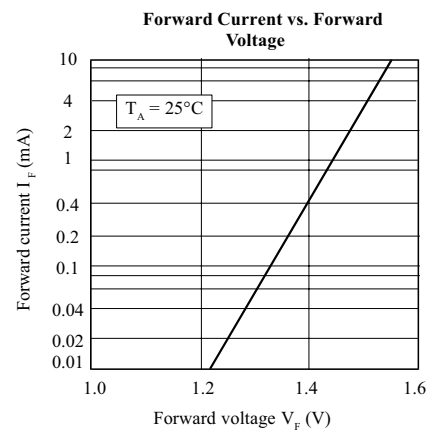
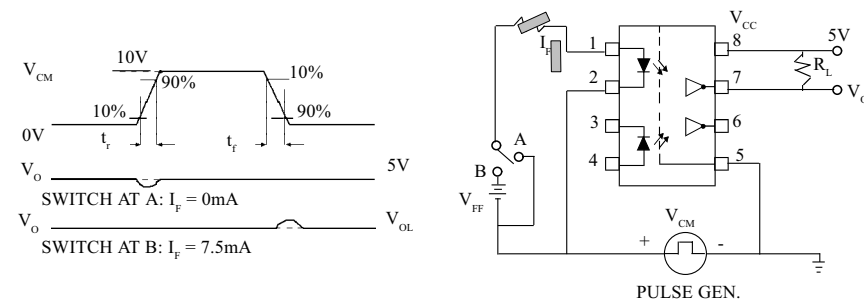


FIG. 2 TEST CIRCUIT FOR TRANSIENT IMMUNITY AND TYPICAL WAVEFORMS





ELECTRONICS, INC.
 44 FARRAND STREET
 BLOOMFIELD, NJ 07003
 (973) 748-5089
 http://www.nteinc.com

NTE859/NTE859SM Integrated Circuit Quad, Low Noise, JFET Input Operational Amplifier

Description:

The NTE859 (14-Lead DIP) and NTE859SM (SOIC-14 Surface Mount) JFET-input operational amplifiers are low noise amplifiers with low noise input bias, offset currents, and fast slew rate. The low harmonic distortion and low noise make these devices ideally suited as amplifiers for high-fidelity and audio preamplifier applications. Each amplifier features JFET-inputs (for high input impedance) coupled with bipolar output stages all integrated on a single monolithic chip.

Features:

- Low Power Consumption
- Wide Common-Mode and Differential Voltage Ranges
- Low Input Bias and Offset Currents
- Output Short-Circuit Protection
- Low Total Harmonic Distortion: 0.003% Typ
- Low Noise: $V_n = 18nV\sqrt{Hz}$ Typ
- High Input Impedance: JFET-Input Stage
- Internal Frequency Compensation
- Latch-Up Free Operation
- High Slew Rate: 13V/ μ s Typ

Absolute Maximum Ratings: ($T_A = 0$ to $+70^\circ\text{C}$ unless otherwise specified)

Supply Voltage (Note 1), $V_{CC}(+)$	18V
Supply Voltage (Note1), $V_{CC}(-)$	-18V
Differential Input Voltage (Note 2), V_{ID}	$\pm 30V$
Input Voltage Range (Note 1, Note 3), V_{IDR}	$\pm 15V$
Duration of Output Short Circuit (Note 4), t_{SC}	Unlimited
Power Dissipation ($T_A = +25^\circ\text{C}$), P_D	680mW
Derate Above 25°C	10mW/ $^\circ\text{C}$
Operating Ambient Temperature Range, T_A	0° to $+70^\circ\text{C}$
Storage Temperature Range, T_{stg}	-65° to $+150^\circ\text{C}$
Lead Temperature (During Soldering, 1/16" from Case for 10sec), T_L	$+260^\circ\text{C}$

- Note 1. All voltage values, except differential voltages, are with respect to the midpoint between $V_{CC}(+)$ and $V_{CC}(-)$.
- Note 2. Differential voltages are at the non-inverting input pin with respect to the inverting pin.
- Note 3. The magnitude of the input voltage must never exceed the magnitude of the supply voltage or 15V, whichever is less.
- Note 4. The output may be shorted to GND or to either supply. Temperature and/or supply voltages must be limited to ensure that the dissipation rating is not exceeded.

Electrical Characteristics: ($V_{CC} = \pm 15V$, $T_A = 0$ to $+70^\circ\text{C}$ unless otherwise specified)

Parameter	Symbol	Test Conditions	Min	Typ	Max	Unit	
Input Offset Voltage	V_{IO}	$V_O = 0$, $R_S = 50\Omega$	$T_A = +25^\circ\text{C}$	-	3	10	mV
				-	-	13	mV
Temperature Coefficient of Input Offset Voltage	αV_{IO}	$V_O = 0$, $R_S = 50\Omega$	-	10	-	$\mu\text{V}/^\circ\text{C}$	
Input Offset Current	I_{IO}	$V_O = 0$, Note 6	$T_A = +25^\circ\text{C}$	-	5	100	pA
				-	-	2	nA
Input Bias Current	I_{IB}	$V_O = 0$, Note 6	$T_A = +25^\circ\text{C}$	-	30	200	pA
				-	-	7	nA
Common-Mode Input Voltage Range	V_{ICR}	$T_A = +25^\circ\text{C}$	± 11	± 12	-	V	
Maximum Peak Output Voltage Range	V_{OM}	$R_L = 10k\Omega$, $T_A = +25^\circ\text{C}$		± 12	± 13.5	-	V
				± 12	-	-	V
				± 10	± 12	-	V
Large-Signal Differential Voltage Amplification	A_{VD}	$V_O = \pm 10V$, $R_L \geq 2k\Omega$	$T_A = +25^\circ\text{C}$	25	200	-	V/mV
				15	-	-	V/mV
Unity-Gain Bandwidth	B_1	$T_A = +25^\circ\text{C}$	-	3	-	MHz	
Input Resistance	r_i	$T_A = +25^\circ\text{C}$	-	10^{12}	-	Ω	
Common-Mode Rejection Ratio	CMRR	$V_{IC} = V_{ICRmin}$, $V_O = 0$, $R_S = 50\Omega$, $T_A = +25^\circ\text{C}$	70	86	-	dB	
Supply Voltage Rejection Ratio ($\Delta V_{CC} / \Delta V_{IO}$)	k_{SVR}	$V_{CC} = \pm 15V$ to $\pm 9V$, $V_O = 0$, $R_S = 50\Omega$, $T_A = +25^\circ\text{C}$	70	86	-	dB	
Supply Current (Per Amplifier)	I_{CC}	No Load, $V_O = 0$, $T_A = +25^\circ\text{C}$	-	1.4	2.5	mA	
Crosstalk Attenuation	V_{O1}/V_{O2}	$A_{VD} = 100$, $T_A = +25^\circ\text{C}$	-	120	-	dB	

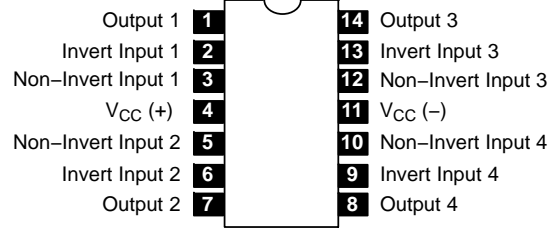
Note 5. All characteristics are measured under open-loop conditions with zero common-mode voltage unless otherwise specified.

Note 6. Input bias currents of a FET-input operational amplifier are normal junction reverse currents, which are temperature sensitive. Pulse techniques must be used that will maintain the junction temperatures as close to the ambient temperature as is possible.

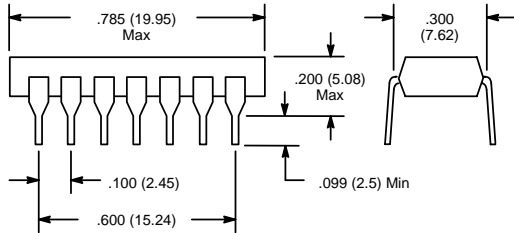
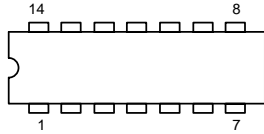
Operating Characteristics: ($V_{CC} = \pm 15V$, $T_A = +25^\circ\text{C}$ unless otherwise specified)

Parameter	Symbol	Test Conditions	Min	Typ	Max	Unit	
Slew Rate at Unity Gain	SR	$V_I = 10V$, $R_L = 2k\Omega$, $C_L = 100pF$	8	13	-	V/ μ s	
Rise Time Overshoot Factor	t_r	$V_I = 10V$, $R_L = 2k\Omega$, $C_L = 100pF$		0.1	-	μ s	
				-	10	-	%
Equivalent Input Noise Voltage	V_n	$R_S = 100\Omega$	$f = 1kHz$	-	18	-	nV/\sqrt{Hz}
			$f = 10Hz$ to $10kHz$	-	4	-	μ V
Equivalent Input Noise Current	I_n	$R_S = 100\Omega$, $f = 1kHz$	-	0.01	-	pA/\sqrt{Hz}	
Total Harmonic Distortion	THD	$V_{O(rms)} = 10V$, $R_S \leq 1k\Omega$, $R_L \geq 2k\Omega$, $f = 1kHz$	-	0.003	-	%	

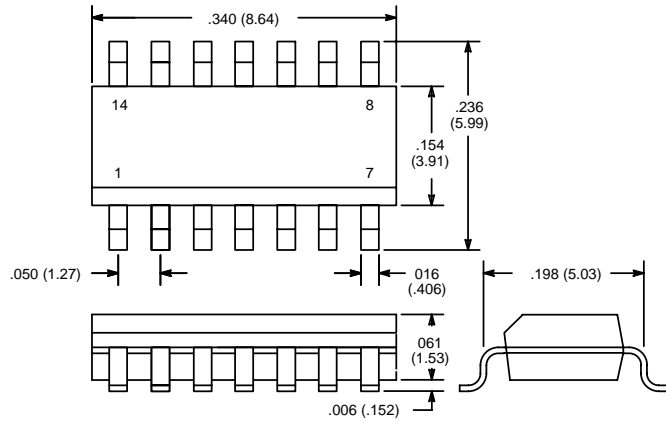
Pin Connection Diagram



NTE859 (14-Lead DIP)



NTE859SM (SOIC-14)



NOTE: Pin1 on Beveled Edge

DATA SHEET

For a complete data sheet, please also download:

- The IC06 74HC/HCT/HCU/HCMOS Logic Family Specifications
- The IC06 74HC/HCT/HCU/HCMOS Logic Package Information
- The IC06 74HC/HCT/HCU/HCMOS Logic Package Outlines

74HC/HCT04 Hex inverter

Product specification
File under Integrated Circuits, IC06

September 1993



Hex inverter

74HC/HCT04

FEATURES

- Output capability: standard
- I_{CC} category: SSI

GENERAL DESCRIPTION

The 74HC/HCT04 are high-speed Si-gate CMOS devices and are pin compatible with low power Schottky TTL (LSTTL). They are specified in compliance with JEDEC standard no. 7A. The 74HC/HCT04 provide six inverting buffers.

QUICK REFERENCE DATA

GND = 0 V; T_{amb} = 25 °C; t_r = t_f = 6 ns

SYMBOL	PARAMETER	CONDITIONS	TYPICAL		UNIT
			HC	HCT	
t _{PHL} / t _{PLH}	propagation delay nA to nY	C _L = 15 pF; V _{CC} = 5 V	7	8	ns
C _I	input capacitance		3.5	3.5	pF
C _{PD}	power dissipation capacitance per gate	notes 1 and 2	21	24	pF

Notes

1. C_{PD} is used to determine the dynamic power dissipation (P_D in μW):

$$P_D = C_{PD} \times V_{CC}^2 \times f_i + \sum (C_L \times V_{CC}^2 \times f_o) \text{ where:}$$

f_i = input frequency in MHz

f_o = output frequency in MHz

Σ (C_L × V_{CC}² × f_o) = sum of outputs

C_L = output load capacitance in pF

V_{CC} = supply voltage in V

2. For HC the condition is V_I = GND to V_{CC}
For HCT the condition is V_I = GND to V_{CC} - 1.5 V

ORDERING INFORMATION

See "74HC/HCT/HCU/HCMOS Logic Package Information".

Hex inverter

74HC/HCT04

PIN DESCRIPTION

PIN NO.	SYMBOL	NAME AND FUNCTION
1, 3, 5, 9, 11, 13	1A to 6A	data inputs
2, 4, 6, 8, 10, 12	1Y to 6Y	data outputs
7	GND	ground (0 V)
14	V _{CC}	positive supply voltage

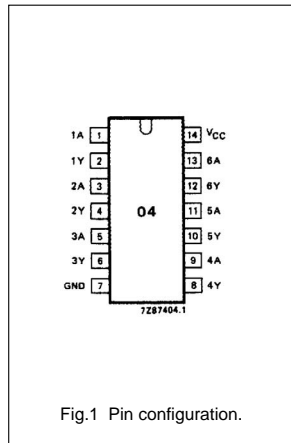


Fig.1 Pin configuration.

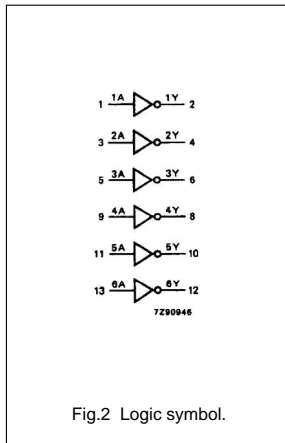


Fig.2 Logic symbol.

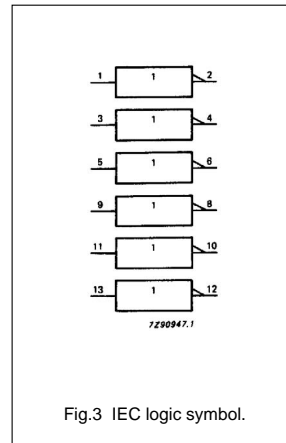


Fig.3 IEC logic symbol.

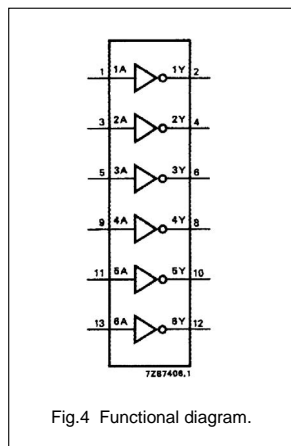


Fig.4 Functional diagram.

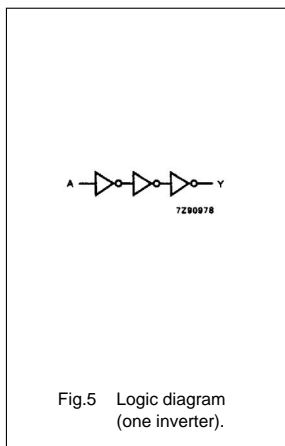


Fig.5 Logic diagram (one inverter).

FUNCTION TABLE

INPUT	OUTPUT
nA	nY
L	H
H	L

Notes

- H = HIGH voltage level
L = LOW voltage level

Hex inverter

74HC/HCT04

DC CHARACTERISTICS FOR 74HC

For the DC characteristics see "74HC/HCT/HCU/HCMOS Logic Family Specifications".

Output capability: standard

I_{CC} category: SSI

AC CHARACTERISTICS FOR 74HC

GND = 0 V; t_r = t_f = 6 ns; C_L = 50 pF

SYMBOL	PARAMETER	T _{amb} (°C)						UNIT	TEST CONDITIONS		
		74HC							V _{CC} (V)	WAVEFORMS	
		+25			-40 to +85		-40 to +125				
		min.	typ.	max.	min.	max.	min.				max.
t _{PHL} / t _{PLH}	propagation delay nA to nY		25 9 7	85 17 14		105 21 18		130 26 22	ns	2.0 4.5 6.0	Fig.6
t _{THL} / t _{TLH}	output transition time		19 7 6	75 15 13		95 19 16		110 22 19	ns	2.0 4.5 6.0	Fig.6

Hex inverter

74HC/HCT04

DC CHARACTERISTICS FOR 74HCT

For the DC characteristics see *"74HC/HCT/HCU/HCMOS Logic Family Specifications"*.

Output capability: standard

I_{CC} category: SSI

Note to HCT types

The value of additional quiescent supply current (ΔI_{CC}) for a unit load of 1 is given in the family specifications.

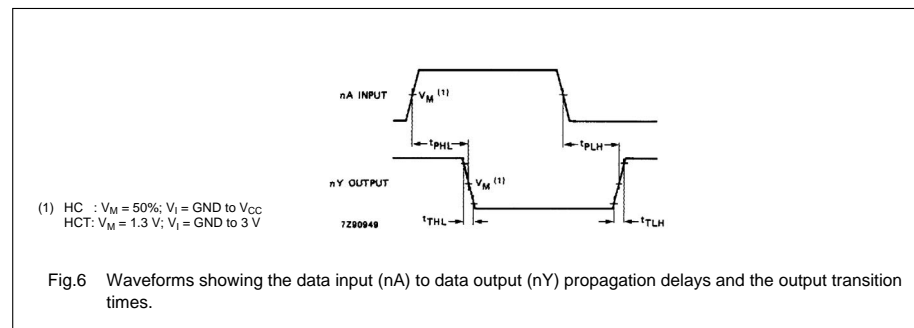
To determine ΔI_{CC} per unit, multiply this value by the unit load coefficient shown in the table below.

INPUT	UNIT LOAD COEFFICIENT
nA	1.20

AC CHARACTERISTICS FOR 74HC

GND = 0 V; $t_r = t_f = 6$ ns; $C_L = 50$ pF

SYMBOL	PARAMETER	T _{amb} (°C)						UNIT	TEST CONDITIONS		
		74HCT							V _{CC} (V)	WAVEFORMS	
		+25			-40 to +85		-40 to +125				
		min.	typ.	max.	min.	max.	min.				max.
t _{PHL} / t _{PLH}	propagation delay nA to nY		10	19		24		29	ns	4.5	Fig.6
t _{THL} / t _{TLH}	output transition time		7	15		19		22	ns	4.5	Fig.6

AC WAVEFORMS**PACKAGE OUTLINES**

See *"74HC/HCT/HCU/HCMOS Logic Package Outlines"*.

LM78XX Series Voltage Regulators

General Description

The LM78XX series of three terminal regulators is available with several fixed output voltages making them useful in a wide range of applications. One of these is local on card regulation, eliminating the distribution problems associated with single point regulation. The voltages available allow these regulators to be used in logic systems, instrumentation, HiFi, and other solid state electronic equipment. Although designed primarily as fixed voltage regulators these devices can be used with external components to obtain adjustable voltages and currents.

The LM78XX series is available in an aluminum TO-3 package which will allow over 1.0A load current if adequate heat sinking is provided. Current limiting is included to limit the peak output current to a safe value. Safe area protection for the output transistor is provided to limit internal power dissipation. If internal power dissipation becomes too high for the heat sinking provided, the thermal shutdown circuit takes over preventing the IC from overheating.

Considerable effort was expended to make the LM78XX series of regulators easy to use and minimize the number of external components. It is not necessary to bypass the out-

put, although this does improve transient response. Input bypassing is needed only if the regulator is located far from the filter capacitor of the power supply.

For output voltage other than 5V, 12V and 15V the LM117 series provides an output voltage range from 1.2V to 57V.

Features

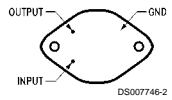
- Output current in excess of 1A
- Internal thermal overload protection
- No external components required
- Output transistor safe area protection
- Internal short circuit current limit
- Available in the aluminum TO-3 package

Voltage Range

LM7805C	5V
LM7812C	12V
LM7815C	15V

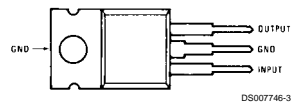
Connection Diagrams

**Metal Can Package
TO-3 (K)
Aluminum**



**Bottom View
Order Number LM7805CK,
LM7812CK or LM7815CK
See NS Package Number KC02A**

**Plastic Package
TO-220 (T)**

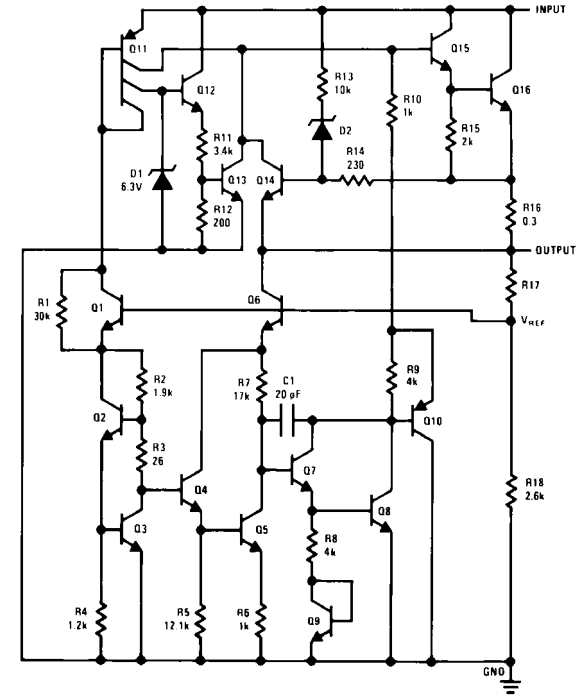


**Top View
Order Number LM7805CT,
LM7812CT or LM7815CT
See NS Package Number T03B**

LM78XX Series Voltage Regulators

LM78XX

Schematic



Absolute Maximum Ratings (Note 3)

If Military/Aerospace specified devices are required, please contact the National Semiconductor Sales Office/Distributors for availability and specifications.

Input Voltage
($V_O = 5V, 12V$ and $15V$) 35V
Internally Limited
Operating Temperature Range (T_A) 0°C to $+70^\circ\text{C}$

Maximum Junction Temperature
(K Package) 150°C
(T Package) 150°C
Storage Temperature Range -65°C to $+150^\circ\text{C}$
Lead Temperature (Soldering, 10 sec.)
TO-3 Package K 300°C
TO-220 Package T 230°C

Electrical Characteristics LM78XXC (Note 2)

$0^\circ\text{C} \leq T_J \leq 125^\circ\text{C}$ unless otherwise noted.

		5V			12V			15V			Units				
Input Voltage (unless otherwise noted)		10V			19V			23V							
Symbol	Parameter	Conditions			Min	Typ	Max	Min	Typ	Max	Min	Typ	Max		
V_O	Output Voltage	$T_J = 25^\circ\text{C}, 5\text{ mA} \leq I_O \leq 1\text{ A}$			4.8	5	5.2	11.5	12	12.5	14.4	15	15.6	V	
		$P_D \leq 15\text{ W}, 5\text{ mA} \leq I_O \leq 1\text{ A}$			4.75	5.25	11.4	12.6	14.25	15.75	V				
		$V_{\text{MIN}} \leq V_{\text{IN}} \leq V_{\text{MAX}}$			$(7.5 \leq V_{\text{IN}} \leq 20)$			$(14.5 \leq V_{\text{IN}} \leq 27)$			$(17.5 \leq V_{\text{IN}} \leq 30)$			V	
ΔV_O	Line Regulation	$I_O = 500\text{ mA}$	$T_J = 25^\circ\text{C}$			3	50	4	120	4	150	mV			
			ΔV_{IN}			$(7 \leq V_{\text{IN}} \leq 25)$			$(14.5 \leq V_{\text{IN}} \leq 30)$			$(17.5 \leq V_{\text{IN}} \leq 30)$			V
			$0^\circ\text{C} \leq T_J \leq +125^\circ\text{C}$			50			120			150			mV
		ΔV_{IN}			$(8 \leq V_{\text{IN}} \leq 20)$			$(15 \leq V_{\text{IN}} \leq 27)$			$(18.5 \leq V_{\text{IN}} \leq 30)$			V	
		$I_O \leq 1\text{ A}$	$T_J = 25^\circ\text{C}$			50			120			150			mV
			ΔV_{IN}			$(7.5 \leq V_{\text{IN}} \leq 20)$			$(14.6 \leq V_{\text{IN}} \leq 27)$			$(17.7 \leq V_{\text{IN}} \leq 30)$			V
$0^\circ\text{C} \leq T_J \leq +125^\circ\text{C}$			25			60			75			mV			
ΔV_{IN}			$(8 \leq V_{\text{IN}} \leq 12)$			$(16 \leq V_{\text{IN}} \leq 22)$			$(20 \leq V_{\text{IN}} \leq 26)$			V			
ΔV_O	Load Regulation	$T_J = 25^\circ\text{C}$			$5\text{ mA} \leq I_O \leq 1.5\text{ A}$			10			50			mV	
					$250\text{ mA} \leq I_O \leq 750\text{ mA}$			25			60			mV	
		$5\text{ mA} \leq I_O \leq 1\text{ A}, 0^\circ\text{C} \leq T_J \leq +125^\circ\text{C}$			50			120			150			mV	
I_O	Quiescent Current	$I_O \leq 1\text{ A}$			$T_J = 25^\circ\text{C}$			8			8			mA	
					$0^\circ\text{C} \leq T_J \leq +125^\circ\text{C}$			8.5			8.5			mA	
ΔI_O	Quiescent Current Change	$5\text{ mA} \leq I_O \leq 1\text{ A}$			0.5			0.5			0.5			mA	
		$T_J = 25^\circ\text{C}, I_O \leq 1\text{ A}$			1.0			1.0			1.0			mA	
		$V_{\text{MIN}} \leq V_{\text{IN}} \leq V_{\text{MAX}}$			$(7.5 \leq V_{\text{IN}} \leq 20)$			$(14.8 \leq V_{\text{IN}} \leq 27)$			$(17.9 \leq V_{\text{IN}} \leq 30)$			V	
		$I_O \leq 500\text{ mA}, 0^\circ\text{C} \leq T_J \leq +125^\circ\text{C}$			1.0			1.0			1.0			mA	
$V_{\text{MIN}} \leq V_{\text{IN}} \leq V_{\text{MAX}}$			$(7 \leq V_{\text{IN}} \leq 25)$			$(14.5 \leq V_{\text{IN}} \leq 30)$			$(17.5 \leq V_{\text{IN}} \leq 30)$			V			
V_N	Output Noise Voltage	$T_A = 25^\circ\text{C}, 10\text{ Hz} \leq f \leq 100\text{ kHz}$			40			75			90			μV	
$\frac{\Delta V_{\text{IN}}}{\Delta V_{\text{OUT}}}$	Ripple Rejection	$I_O \leq 1\text{ A}, T_J = 25^\circ\text{C}$ or $I_O \leq 500\text{ mA}$			62			80			55			72	dB
		$0^\circ\text{C} \leq T_J \leq +125^\circ\text{C}$			62			55			54			70	dB
		$V_{\text{MIN}} \leq V_{\text{IN}} \leq V_{\text{MAX}}$			$(8 \leq V_{\text{IN}} \leq 18)$			$(15 \leq V_{\text{IN}} \leq 25)$			$(18.5 \leq V_{\text{IN}} \leq 28.5)$			V	
R_O	Dropout Voltage Output Resistance	$T_J = 25^\circ\text{C}, I_{\text{OUT}} = 1\text{ A}$			2.0			2.0			2.0			V	
		$f = 1\text{ kHz}$			8			18			19			$\text{m}\Omega$	

Electrical Characteristics LM78XXC (Note 2) (Continued)

$0^\circ\text{C} \leq T_J \leq 125^\circ\text{C}$ unless otherwise noted.

		5V			12V			15V			Units			
Input Voltage (unless otherwise noted)		10V			19V			23V						
Symbol	Parameter	Conditions			Min	Typ	Max	Min	Typ	Max	Min	Typ	Max	
V_{IN}	Short-Circuit Current	$T_J = 25^\circ\text{C}$			2.1			1.5			1.2			A
		$T_J = 25^\circ\text{C}$			2.4			2.4			2.4			A
		$0^\circ\text{C} \leq T_J \leq +125^\circ\text{C}, I_O = 5\text{ mA}$			0.6			1.5			1.8			$\text{mV}/^\circ\text{C}$
V_{IN}	Input Voltage Required to Maintain Line Regulation	$T_J = 25^\circ\text{C}, I_O \leq 1\text{ A}$			7.5			14.6			17.7			V

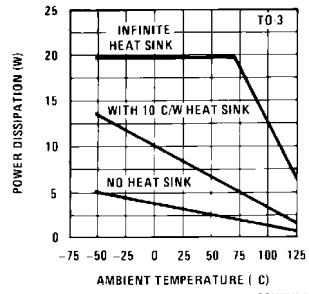
Note 1: Thermal resistance of the TO-3 package (K, KC) is typically $4^\circ\text{C}/\text{W}$ junction to case and $35^\circ\text{C}/\text{W}$ case to ambient. Thermal resistance of the TO-220 package (T) is typically $4^\circ\text{C}/\text{W}$ junction to case and $50^\circ\text{C}/\text{W}$ case to ambient.

Note 2: All characteristics are measured with capacitor across the input of $0.22\text{ }\mu\text{F}$, and a capacitor across the output of $0.1\text{ }\mu\text{F}$. All characteristics except noise voltage and ripple rejection ratio are measured using pulse techniques ($t_w \leq 10\text{ ms}$, duty cycle $\leq 5\%$). Output voltage changes due to changes in internal temperature must be taken into account separately.

Note 3: Absolute Maximum Ratings indicate limits beyond which damage to the device may occur. For guaranteed specifications and the test conditions, see Electrical Characteristics.

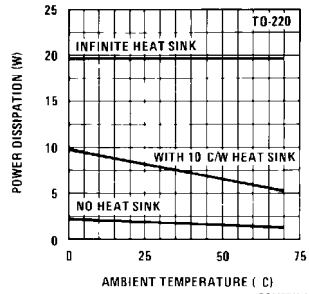
Typical Performance Characteristics

Maximum Average Power Dissipation



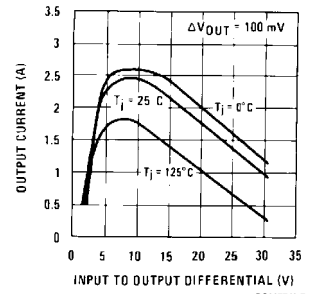
DS007746-5

Maximum Average Power Dissipation



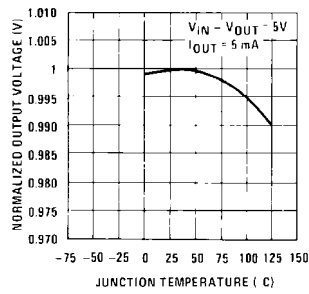
DS007746-6

Peak Output Current



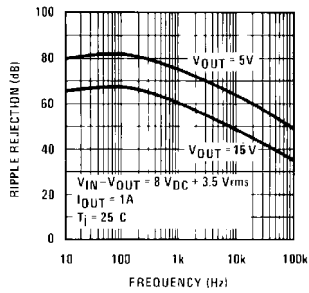
DS007746-7

Output Voltage (Normalized to 1V at $T_j = 25^\circ\text{C}$)



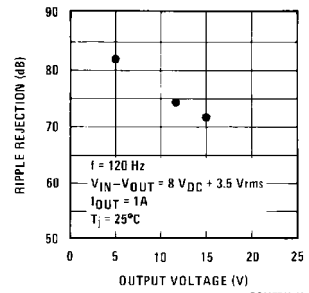
DS007746-8

Ripple Rejection



DS007746-9

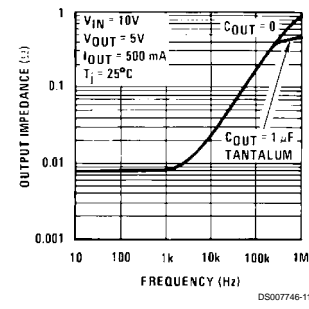
Ripple Rejection



DS007746-10

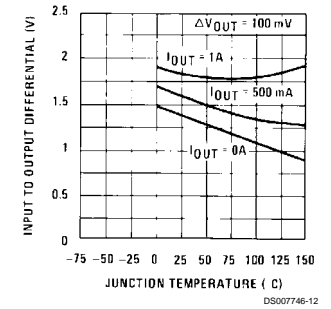
Typical Performance Characteristics (Continued)

Output Impedance



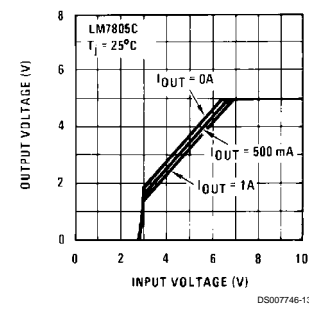
DS007746-11

Dropout Voltage



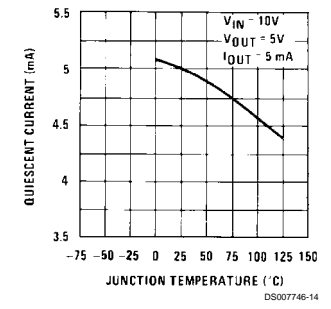
DS007746-12

Dropout Characteristics



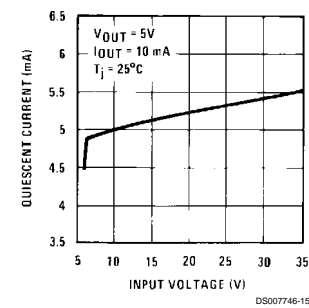
DS007746-13

Quiescent Current



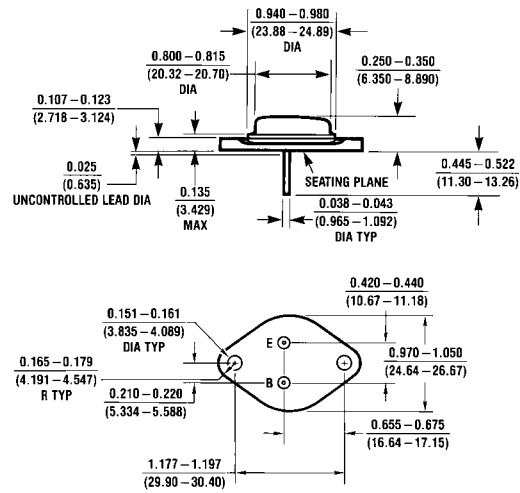
DS007746-14

Quiescent Current



DS007746-15

Physical Dimensions inches (millimeters) unless otherwise noted



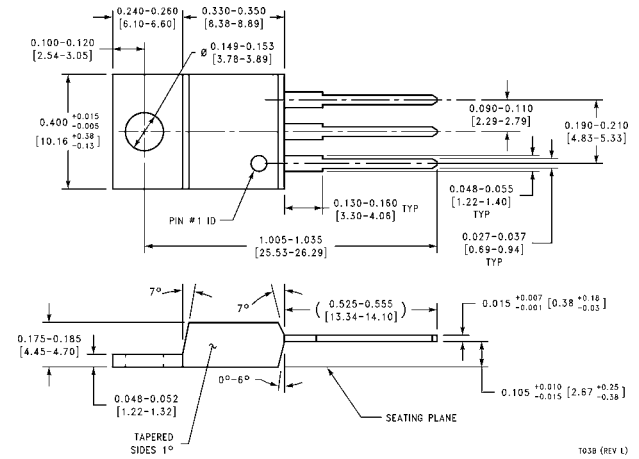
Aluminum Metal Can Package (KC)
Order Number LM7805CK, LM7812CK or LM7815CK
NS Package Number KC02A

KC02A (REV C)

LM78XX

LM78XX Series Voltage Regulators

Physical Dimensions inches (millimeters) unless otherwise noted (Continued)



TO-220 Package (T)
Order Number LM7805CT, LM7812CT or LM7815CT
NS Package Number T03B

T03B (REV L)

LIFE SUPPORT POLICY

NATIONAL'S PRODUCTS ARE NOT AUTHORIZED FOR USE AS CRITICAL COMPONENTS IN LIFE SUPPORT DEVICES OR SYSTEMS WITHOUT THE EXPRESS WRITTEN APPROVAL OF THE PRESIDENT AND GENERAL COUNSEL OF NATIONAL SEMICONDUCTOR CORPORATION. As used herein:

1. Life support devices or systems are devices or systems which, (a) are intended for surgical implant into the body, or (b) support or sustain life, and whose failure to perform when properly used in accordance with instructions for use provided in the labeling, can be reasonably expected to result in a significant injury to the user.
2. A critical component is any component of a life support device or system whose failure to perform can be reasonably expected to cause the failure of the life support device or system, or to affect its safety or effectiveness.

	National Semiconductor Corporation Americas Tel: 1-800-272-9959 Fax: 1-800-737-7018 Email: support@nsc.com www.national.com	National Semiconductor Europe Fax: +49 (0) 180-530 85 86 Email: europe.support@nsc.com Deutsch Tel: +49 (0) 69 9508 6208 English Tel: +44 (0) 870 24 0 2171 Français Tel: +33 (0) 1 41 91 8790	National Semiconductor Asia Pacific Customer Response Group Tel: 65-2544466 Fax: 65-2504466 Email: ap.support@nsc.com	National Semiconductor Japan Ltd. Tel: 81-3-5639-7560 Fax: 81-3-5639-7507
--	---	--	---	--

LM79XX Series 3-Terminal Negative Regulators

General Description

The LM79XX series of 3-terminal regulators is available with fixed output voltages of $-5V$, $-8V$, $-12V$, and $-15V$. These devices need only one external component—a compensation capacitor at the output. The LM79XX series is packaged in the TO-220 power package and is capable of supplying 1.5A of output current.

These regulators employ internal current limiting safe area protection and thermal shutdown for protection against virtually all overload conditions.

Low ground pin current of the LM79XX series allows output voltage to be easily boosted above the preset value with a resistor divider. The low quiescent current drain of

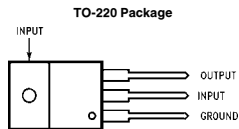
these devices with a specified maximum change with line and load ensures good regulation in the voltage boosted mode.

For applications requiring other voltages, see LM137 data sheet.

Features

- Thermal, short circuit and safe area protection
- High ripple rejection
- 1.5A output current
- 4% tolerance on preset output voltage

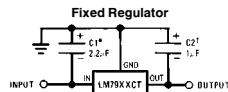
Connection Diagrams



Front View

Order Number LM7905CT, LM7912CT or LM7915CT
See NS Package Number TO3B

Typical Applications



TL/H/7340-3

*Required if regulator is separated from filter capacitor by more than 3". For value given, capacitor must be solid tantalum. 25 μ F aluminum electrolytic may be substituted.

†Required for stability. For value given, capacitor must be solid tantalum. 25 μ F aluminum electrolytic may be substituted. Values given may be increased without limit.

For output capacitance in excess of 100 μ F, a high current diode from input to output (1N4001, etc.) will protect the regulator from momentary input shorts.

LM79XX Series 3-Terminal Negative Regulators

Absolute Maximum Ratings (Note 1)

If Military/Aerospace specified devices are required, please contact the National Semiconductor Sales Office/Distributors for availability and specifications.

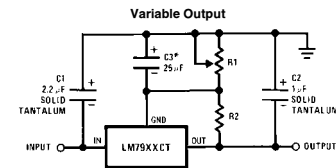
Input Voltage
($V_O = -5V$) $-25V$
($V_O = -12V$ and $-15V$) $-35V$

Input-Output Differential
($V_O = -5V$) 25V
($V_O = -12V$ and $-15V$) 30V
Power Dissipation (Note 2) Internally Limited
Operating Junction Temperature Range $0^\circ C$ to $+125^\circ C$
Storage Temperature Range $-65^\circ C$ to $+150^\circ C$
Lead Temperature (Soldering, 10 sec.) $230^\circ C$

Electrical Characteristics Conditions unless otherwise noted: $I_{OUT} = 500$ mA, $C_{IN} = 2.2$ μ F, $C_{OUT} = 1$ μ F, $0^\circ C \leq T_J \leq +125^\circ C$, Power Dissipation $\leq 1.5W$.

Part Number		LM7905C			Units	
Output Voltage		-5V				
Input Voltage (unless otherwise specified)		-10V				
Symbol	Parameter	Conditions	Min	Typ	Max	
V_O	Output Voltage	$T_J = 25^\circ C$ 5 mA $\leq I_{OUT} \leq 1$ A, $P \leq 15W$	-4.8	-5.0	-5.2	V
			-4.75		-5.25	V
			(-20 $\leq V_{IN} \leq -7$)			V
ΔV_O	Line Regulation	$T_J = 25^\circ C$, (Note 3)	8	50		mV
			(-25 $\leq V_{IN} \leq -7$)			V
			2	15		mV
			(-12 $\leq V_{IN} \leq -8$)			V
ΔV_O	Load Regulation	$T_J = 25^\circ C$, (Note 3) 5 mA $\leq I_{OUT} \leq 1.5$ A 250 mA $\leq I_{OUT} \leq 750$ mA	15	100		mV
			5	50		mV
I_Q	Quiescent Current	$T_J = 25^\circ C$	1	2		mA
ΔI_Q	Quiescent Current Change	With Line		0.5		mA
		With Load, 5 mA $\leq I_{OUT} \leq 1$ A		(-25 $\leq V_{IN} \leq -7$)	0.5	mA
V_N	Output Noise Voltage	$T_A = 25^\circ C$, 10 Hz $\leq f \leq 100$ Hz		125		μ V
	Ripple Rejection	$f = 120$ Hz	54	66		dB
			(-18 $\leq V_{IN} \leq -8$)			V
	Dropout Voltage	$T_J = 25^\circ C$, $I_{OUT} = 1$ A		1.1		V
I_{OMAX}	Peak Output Current	$T_J = 25^\circ C$		2.2		A
	Average Temperature Coefficient of Output Voltage	$I_{OUT} = 5$ mA, $0^\circ C \leq T_J \leq 100^\circ C$		0.4		mV/ $^\circ C$

Typical Applications (Continued)



TL/H/7340-2

*Improves transient response and ripple rejection. Do not increase beyond 50 μ F.

$$V_{OUT} = V_{SET} \left(\frac{R1 + R2}{R2} \right)$$

Select $R2$ as follows:
LM7905CT 300 Ω
LM7912CT 750 Ω
LM7915CT 1k

Electrical Characteristics (Continued) Conditions unless otherwise noted: $I_{OUT} = 500 \text{ mA}$, $C_{IN} = 2.2 \mu\text{F}$, $C_{OUT} = 1 \mu\text{F}$, $0^\circ\text{C} \leq T_J \leq +125^\circ\text{C}$, Power Dissipation = 1.5W.

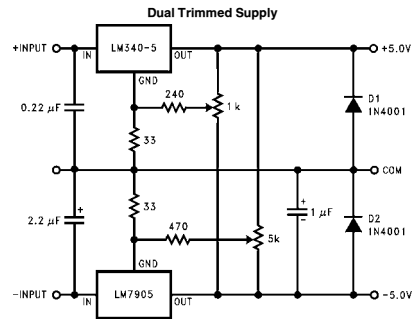
Part Number		LM7912C	LM7915C	Units					
Output Voltage		-12V	-15V						
Input Voltage (unless otherwise specified)		-19V	-23V						
Symbol	Parameter	Conditions	Min	Typ	Max	Min	Typ	Max	
V_O	Output Voltage	$T_J = 25^\circ\text{C}$ $5 \text{ mA} \leq I_{OUT} \leq 1 \text{ A}$, $P \leq 15 \text{ W}$	-11.5 -11.4 ($-27 \leq V_{IN} \leq -14.5$)	-12.0 -12.6 ($-30 \leq V_{IN} \leq -14.5$)	-12.5 -12.6 ($-30 \leq V_{IN} \leq -14.5$)	-14.4 -14.25 ($-30 \leq V_{IN} \leq -17.5$)	-15.0 -15.75 ($-30 \leq V_{IN} \leq -17.5$)	-15.6 -15.75 ($-30 \leq V_{IN} \leq -17.5$)	V V V
ΔV_O	Line Regulation	$T_J = 25^\circ\text{C}$, (Note 3)	5 3 ($-22 \leq V_{IN} \leq -16$)	80 30 ($-30 \leq V_{IN} \leq -16$)		5 3 ($-26 \leq V_{IN} \leq -20$)	100 50 ($-30 \leq V_{IN} \leq -20$)		mV V mV V
ΔV_O	Load Regulation	$T_J = 25^\circ\text{C}$, (Note 3) $5 \text{ mA} \leq I_{OUT} \leq 1.5 \text{ A}$ $250 \text{ mA} \leq I_{OUT} \leq 750 \text{ mA}$	15 5	200 75		15 5	200 75		mV mV
I_Q	Quiescent Current	$T_J = 25^\circ\text{C}$	1.5	3		1.5	3		mA
ΔI_Q	Quiescent Current Change	With Line With Load, $5 \text{ mA} \leq I_{OUT} \leq 1 \text{ A}$		0.5 0.5			0.5 0.5		mV mV
V_n	Output Noise Voltage	$T_A = 25^\circ\text{C}$, $10 \text{ Hz} \leq f \leq 100 \text{ Hz}$	300			375			μV
	Ripple Rejection	$f = 120 \text{ Hz}$	54 ($-25 \leq V_{IN} \leq -15$)	70		54 ($-30 \leq V_{IN} \leq -17.5$)	70		dB V
	Dropout Voltage	$T_J = 25^\circ\text{C}$, $I_{OUT} = 1 \text{ A}$	1.1			1.1			V
$I_{O\text{MAX}}$	Peak Output Current	$T_J = 25^\circ\text{C}$	2.2			2.2			A
	Average Temperature Coefficient of Output Voltage	$I_{OUT} = 5 \text{ mA}$, $0^\circ\text{C} \leq T_J \leq 100^\circ\text{C}$	-0.8			-1.0			$\text{mV}/^\circ\text{C}$

Note 1: Absolute Maximum Ratings indicate limits beyond which damage to the device may occur. Operating Ratings indicate conditions for which the device is intended to be functional, but do not guarantee Specific Performance limits. For guaranteed specifications and test conditions, see the Electrical Characteristics.

Note 2: Refer to Typical Performance Characteristics and Design Considerations for details.

Note 3: Regulation is measured at a constant junction temperature by pulse testing with a low duty cycle. Changes in output voltage due to heating effects must be taken into account.

Typical Applications (Continued)



TL/H/7340-4

Design Considerations

The LM79XX fixed voltage regulator series has thermal overload protection from excessive power dissipation, internal short circuit protection which limits the circuit's maximum current, and output transistor safe-area compensation for reducing the output current as the voltage across the pass transistor is increased.

Although the internal power dissipation is limited, the junction temperature must be kept below the maximum specified temperature (125°C) in order to meet data sheet specifications. To calculate the maximum junction temperature or heat sink required, the following thermal resistance values should be used:

Package	Typ θ_{JC} °C/W	Max θ_{JC} °C/W	Typ θ_{JA} °C/W	Max θ_{JA} °C/W
TO-220	3.0	5.0	60	40

$$P_{D\text{ MAX}} = \frac{T_{J\text{ MAX}} - T_A}{\theta_{JC} + \theta_{CA}} \text{ or } \frac{T_{J\text{ MAX}} - T_A}{\theta_{JA}}$$

$$\theta_{CA} = \theta_{CS} + \theta_{SA} \text{ (without heat sink)}$$

Solving for T_J :

$$T_J = T_A + P_D(\theta_{JC} + \theta_{CA}) \text{ or } T_J = T_A + P_D\theta_{JA} \text{ (without heat sink)}$$

Where:

T_J = Junction Temperature

T_A = Ambient Temperature

P_D = Power Dissipation

θ_{JA} = Junction-to-Ambient Thermal Resistance

θ_{JC} = Junction-to-Case Thermal Resistance

θ_{CA} = Case-to-Ambient Thermal Resistance

θ_{CS} = Case-to-Heat Sink Thermal Resistance

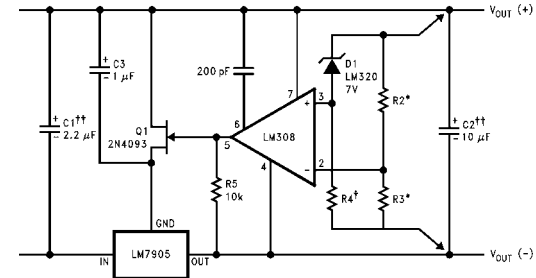
θ_{SA} = Heat Sink-to-Ambient Thermal Resistance

Typical Applications (Continued)

Bypass capacitors are necessary for stable operation of the LM79XX series of regulators over the input voltage and output current ranges. Output bypass capacitors will improve the transient response by the regulator.

The bypass capacitors, (2.2 μF on the input, 1.0 μF on the output) should be ceramic or solid tantalum which have good high frequency characteristics. If aluminum electrolytics are used, their values should be 10 μF or larger. The bypass capacitors should be mounted with the shortest leads, and if possible, directly across the regulator terminals.

High Stability 1 Amp Regulator



TL/H/7340-5

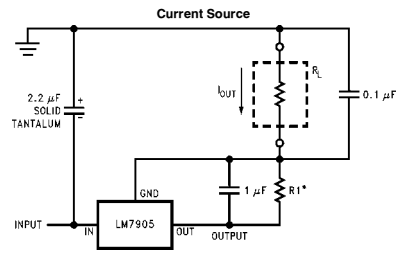
Load and line regulation < 0.01% temperature stability $\leq 0.2\%$

*Determine Zener current

†Solid tantalum

*Select resistors to set output voltage. 2 ppm/°C tracking suggested

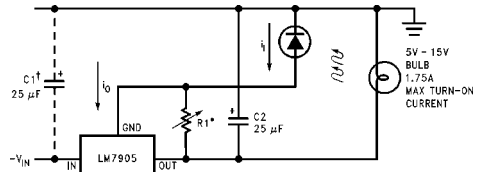
Typical Applications (Continued)



$$I_{OUT} = 1 \text{ mA} + \frac{5V}{R1}$$

TL/H/7340-7

Light Controller Using Silicon Photo Cell



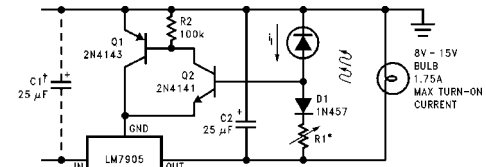
*Lamp brightness increase until $I_i = I_0 (\approx 1 \text{ mA}) + 5V/R1$.

†Necessary only if raw supply filter capacitor is more than 2* from LM7905CT

TL/H/7340-8

Typical Applications (Continued)

High-Sensitivity Light Controller

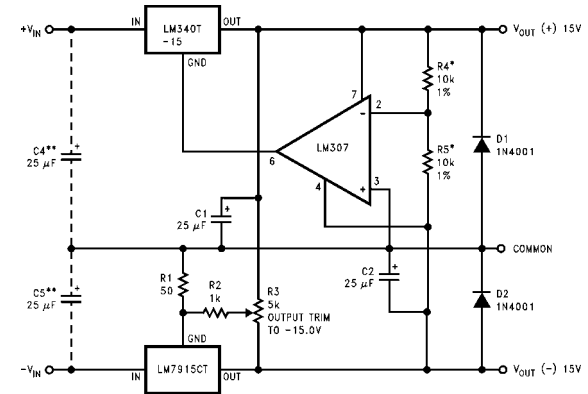


*Lamp brightness increases until $I_i = 5V/R1$ (I_i can be set as low as 1 μA)

†Necessary only if raw supply filter capacitor is more than 2* from LM7905

TL/H/7340-9

±15V, 1 Amp Tracking Regulators



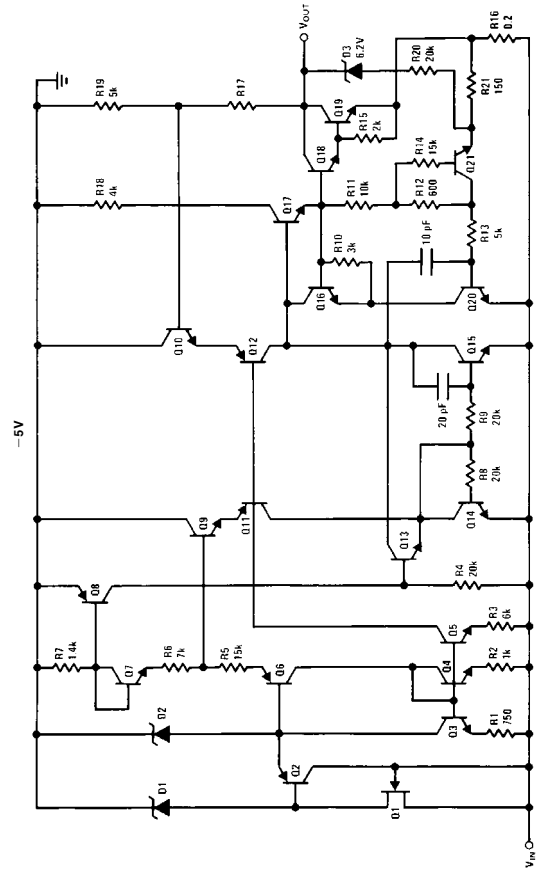
TL/H/7340-1

	(-15)	(+15)
Load Regulation at $\Delta I_L = 1\text{A}$	40 mV	2 mV
Output Ripple, $C_{IN} = 3000 \mu\text{F}$, $I_L = 1\text{A}$	100 μVrms	100 μVrms
Temperature Stability	50 mV	50 mV
Output Noise 10 Hz $\leq f \leq 10$ kHz	150 μVrms	150 μVrms

*Resistor tolerance of R4 and R5 determine matching of (+) and (-) outputs.

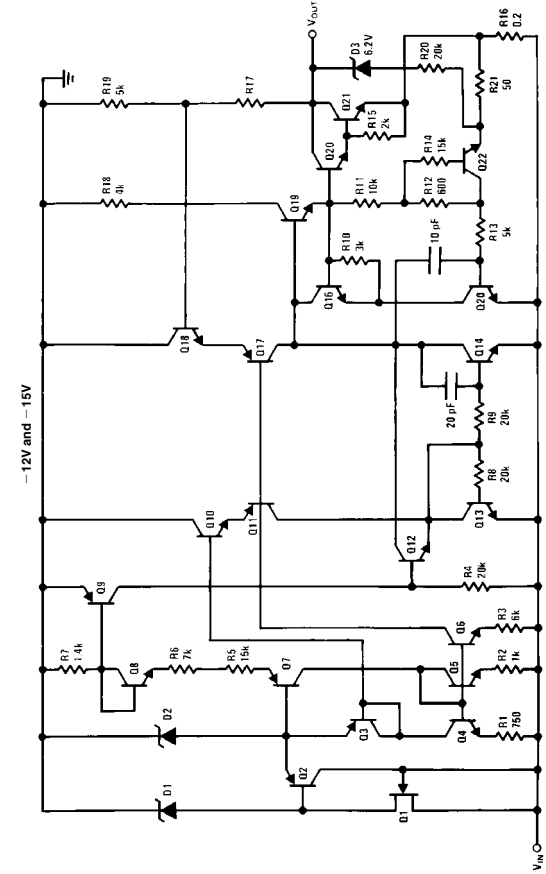
**Necessary only if raw supply filter capacitors are more than 3* from regulators.

Schematic Diagrams



TU/H7340-12

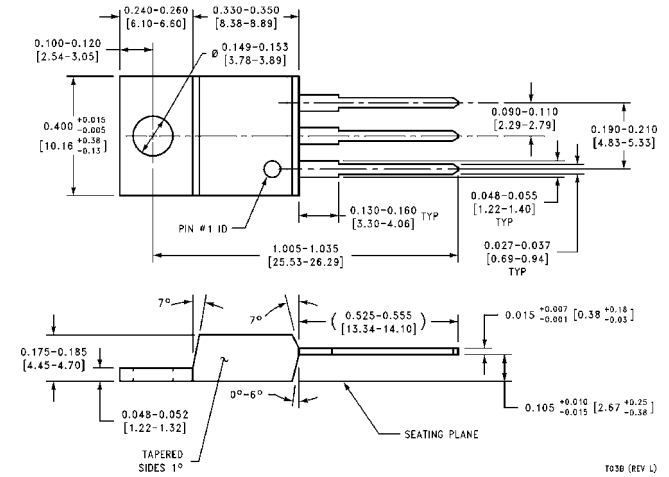
Schematic Diagrams (Continued)



TU/H7340-13

LM79XX Series 3-Terminal Negative Regulators

Physical Dimensions inches (millimeters)




TO-220 Outline Package (T)
Order Number LM7905CT, LM7912CT or LM7915CT
NS Package Number T03B

T03B (REV L)

LIFE SUPPORT POLICY

NATIONAL'S PRODUCTS ARE NOT AUTHORIZED FOR USE AS CRITICAL COMPONENTS IN LIFE SUPPORT DEVICES OR SYSTEMS WITHOUT THE EXPRESS WRITTEN APPROVAL OF THE PRESIDENT OF NATIONAL SEMICONDUCTOR CORPORATION. As used herein:

1. Life support devices or systems are devices or systems which, (a) are intended for surgical implant into the body, or (b) support or sustain life, and whose failure to perform, when properly used in accordance with instructions for use provided in the labeling, can be reasonably expected to result in a significant injury to the user.
2. A critical component is any component of a life support device or system whose failure to perform can be reasonably expected to cause the failure of the life support device or system, or to affect its safety or effectiveness.

 <p>National Semiconductor Corporation 1111 West Bardin Road Arlington, TX 76017 Tel: (800) 272-9959 Fax: (800) 737-7018</p>	<p>National Semiconductor Europe Fax: (+49) 0-180-530 85 86 Email: cnjwge@tevm2.nsc.com Deutsch Tel: (+49) 0-180-530 85 85 English Tel: (+49) 0-180-532 78 92 Français Tel: (+49) 0-180-532 93 58 Italiano Tel: (+49) 0-180-534 16 80</p>	<p>National Semiconductor Hong Kong Ltd. 13th Floor, Straight Block, Ocean Centre, 5 Canton Rd., Tsimshatsui, Kowloon Hong Kong Tel: (852) 2737-1600 Fax: (852) 2736-9960</p>	<p>National Semiconductor Japan Ltd. Tel: 81-043-299-2309 Fax: 81-043-299-2408</p>
--	--	--	---

National does not assume any responsibility for use of any circuitry described, no circuit patent licenses are implied and National reserves the right at any time without notice to change said circuitry and specifications.